Programme opérationnel Interreg IVA

France-Espagne-Andorre 2007 – 2013

SISPYR

Sistema de Información Sísmica del Pirineo

Système d’Information Sismique des Pyrénées

Sistema d'InformacióSísmicadelsPirineus

Seismic Attenuation

Action 3

Main contributor: OMP

2013-04-03

Authors: Marie CALVET (2)

Keywords:

Seismic attenuation, wave scattering, anelastic attenuation

1. IGC, IntitutGeològic de Catalunya
2. OMP, Université Paul Sabatier, Observatoire Midi-Pyrénées
3. UPC, UniversitatPolitècnica de Catalunya
4. IGN, Instituto Geografico Nacional
5. BRGM, Bureau de Recherches Géologiques et Minières
6. GEOCAT

Abstract

The coda quality factor of short-period S waves Qc excited by local earthquakes in the Pyrenees has been measured as a function of the length of the coda window Lw for different choices of the onset time of the coda (tw). In the 2-16Hz frequency band, we observe a transient regime characterized by an increase of Qc with Lw, followed by a stabilization around a plateau whose value depends on the central frequency of the signal. Using Monte Carlo simulations of wave transport in a variety of random media (about 1200 models), we demonstrate that the lapse-time dependence of Qc in the Pyrenees may be modeled by multiple anisotropic scattering of seismic waves, without invoking any depth dependence of the attenuation properties in the crust. In our model, anisotropic scattering is quantified by the ratio between the transport mean free path and the mean path (l*/l). At 6 Hz, the data require an anisotropy factor l*/l>5, a transport mean free path l*≈400km, and an intrinsic quality factor Qi≈800. From the frequency-dependent plateau of Qc at large lapse time, we infer an intrinsic quality factor of the form Qi≈400 $f^{0.4}$ in the Pyrenees. We also show how the rapid increase of the lapse-time dependence of Qc with frequency may be exploited to put constraints on the power spectrum of heterogeneities in the crust.

Next, lateral variations of seismic attenuation in the Pyrenees have been explored from the analysis of local earthquakes records. Scattering loss and intrinsic absorption both control the propagation of short period S waves through the crust. These two parameters have different effects: the shape of the S-wave energy envelope strongly depends on scattering while intrinsic absorption produces an exponential decay. The role of intrinsic and scattering attenuation is analyzed in two steps. Firstly, the coda quality factor Qc which quantifies the energy decay of coda waves, is estimated at large lapse time in five frequency bands and interpreted as intrinsic absorption. Because of the apparent lapse time dependence of Qc, the choice of coda window is crucial to map the lateral variations of seismic attenuation. If different coda windows are mixed (early and late coda window), it may happen that the lateral variations of Qc are measurement artifacts. Next, we systematically measure the peak delay time, defined as the time lag from the direct S-wave onset to the maximum amplitude arrival. This parameter quantifies the strength of multiple forward scattering due to random inhomogeneities along the seismic ray path. Comparison of coda Q and peak delay time measurements allows a qualitative interpretation of the origin of seismic attenuation (scattering/absorption) in the Pyrenean crust.

In all frequency bands, peak delay time measurements systematically show stronger scattering in the Western Pyrenees. At low frequency, Qc variations mainly depend on the tectonic units of the Pyrenees, with stronger absorption in sedimentary materials and basins, and smaller absorption in Paleozoic basements. At high frequency, coda Q is low at the location of Neogene structures in the Eastern Pyrenees. A more enigmatic low-Q anomaly is also observed at the location of the Maladeta Massif in the Central Pyrenees. In the Western Pyrenees, at the location of the Labourd-Maul\'eon region, absorption and scattering are both important at low frequency. This region also corresponds to a high-velocity/density anomaly revealed from tomography and gravity data analysis. It suggests that the high level of

inhomogeneities and absorption in the Labourd region may be related to intrusion of mantle and/or sub-crustal materials. In the Eastern Pyrenees, absorption appears dominant over scattering at high frequency. We hypothesize that thermal effects induced by crustal thinning may explain the strong absorption observed in this area.

Content

I – Introduction

In complement to seismic velocity measurements, attenuation provides valuable informations about the structure of the Earth. It is also an important parameter for the quantitative evaluation of large earthquake strong motion. Three mechanisms can be invoked to explain seismic waves attenuation: (1) anelastic absorption which mainly depends on temperature, melt or fluid content, and chemical composition, (2) scattering of seismic waves generated by small-scale velocity fluctuations and (3) focusing due to propagation in 3-D structures. The separation of these different effects is still a significant challenge but various methods have been proposed to estimate the relative contribution of anelasticity and scattering to the seismic attenuation in the Earth lithosphere (see Sato et al., 2012, for a review).

Because of easy applicability, many determinations of seismic attenuation have involved so far the use of coda waves of local earthquakes. Coda Q measurements (noted Qc hereafter) was extensively used in seismology for lithospheric or crustal attenuation studies. However Qc depends simultaneously on the scattering and anelastic properties of the crust. By using the MLTWA method developed by Fehler et al. (1992), Carcolé and Sato (2010) have recently obtained high resolution maps of scattering attenuation and intrinsic for Japan. They also demonstrated that the spatial variations of intrinsic absorption and Qc are highly correlated. But many studies have also shown that Qc depends on the lapse time in the coda. This observation is usually interpreted as an evidence of depth dependence of attenuation in the lithosphere. In complement to coda Q measurements, analyses of high-frequency seismic envelopes have been used to discuss the relative contribution of intrinsic absorption and scattering loss to the total seismic attenuation

In this project, we have examined the following points:

(1) What is the physical interpretation of Qc at short and large lapse time ?
(2) What is the relative contribution of intrinsic absorption and scattering loss to the total seismic attenuation in the Pyrenees?
(3) What are the lateral variations of seismic attenuation in the Pyrenean crust?

We analyse about 700 local earthquakes recorded at the pyrenean seismic stations managed by the partners of the SISPYR project. We also perform numerical simulations of wave transport in heterogeneous random media.

II – Catalogue of Pyrenean waveforms

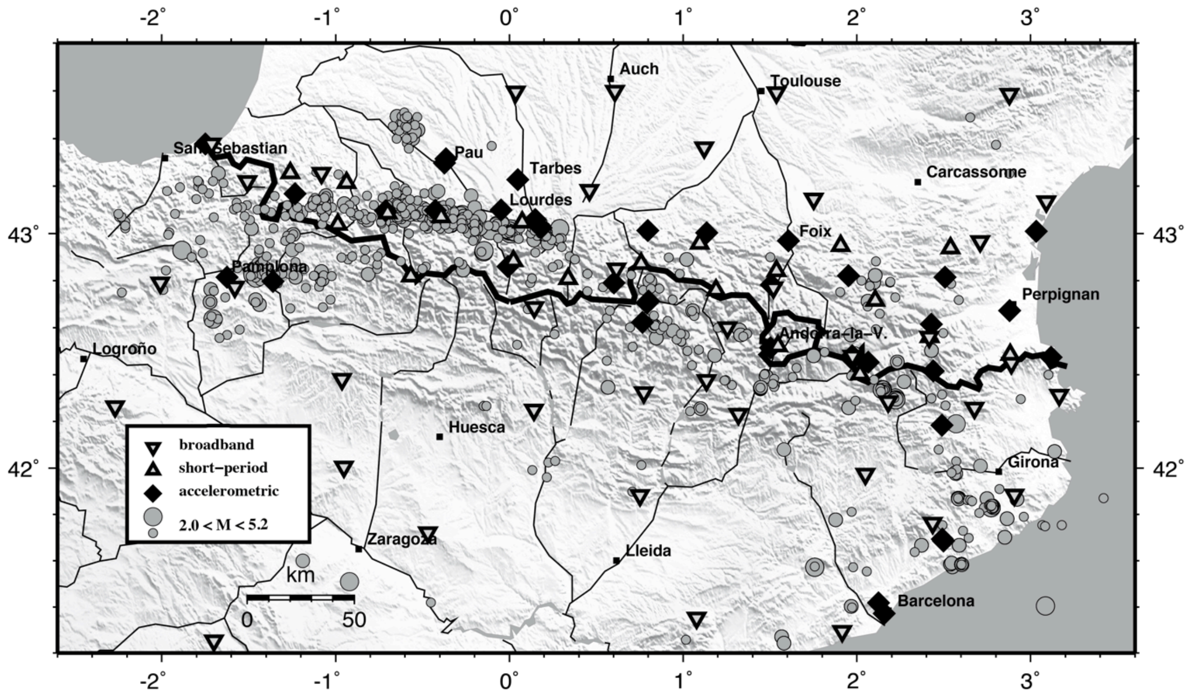

Figure 1: Location map of earthquakes and seismological stations.

We collect around 10000 waveform data recorded at 117 stations from 741 earthquakes which occured between 2001 and 2011, with a local magnitude (Ml) larger than 2.0. Focal depths vary between 1 km and 20 km. Location of epicenters, local magnitude and origin time of earthquakes have been determined by the Réseau de Surveillance Sismique des Pyrénées (RSSP). Our dataset mainly contains short period velocimetric waveforms from RSSP (20 stations). We also include accelerometric data from RAP (Réseau Accéléerométrique Permanent - 23 stations) and IGC (Institut Geològic de Catalunya - 13 stations), and broadband velocimetric data from IGC (14 stations) and IGN (Instituto Geogràfico Nacional - 8 stations). We also selected a few broadband records from the PYROPE (http://w3.dtp.obs-mip.fr/RSSP/PYROPE/) and IBERARRAY (http://iberarray.ictja.csic.es) experiments which have been deployed in the Pyrenees at the end of 2010. Most of the short period velocimetric and accelerometric data are recorded by triggered systems whereas broadband stations record continuously. Locations of epicenters and stations are reported on Figure 1. Epicentral distances range from 1 km to 400 km.

III – Lapse time dependence of coda-Q: interpretation

III.1 - Coda-Q interpretation: State of art

Since its inception by Aki and Chouet (1975), the interpretation of the quality factor of coda waves Qc has been the subject of numerous debates in the seismological literature. Aki and Chouet (1975) observed that the shape of the coda envelope of local earthquakes was remarkably independent of the source location and orientation. In addition, they found that a simple algebro-exponential formula could be used to parameterize the coda decay as follows:

$$\mathrm{E}(\mathrm{t},\mathrm{f}) = \mathrm{S}(\mathrm{f})\, t^{-\alpha}\, \mathrm{e}^{-2\pi \mathrm{f} \mathrm{t}/Q_c} \qquad (1)$$

where E is the power spectrum, S(f) is a frequency dependent source (and/or site) term, t is the lapse time, f is the frequency, α is a positive exponent, and Qc is the frequency dependent quality factor of coda waves. The exponent α cannot be determined from the data only. Indeed, the coda decay may be fitted equally well by different values of α with an impact typically less than 20% on the estimated Qc value. Hence, in data analyses the value of α is fixed a priori.

In the early years of coda studies, most investigators favored a single scattering interpretation in a homogeneous half-space. This model is compatible with formula (1) with an exponent α equal to 2 and a quality factor Qc which depends simultaneously on scattering and absorption

$$Q_c^{-1} = Q_{sc}^{-1} + Q_i^{-1} \qquad (2)$$

where Qsc and Qi denote the scattering and absorption quality factor, respectively. As array analyses demonstrated that coda waves were likely dominated by shear waves, Qc was thought to represent the quality factor of shear waves including scattering and absorption processes. In the late eighties and early nineties, the single-scattering model was challenged by the introduction of the radiative transfer equation and numerical Monte Carlo simulations which put forward the important role of multiple scattering in the generation of coda waves. Direct confirmations of the importance of multiple scattering were provided by the observation of seismic wave equipartition (Hennino et al., 2001) and weak localization (Larose et al., 2004). Multiple-scattering leads to a radically different interpretation of Qc. In particular, at long lapse time, coda waves enter in the diffusive regime which implies:

$$Q_c^{-1} = Q_i^{-1} \qquad (3)$$

in a simple uniform half-space. Comparison of formulas (2) and (3) highlights the role of the physical model underlying the interpretation of Qc.

The dependence of Qc on the lapse time in the coda and its relation to the depth dependence of attenuation properties in the lithosphere is another topic of interest which has been discussed recurrently in the literature. Rautian and Khalturin (1978) were among the first authors to propose that while remarkably stable, the envelope of coda waves could not be fitted with a single Qc parameter, independent of the time in the coda. Combining coda observations in different epicentral distance ranges and lapse times, they found the general trend that coda waves are generally less attenuated (show higher Qc) at long lapse times (large epicentral distances) than at short lapse times (short epicentral distances). The lapse time dependence of coda Q was interpreted by Rautian and Kalturin as a consequence of the overall decrease of attenuation of seismic waves with depth. Elaborating further on this idea and using a single-scattering interpretation, Gusev (1995) developed a stratified model of scattering properties in the lithosphere exhibiting a strong decrease of the strength of the scattering with depth. A number of studies throughout the world reported an increase of Qc with lapse time (Ibanez et al., 1990; Tselentis, 1993; Woodgold, 1994; Mukhopadhyay et al., 2008) and with few exceptions, generally ascribed this observation to depth-dependent attenuation properties in the Earth. Del Pezzo et al. (1990) nevertheless pointed out that the increase of Qc with time may stem simply from the inability of formula (1) to capture the full complexity of the scattering process in the Earth. For instance, the transition from the single scattering to the diffusive regime may result in an apparent dependence of Qc with lapse time, even in a half-space with uniform attenuation properties. However, as pointed out by Hoshiba (1991) based on a multiple isotropic scattering model, such an effect is too small to explain the full dependence of Qc with lapse time. Isotropic scattering, i.e. the independence of the scattering pattern on the incoming and outgoing propagation directions, does generally a poor job at fitting the shape of S coda envelopes at short lapse time (e.g., Gusev and Abubakirov, 1987; Hoshiba, 1995). Gusev and Abubakirov (1987) showed that envelope records of body waves are generally much better fitted by anisotropic scattering models and proposed a generic model of heterogeneity compatible with seismological observations. The broadening of energy envelopes with epicentral distance is a clear manifestation of multiple forward scattering in Earth's lithosphere (Sato, 1989; Saito et al., 2002).

In this study, we show the role of multiple anisotropic scattering in the lapse time dependence of coda Q using numerical simulations and observations from the Pyrenees.

III.2 – Data Processing

We estimate the power spectral density E(t,f) at lapse time t in the coda using the procedure outlined by Aki and Chouet (1975). The waveforms are deconvolved from the station response and acceleration records are integrated to get the three components of velocity. Bandpass Butterworth filters of order 4 are applied to the data in three frequency bands: 2-4Hz, 4-8Hz, 8-16Hz. The squared vertical traces are smoothed with a moving average window whose typical duration is of the order of 16 cycles. The coda envelopes are subsequently corrected for the algebraic term $t^{-\alpha}$ of Eq. (1) with α=3/2. After selecting a time window of duration Lw starting at a lapse time tw after the earthquake occurrence, a least-squares linear fit of $\ln\left(E(t,f)t^{3/2}\right)$ as a function of t yields an estimate of Qc in each frequency band. The values of Qc are accepted when the signal-to-noise ratio is greater than 4 and the correlation coefficient of the linear regression is greater than 0.98. At this point, it seems worthwhile to justify the value α=3/2 adopted in this work which differs from previous investigations. Rautian and Khalturin (1978) examined this point in detail and concluded that the data cannot guide us in the choice of α. The value of α must therefore be fixed a priori in accordance with the interpretation model. Because our approach relies on wave multiple scattering which is known to converge towards a diffusion process after a few mean free times (Sato et al., 2012), we adopt the value α=3/2 expected from 3-D diffusion.

III.3 – Observations

First, we consider data band-passed around a central frequency of 6 Hz. To characterize the lapse time dependence of Qc, we vary the position of the coda window with respect to the origin time of the earthquakes tw∈[30-120]s and/or the length of the coda window Lw∈[20-135]s. As the shape of the seismogram envelope is strongly affected by the source-station distance, we select local records with epicentral distances between 50km and 80km. Figure 2 shows the values of Qc at 6Hz as a function of the window length Lw for two onset times of the coda (tw=30s and tw=50s). Note that twice the ballistic time of shear waves lies in the range [28 - 45]s, so that our choice of coda onset time is close to the classical 2ts introduced by Aki and Chouet (1975). Figure 2 compiles all measurements along the pyrenean range and clearly displays an overall increase of Qc with Lw, as previously reported in the literature. Some nuance must nevertheless be brought to this statement because the dependence of Qc on Lw is strongly affected by the value of tw. As show in Figure 2, Qc typically ranges from 450 to 800 for Lw∈[30-130]s at tw=30s, but Qc is largely time-independent at tw=50s. Similarly, for sufficient large Lw, we observe that Qc tends to a constant 800 ±200, independent of tw. We emphasize that the range of fluctuations of Qc (±200) is likely due to strong lateral variations of the attenuation in the Pyrenees (see section 4) and does not reflect the uncertainty of individual measurements, which is typically one order of magnitude lower.

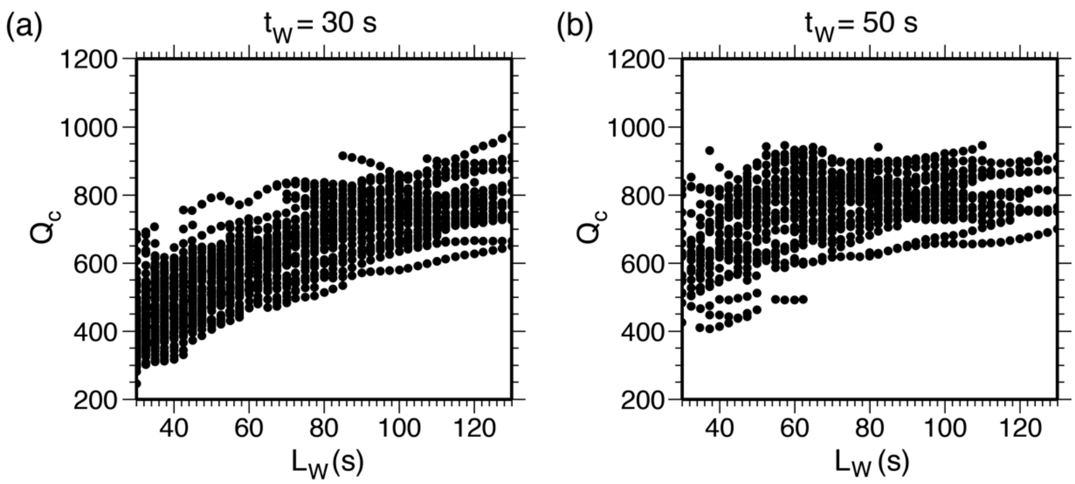

Figure 2: Qc at 6 Hz as a function of Lw for two coda onsets tw

Next, we compare the lapse time dependence of Qc in the three frequency bands at fixed coda onset tw=30s. Figure 3 clearly illustrates the increase of Qc with the length of the coda window up to Lw≈80s in all frequency bands. After this transient regime, Qc reaches a plateau which globally increases with frequency. The overall increase of the lapse-time dependence of Qc from low to high frequencies is a key observation to constrain the form of heterogeneity in the Pyrenees. To facilitate the comparison with other studies, the measurements are summarized by a simple power law of the form $Q_c = Q_0 f^n$. At large Lw (typically Lw~120s), Qc varies as $295(\pm25)f^{0.55(0.015)}$ while at shorter Lw (Lw~35s), Qc varies as $106(\pm21)f^{0.75(\pm0.08)}$. Although earlier studies reported on the frequency dependence of Qc in the Pyrenees, a straightforward comparison is problematic because the choice of coda window varies from one author to the other (Gagnepain-Beinex, 1987; Mitchell et al., 2008). On the one hand, Gagnepain-Beinex (1987) finds Q0 and n in the range [30-140] and [0.7-1.1], respectively. These measurements are compatible with our results for short lapse time. On the other hand Mitchell et al. (2008) find Q0 and n in the range [200-300] and [0.6-0.7], respectively. These measurements are consistent with our findings at large lapse time. The differences among the various studies published so far on the Pyrenees may presumably be ascribed to the choice of coda window. Indeed, Gagnepain-Beinex (1987) analyzed data from nearby earthquakes (r<30 km) using tw=2ts and a window length Lw∈[20-50]s, which mostly samples the early coda. This is in sharp contrast with the work of Mitchell et al. (2008) who used earthquakes recorded at regional distances, and analyzed the coda starting at a group velocity u=3.15km/s, with a time window of several hundreds of seconds. The systematic exploration of the relation between Qc and Lw applied to our dataset therefore reconciles the observations of Gagnepain-Beyneix and Mitchell.

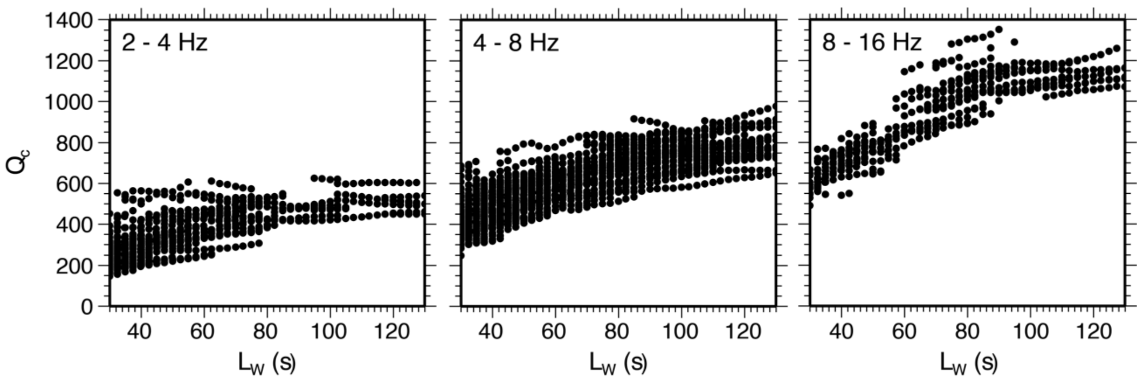

Figure 3: Qc as a function of Lw in three frequency bands (tw=30s).

III.4 – Numerical results

III.4.1 – Heterogeneity and multiple scattering model

In Earth's lithosphere the fluctuations of velocity are conveniently encapsulated in the formula:

$$V(x) = c\,(1+\xi(x))\ (4)$$

where c is the background velocity and $\xi(x)$ is a random function of position (Sato et al., 2012). In this study, the mean velocity is fixed at c=3.5km/s which is a good approximation of the S-wave velocity in the pyrenean crust (Souriau and Granet, 1995). In multiple scattering applications, random media are usually characterized by the autocorrelation function of the fluctuations defined as:

$$R(x,y) = \langle \xi(x)\xi(x+y) \rangle\ \ (5)$$

where the brackets denote an average over an ensemble of realization (Sato et al., 2012). We assume that the random medium is homogeneous and isotropic which implies that the autocorrelation function depends on r=|x-y| only. The magnitude of the fluctuations is quantified by the mean-squared velocity fluctuation ε^2=R(0). A completely equivalent description of the random medium is provided by the heterogeneity power spectrum P(k) which is the Fourier transform of R(r). A large variety of power spectra relevant to geophysical applications has been proposed by (Klimes, 2002). In this work, the usual Gaussian and Von-Karman power spectra will be adopted to represent the crustal heterogeneity. The Gaussian power spectrum is used to describe smooth random media where fluctuations all have a similar size a, also known as the correlation length. Von-Karman spectra are characterized by three parameters (a, ε^2, ν) and describe a large variety of random media where small-scale fluctuations are superposed on a smooth background. The roughness of the medium -- i.e. its content in short wavelength features-- is controlled by the exponent ν>0. The most frequently encountered version of the Von-Karman spectrum is the exponential medium which corresponds to ν= 0.5. Media with 0<ν<1 are said to be rich in short wavelength. Note that ν may also be taken greater than 1.

The gross scattering properties of random media are encapsulated in two parameters: the mean free path l and the transport mean free path l*. l is the characteristic length between two scattering events and l* is the propagation distance required for a wave to lose ``memory'' of its initial direction. The ratio l*/l, called anisotropy factor hereafter, quantifies the amount of anisotropic scattering. l and l* scale like $k^{-4}\ a^{-3}$ at low adimensional frequency (k a <<1). At large adimensional frequency (k a >> 1), l and l* scale like $k^{-2}\ a^{-1}$ and a, respectively. The anisotropy factor l*/l tends to 1 at small correlation length a, and increases like $k^2\ a^2$ at large correlation length. At fixed correlation length, l*/l increases like 2 ν-1 (ka >> 1).

Multiple anisotropic scattering is accurately modeled with the radiative transfer equation (Ryzhik et al., 1996) which can be solved numerically with the aid of Monte-Carlo simulations. We employ a simplified version of the Monte Carlo code developed by (Margerin et al., 2000). The main steps are summarized hereafter. A number of particles (typically 10^7) are launched isotropically from a point source. The distance between two collisions follows an exponential distribution with parameter l and absorption is simply taken into account by decreasing the weight of each particle by a factor $e^{-2\pi f t/Q_i}$. At each scattering event, the direction of the particle is modified by selecting randomly two angles that statistically reproduce the angular anisotropy of the single-scattering process. This free propagation+scattering process is repeated until the traveltime of the particle exceeds the time window of interest. The position of the particle is tracked during its random walk through the scattering medium to obtain the energy distribution as a function of time.

III.4.2 – Multiple-scattering models

We now propose to discuss the effects of scattering parameters (anisotropy factor and transport mean free path), heterogeneity power spectrum, and intrinsic absorption on the lapse time dependence of Qc at 6Hz. A large number of coda envelopes (around 1200) spanning a large set of random media was computed using the Monte Carlo method. Synthetic curves of Qc v.s. lapse time were obtained and compared to the pyrenean. Our goal is to find a scattering model which can explain the increase of Qc as a function of lapse-time as observed in the Pyrenees at 6Hz: a monotonic increase of Qc from Qc~450 at Lw=30s to Qc~800 at Lw=130s.

We first demonstrate explicitly that isotropic multiple scattering (l*=l) is incompatible with the lapse time dependence of Qc observed in the Pyrenees (Figure 4). Although the mean free path varies over one order of magnitude, it has little impact on the overall shape and amplitude of the lapse-time dependence of Qc. Multiple isotropic scattering may explain at most 25% of the observed variation of Qc which motivates the introduction of anisotropic scattering models.

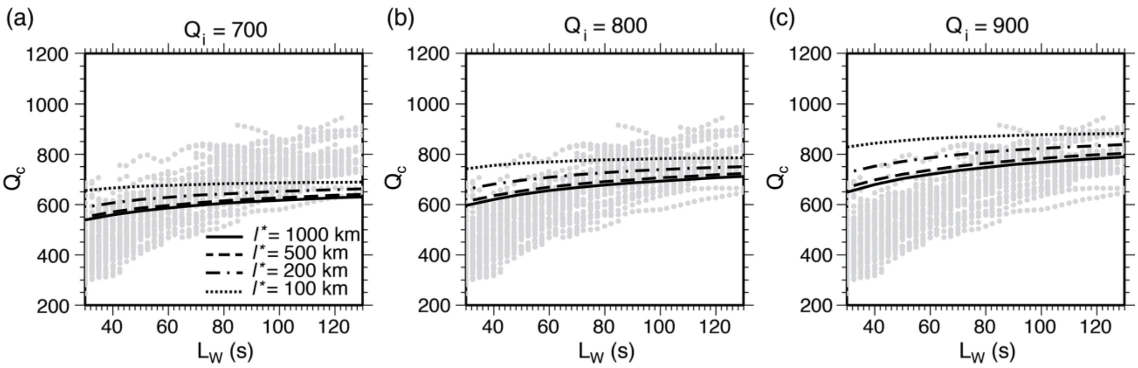

Figure 4: Lapse time dependence of synthetic codas computed at 6 Hz in a series of isotropic multiple-scattering models with l*=1000 km (solid line), l*=500 km (dashed line), and l*=200 km (dot-dashed line) and l*=100 km (dotted line). Three values of intrinsic quality factor are investigated: (a) Qi=700, (b) Qi=800 and (c) Qi=900. The numerical results (black lines) are superposed on the data (gray dots). The onset of the coda window is the same for synthetics and observations (tw=30s).

We now propose to examine the effect of scattering anisotropy. We fix intrinsic absorption (Qi=800). Figures 5(a-c) show that in an exponential medium, scattering anisotropy increases the lapse time dependence of Qc by a factor of roughly 2 compared to the isotropic case (Figure 4b). The effect is more pronounced at short window length Lw but is rather insensitive to the value of the anisotropy factor l*/l and of the transport mean free path l*. Rather, the transport mean free path (together with the intrinsic attenuation Qi) controls the overall amplitude of Qc.

To illustrate the role of the heterogeneity power spectrum, we also consider a Von-Karman medium poor in short-wavelength features (ν=5) for the same set of anisotropy factors and transport mean free paths as above (Figure 5, lower panels). As previously noted, the introduction of scattering anisotropy increases the lapse time dependence of Qc. In particular for ν=5, Qc rises all the more rapidly at short window length as the anisotropy factor is large, and the effect is all the more pronounced as the transport mean free path is short. The two Von-Karman power spectra can hardly be distinguished for small anisotropy factors (Figure 5(a and d)) but there are striking differences between the two at sufficiently large anisotropy factors. Comparison of panels c and f in Figure 5 shows that the transport mean free path has little effect on the lapse time dependence of Qc in an exponential medium, whereas the rise of Qc at short time windows is all the more rapid as the transport mean free path l* is short, in a Von-Karman medium poor in short wavelength ν=5. Hence, Figure 5 reveals that in addition to the scattering parameters l and l*, the medium roughness plays a crucial role in the lapse time dependence of Qc. The increase of Qc observed in our dataset --Qc varies from 450 at Lw=30s to 800 at Lw=130s -- requires an anisotropy factor typically larger than 5 and a smoothness exponent typically larger than 1.

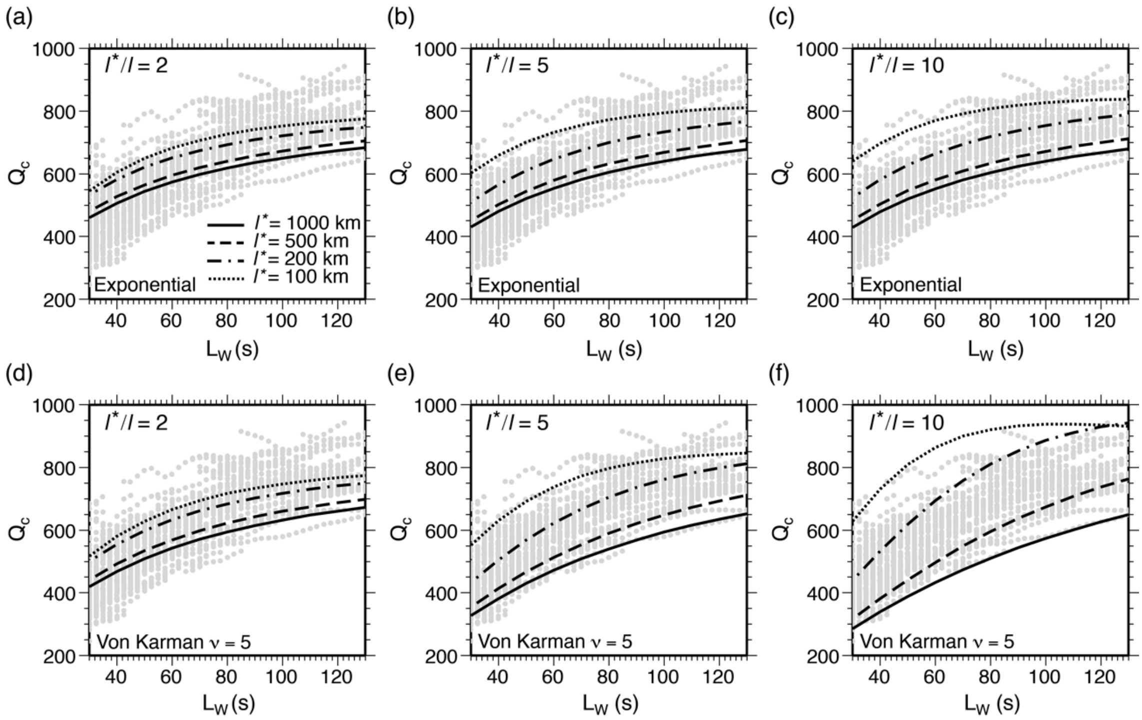

Figure 5: Lapse time dependence of synthetic codas computed at 6Hz in a series of anisotropic scattering models with l*=1000 km (solid line), l*=500 km (dashed line), l*=200 km (dot-dashed line) and l*=100km (dotted line) for two heterogeneity power spectra: exponential (top) and Von-Karman with ν=5 (bottom). Three values of the anisotropy factor are investigated: l*/l=2 (a, d), l*/l=5 (b, e) and l*/l=10 (c, f). The intrinsic quality factor is fixed: Qi=800. The numerical results (black lines) are superposed on the data (gray dots). The onset of the coda window is the same for synthetics and observations (tw=30s).

We remark that in the case of smooth media (Figure 5 e-f), the quality factor seems to increase indefinitely with lapse time depending on the l*/l and l* values. However, when the calculations are performed at sufficiently large window length Lw as in Figure 6, we find that the synthetic Qc curve can present an overshoot before converging to a plateau determined by the intrinsic quality factor. The overshoot is all the more pronounced as the anisotropy factor l^*/l and the smoothness exponent ν are larger and is associated with a very rapid increase of Qc at short lapse time (Lw$\in$[30-80]s). We may exploit this theoretical prediction to put some loose constraints on the anisotropy factor and on the medium roughness. In particular, smooth media (e.g. Gaussian media) with large anisotropy factor are less likely to represent the heterogeneity of the pyrenean crust because they predict an increase of Qc with lapse time usually faster than observed.

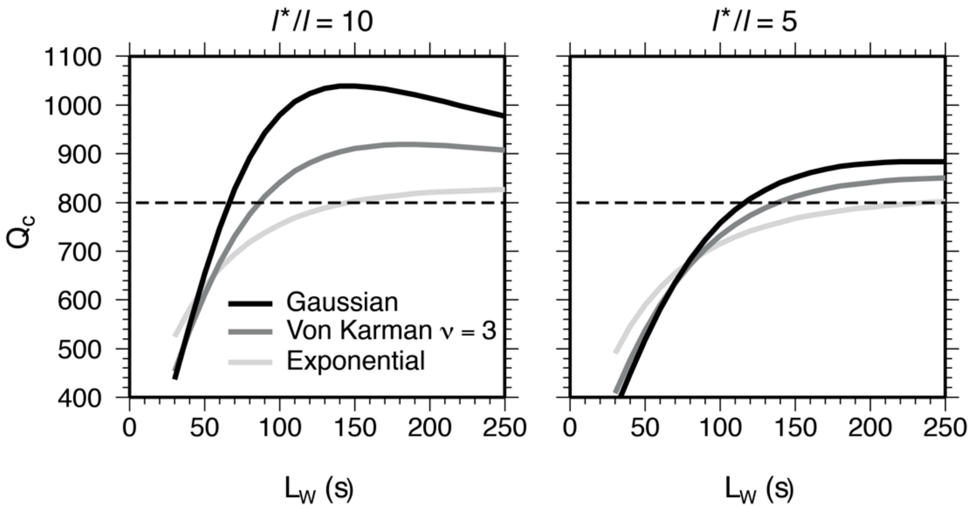

Figure 6: Illustration of the convergence of the coda quality factor Qc towards the intrinsic quality factor Qi=800 at large lapse time for three anisotropic scattering models with anisotropy factors l*/l=10 (left) and l*/l=5 (right) and transport mean free path l*=200 km: gaussian medium (black line), Von-Karman medium with ν=3 (dark gray line) and exponential medium (light gray line). The coda starts at tw=30s and the length of the coda window Lw is indicated on the horizontal axis.

III.5 – On the average attenuation properties of the Pyrenees

In the previous section, we made a case that a large part if not all the lapse-time dependence of Qc in the Pyrenees may be ascribed to anisotropic scattering without invoking any depth dependence of the attenuation properties. Following this idea, we combine Qc measurements in different frequency bands to put some constraints on the nature of heterogeneities in the pyrenean crust. The main purpose is to develop a preliminary scattering model which captures the gross features of the lapse-time dependence of Qc in the Pyrenees. Let us first recapitulate the principal conclusions that can be drawn from the confrontation of observations and numerical models at 6

Hz. The lapse-time dependence of Qc requires: (1) anisotropy factors of the order of 5 or larger; (2) smoothness exponent ν larger than 1; (3) intrinsic quality factor of the order of 900±300; (4) transport mean free path larger than 100 km. Considering the non-linearity of the model and the number of parameters, we do not make any attempt to solve an inverse problem. Our modest goal is to show that the frequency dependence of Qc may give some constraint on the roughness of the crust, i.e. its content in short wavelength features. We adopt the following two-step approach: (1) We infer the frequency dependence of absorption properties using the close correspondence between Qi and the coda quality factor Qc estimated from late coda windows, as put forward in the previous section. The frequency-dependent plateau of Qc apparent in Figure 3 is parametrized in the form $Q_c = Q_0 f^n$. For the Pyrenees, the values of Q0 and n deduced from a least-squares fit of the average value of Qc are 300 and 0.6, respectively. Because Qc tends to Qi at large lapse time, it appears reasonable to propose a frequency-dependent intrinsic quality factor of the form $Qi=300f^{0.6}$. Because the standard deviation of the data is rather large (±100) other parameterizations that fall within the uncertainty range are possible. As an example the frequency-dependent relation $Qi=400f^{0.4}$ is equally acceptable and will also be implemented. (2) Assuming an anisotropy factor l*/l=5, we select a set of Von-Karman random media with ν={1,3,5} which best fit the lapse time dependence of Qc at 6~Hz. Considering the different parameterizations of Qi, three transport mean free paths l*={250,500,1000}km may adequately explain the data. For each power spectrum (ν=1, 3, 5), we calculate the pair (a,ε) which corresponds to a given pair (l*/l,l*) at 6Hz. This yields three different heterogeneity models for each value of νas summarized in Table 1. From the knowledge of (a,ε,ν) we deduce the transport parameters (l, l*) and the scattering pattern in the [2-4]Hz and [8-16]Hz frequency bands. By numerically solving the radiative transfer equation for each heterogeneity model (a, ε,ν) given in Table 1, we theoretically predict the lapse time dependence of Qc in all frequency bands. Numerical results are confronted with observations in Figure7.

Power Spectrum	Model	a (m)	ε(%)	l (km) 3 Hz	l (km) 6 Hz	l (km) 12 Hz	l* (km) 3 Hz	l* (km) 6 Hz	l* (km) 12 Hz
Von-Karman v = 1.0	Model 1	160	3.7	230	50	13	485	250	190
	Model 2	160	2.6	460	100	25	970	500	380
	Model 3	160	1.8	920	200	50	1930	1000	760
Von-Karman v = 3.0	**Model 1**	**90**	**3.5**	**230**	**50**	**13**	**420**	**250**	**235**
	Model 2	**90**	**2.5**	**450**	**100**	**25**	**830**	**500**	**470**
	Model 3	90	1.8	900	200	50	1650	1000	940
Von-Karman v = 5.0	Model 1	70	3.6	220	50	13	390	250	250
	Model 2	70	2.5	430	100	25	780	500	490
	Model 3	70	1.8	870	200	50	1560	1000	980

Table 1: Statistical and scattering properties of the random media investigated in this study.

In the [2-4]Hz frequency band, the three Von-Karman random media yield very similar predictions. This does not come as a surprise since, as shown in the previous section, Qc is essentially controlled by the intrinsic quality factor and the transport mean free path for anisotropy factors typically less than 2 (see Table 1) The agreement with observations in the [2-4]Hz frequency band is worth noting and is consistent with the dominance of non-preferential scattering around 3Hz in the Pyrenees (Figure7 a, d, g). Since the lapse time low-frequency Qc measurements do not provide strong constraints on the medium roughness and on the transport mean free path. The comparison of panels (a,d,g) and (c,f,i) in Figure 12 reveals that only high-frequency data may help discriminate the models presented in Table 1. Independent of the medium roughness, the anisotropy factor increases while the transport mean free path decreases at high-frequency, which in turn implies a stronger lapse-time dependence of Qc as observed in pyrenean data in the [8-16] Hz band.

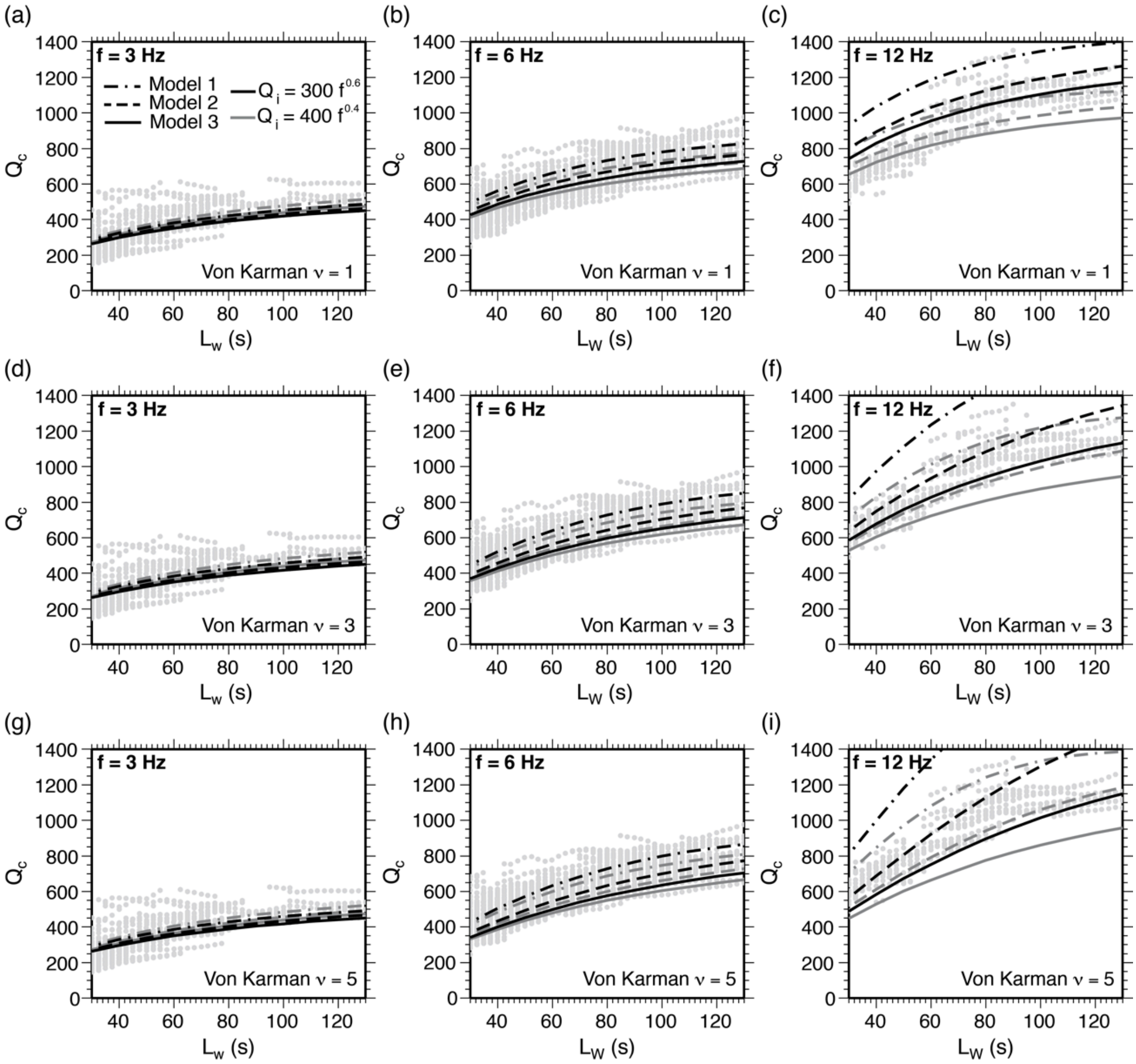

Figure 7: Lapse time dependence of Qc for synthetic codas computed at 3 Hz, 6 Hz and 12 Hz. Three Von-Karman power spectra with ν=1.0 (top), ν=3.0 (middle) and ν=5.0 (bottom) are considered. In each panel, three couples of statistical parameters (a,ε) given in Table 1 are investigated: Model 1 (dot-dashed lines), Model 2 (dashed lines) and Model 3 (solid lines). Two frequency-dependent intrinsic quality factors are explored: Qi=300 $f^{0.6}$ (black lines) and Qi=400 $f^{0.4}$ (gray lines). The numerical results (black and gray lines) are superposed on the data (gray dots). The onset of the coda window is the same for synthetics and observations (tw=30s) in the three frequency bands.

Comparison of panels c,f and i in Figure 7 leads us to select preferred average models of heterogeneity for the pyrenean range, also indicated in boldface in Table 1. A Von-Karman medium with a smoothness exponent ν=3, a correlation length a=90 m, root mean-squared velocity fluctuations $\varepsilon\in$[2.5-3.5]%, and intrinsic quality factor of the form Qi=400 $f^{0.4}$ agrees well with observations at all frequencies. Von Karman models with ν=1 (resp. ν=5) predict too weak (resp. strong) lapse time dependence of Qc in the [8,16]Hz frequency band. Our preferred models yield a transport mean path l*$\in$[420-830]km and an intrinsic quality factor Qi=620 at 3 Hz, in excellent agreement with previous estimates by Sens-Shonfelder et al. (2009) who obtained Qi=623 and l*=761km from the analysis of Lg coda at 3 Hz.

IV – Spatial variations of attenuation in the Pyrenees

IV.1 – Coda-Q Maps

IV.1.1 – Methodology

Because of the apparent lapse time dependence of Qc, the choice of coda window is crucial to map the lateral variations of seismic attenuation. If different coda windows are mixed (early and late coda window), it may happen that the lateral variations of Qc are measurement artifacts. For a selected range of epicentral distances, we must fix the coda onset tw and the coda window length Lw. Indeed, to facilitate the physical interpretation of Qc, we must be sure that its estimate is not hampered by the transient regime occurring at short lapse time (see Figure 2). However the number of signals which allow measurements at sufficiently large lapse time is limited by the length of the triggered seismic records and by the noise level. The best compromise is to measure Qc for epicentral distances smaller than 90km and for a 30s coda window starting 50s after the origin time of the earthquakes. This range of parameters corresponds to the plateau apparent in Figure2 and 3. Our choice of coda window allows good spatial coverage of the Pyrenees and ensures that Qc provides a reliable estimate of the absorption quality factor Qi. Absorption is to be understood as the combined effect of anelasticity and leakage (Margerin et al., 2009), the latter being negligible except in locally strongly scattering area.

The range of fluctuations (±250) around the plateau value (~800 in the frequency band 4-8Hz) is typically one order of magnitude larger than the uncertainty of individual measurements. We can thus confidently propose that the fluctuations are due to strong variations of absorption properties along the Pyrenean range. Adopting the selection criteria discussed above, the total numbers of Qc measurements in the five frequency bands are: 2190 (1-2Hz), 2260 (2-4Hz), 2296 (4-8Hz), 2293 (8-16Hz), 2035 (16-32Hz). We adopt a very simple Qc regionalization approach which consists of assigning Qc values to ray paths between stations and hypocentres. As the sensitivity of coda waves may be stronger near the station and the source, we should select Qc measurements for rather small epicentral distances. We tested various epicentral distance ranges, but to preserve good spatial coverage in Qc maps, we decided to select all the data for epicentral distance smaller than 90km. For simplicity, we only consider 2D lateral variations of Qc. Seismic ray paths are calculated considering that the S-wave velocity is homogeneous (about 3.5km/s). The depth distribution of hypocentres, indicates that most of the ray paths are located in the first 20kms of the crust. We divide the Pyrenean crust into rectangular 0.1°× 0.1° blocks. As many ray paths propagate through one block and each ray path indicates a different value of Qc we propose to allocate the mean values of Qc to each block. Only blocks crossed by more than 2 ray paths are retrieved. Finally, for each block, we take an average of the mean value over the nearest nine blocks to smooth the spatial variations.

IV.1.2 – Main characteristics of Qc maps

Figure 8 shows the spatial distribution of Qc and the ray path density in the five frequency bands. The spatial coverage of the Pyrenees is rather good, more particularly in areas characterized by a strong density of seismic stations and earthquakes. Strong absorption (small Qc values) is indicated in red colors whereas low absorption (large Qc values) is indicated in blue colors.

At low-frequency, we observe a rather good correlation between attenuation structures and the main tectonic units of the Pyrenees described by Choukroune et al. (1982) In the 1-2Hz map, Precambrian and Paleozoic basements in the Eastern (from NPF to the Catalan Coastal Range) and the Central Pyrenees (between the North Pyrenean Thrust and the southern limit of the PAZ) are characterized by smaller attenuation (larger Qc values) than the South Pyrenean Zone, the Mauléon, Pau and Pampelona Basins. However, the Paleozoic Basque Massifs exhibit stronger attenuation than other Paleozoic structures of the Pyrenees. Qc maps also reveal a North-South low-Qc anomaly at the longitude of the hercynian Maladetta Massifs (longitude 1.5°) which crosses the Pyrenees from the Aquitaine Basin to the Ebro Basin. On average, similar Qc structures are observed in the 2-4Hz map, except for the Mauléon Basin where attenuation becomes smaller than in the sediments of Pamplona and Pau Basins. In conclusion, our low-frequency Qc maps are characterized by rather strong absorption in the Western Pyrenees and small absorption in the Eastern Pyrenees with in average stronger absorption in sedimentary structures than in Paleozoic materials.

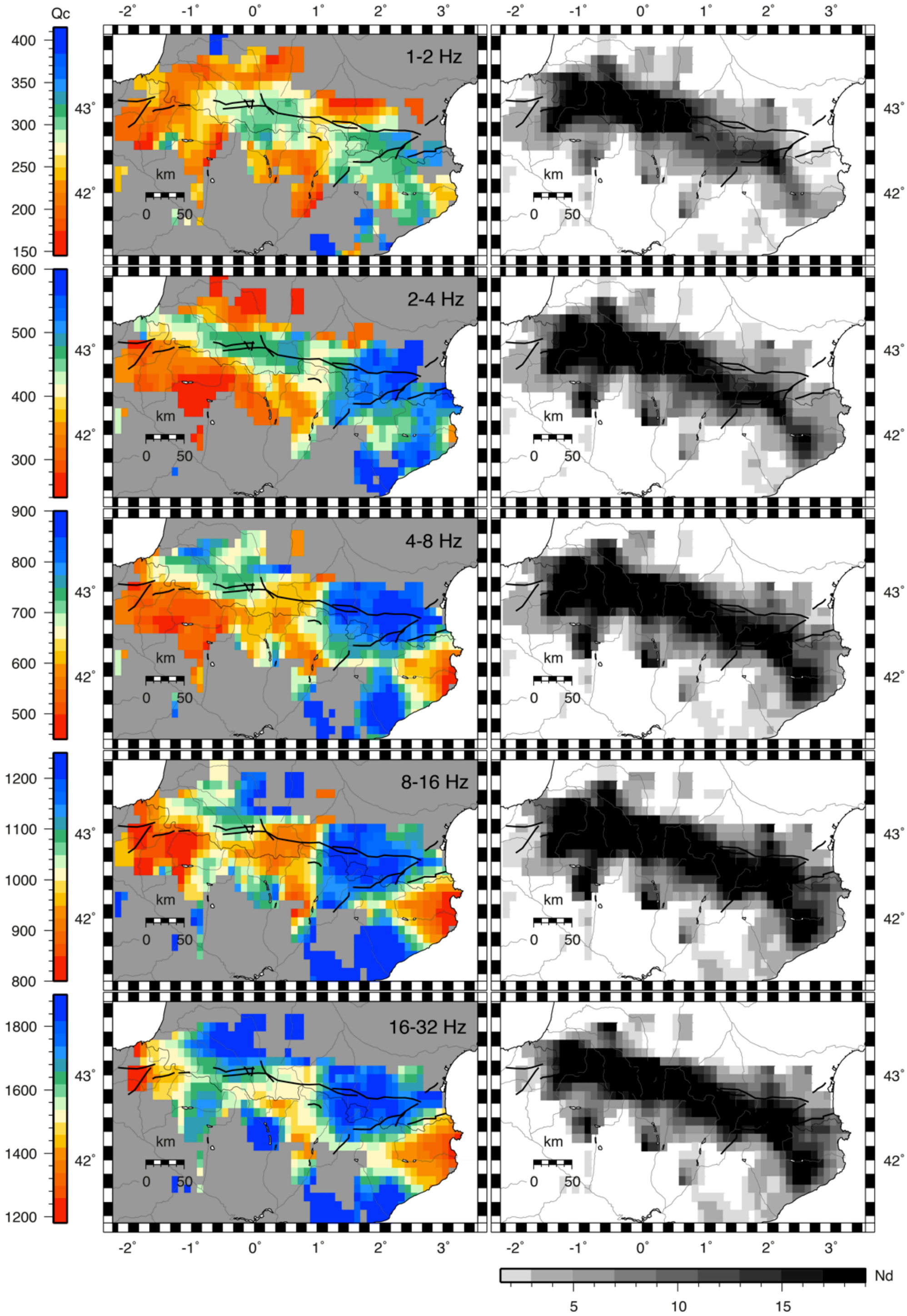

Figure 8: Regional variations of Qc (left) and ray path density (right). Qc is estimated in five frequency bands from [1- 2]Hz (top) to [16 - 32]Hz (bottom). Blocks with less than two measurements are shown in gray in Qc maps.

At high frequency (>4 Hz), the Qc pattern in the Pyrenees change drastically and cannot be easily related to the principal tectonic units. The most striking feature is the low Qc anomaly clearly delimited by the Neogene structures (Olot and La Selva volcanic areas) in the Eastern Pyrenees. We also observe that the North-South low-Qc anomaly already detected at low frequency spreads from the Maladeta Massif to the

Adour Fault. Surprisingly, the sediments in Aquitain and Ebro Basins as well as the Hercynian massifs of the Paleozoic Axial Zone in the Eastern Pyrenees exhibit similar seismic absorption. In the Westernmost Pyrenees, the strong attenuation anomaly is now limited to the Basque Massifs.

IV.2 – Pulse broadening Analysis

In complement to coda Qc measurements, analyses of high-frequency seismic envelopes have been used to discuss the relative contribution of intrinsic absorption and scattering loss to the total seismic attenuation (Sato,1989; Obara et al., 1995; Saito et al., 2002; Petukhin and Gusev, 2003; Takahashi et al., 2007). Multiple scattering due to random velocity inhomogeneities in the crust increases the apparent duration of the S-wave pulse. On the contrary, intrinsic absorption truncates it. The seismic wave envelop results from a competition between scattering and absorption (Saito et al., 2005). We thus propose to explore more systematically the regional variations of Qc and pulse broadening in order to discuss the origin (scattering and/or absorption) of the lateral variations of seismic attenuation in the Pyrenees.

IV.2.1 – Methodology

The strength of multiple scattering due to random heterogeneities along the seismic ray path can be quantified by the peak delay time (noted Tpd hereafter) defined as the time lag from the S-wave onset to the maximum of the amplitude.

We consider records with hypocentral distances smaller than 80 km in order to focus on crustal phases only. The waveforms are first deconvolved from the recording system response. Seismograms are filtered in four frequency bands (2-4Hz, 4-8Hz, 8-16Hz, 16-32Hz) in forward and backward directions to avoid any phase delay caused by using the fourth-order bandpass Butherworth filter. Next, we compute the root mean square of the sum of the two horizontal velocity components. The envelopes are smoothed with a moving time window whose typical duration is twice the central period of each frequency band. We only used waveform data which show a clear S-wave onset (quantified by the picking weight). S-wave onsets have been collected from local seismicity catalogues and are the same for each frequency band. Tpd is measured in seconds in a 40s time window starting from the S-wave onset. We obtained 5157 Tpd measurements in each frequency band.

Figure 9 shows Tpd as a function of the hypocentral distance R in the four frequency bands. Typically, at 80km epicentral distance, the peak delay time can reach 4s. Large values of Tpd, while absorption is also important (see section 3), reveal that scattering is rather strong in the Pyrenean crust. Although data are widely scattered, we observed that log(Tpd) increases almost linearly with the logarithm of the hypocentral distance. Indeed, at fixed frequency, it can be shown that log(T_pd) varies linearly with the logarithm of the hypocentral distance depending on the heterogeneity power spectrum of the random medium and on intrinsic absorption (Saito et al., 2002). Black solid lines in Figure 8 show the linear regression of log(Tpd) against hypocentral distance log(R):

$$\log\left(T_{pd}\ (f)\right) = A_R(f) + B_R(f)\log\ (R)$$

The regression coefficients are given in Figure 9.

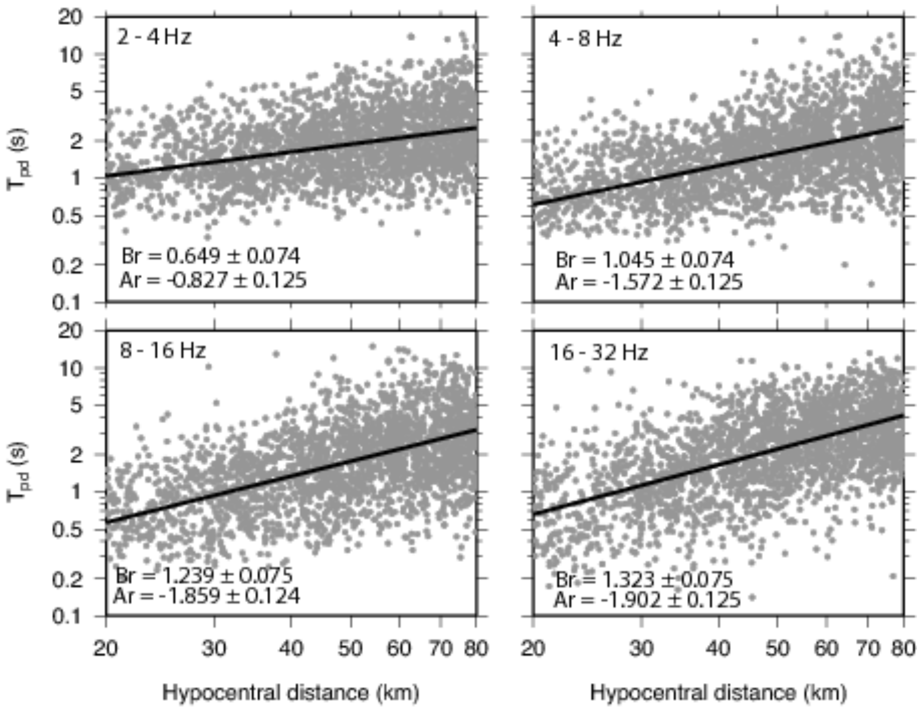

Figure 9: Tpd as a function of the hypocentral distance

A part of the dispersion of Tpd measurements at a given hypocentral distance could be due to regional variations of scattering along the range. Thus, we propose to explore the spatial variations of envelope broadening after removing the hypocentral dependence. For the mapping of peak delay times, we follow the method proposed by Takahashi et al. (2007). First, for each frequency band, we remove the hypocentral dependence by computing the peak delay time deviation defined as follows:

$$\Delta\left(\log(T_{pd})\ (f)\right) = \log\ (\ T_{pd}(f)) - A_R(f) - B_R(\mathrm{f})\ \log\ (R)$$

As envelope broadening is considered to be the result of multiple forward scattering by inhomogeneities, Δ(logTpd) may represent the relative strength of accumulated scattering contribution along each ray path. A small Δ(logTpd) thus implies the absence of strong medium heterogeneities along the ray path from the hypocentre to the station, whereas strong Δ(logTpd) indicates that a strongly inhomogeneous region is located somewhere along the ray path. For the mapping, we adopt the same approach as the one used for Qc maps. We only consider 2D spatial variations and we divide the Pyrenean crust into rectangular 0.1°×0.1° blocks. Next, we allocate the mean values of Δ(logTpd) to each block. Only blocks that are crossed by more than 5 ray paths are considered. Finally, in each block, we take an average of the mean values over the nearest nine blocks to smooth the spatial variations.

IV.2.2 – Tpd maps

Figure 10 shows the distribution of peak delay time deviation in four frequency bands. Blocks with small values of Δ(logTpd) are indicated by blue colors while blocks of large Δ(logTpd) values are in red. The top panel shows the ray path density. First we observe that there is no clear correlation between the Δ(logTpd) maps and the three main tectonic units.

The main feature is an East-West dichotomy in the Δ(logTpd) spatial distribution. The Western Pyrenees (west to the Adour Fault) exhibit larger Δ(logTpd) values than the Central and Eastern Pyrenees. It may indicate the presence of strong inhomogeneities in the western part of the range. Indeed, as absorption and scattering have a competitive effect on the peak delay time, large Δ(logTpd) values suggest that scattering may be dominant, at least equal, in comparison to absorption at low frequency. The small variations of Δ(logTpd) with frequency also suggest that the power spectrum of inhomogeneities is poor in small-scale components (Sato, 1989; Saito et al., 2002). In the Central and Eastern Pyrenees, the Paleozoic Axial Zone and the North Pyrenean Zone show rather small Δ(logTpd) values in all frequency bands. This feature could be due either to weak scattering or to strong absorption. But Qc maps show that absorption is low in the PAZ except around the Maladetta Massif. Thus, scattering is probably weak on average in the PAZ and NPZ. In the Eastern Pyrenees, more particularly to the east of intermountain basins of Empordà and La Selva, exhibit rather strong Δ(logTpd) values in the 2-4Hz frequency band. But the amplitude of the peak delay time deviation decreases as frequency increases. This frequency feature suggests that the crust in the Eastern Pyrenees is richer in small-scale structures than in the Western Pyrenees. However the effect of absorption should be also taken into account to propose a robust conclusion. In the Eastern Pyrenees, we also observe two high Δ(logTpd) regions located in the southern thrusts of the Axial zone, close to the compressive faults of Tech and Ribes Cambredon .

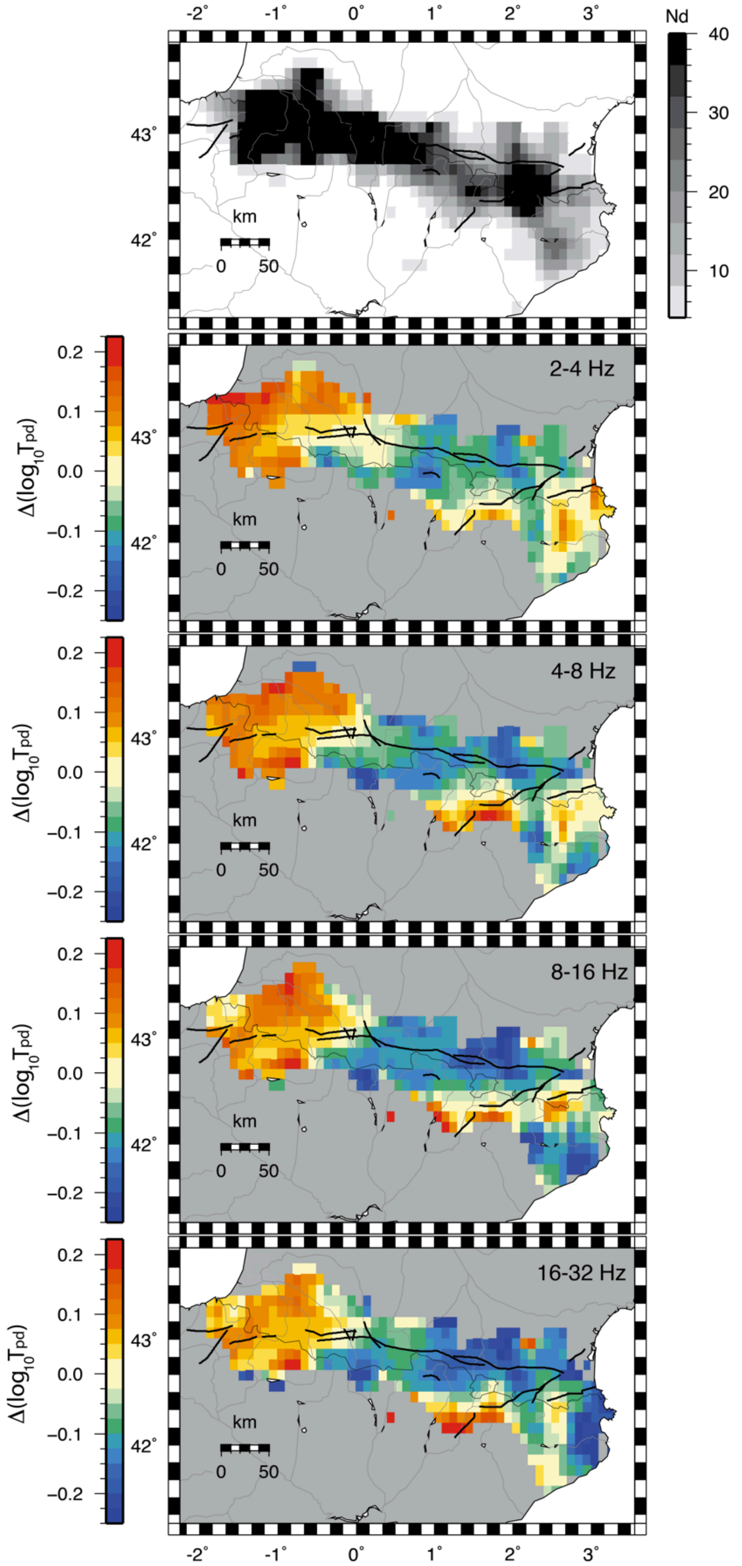

Figure 10: Tpd maps in four frequency band. Top panel gives the ray path density.

V – Conclusions

(1) A first message conveyed by this study is that most if not all the lapse time dependence of Qc observed in the Pyrenees may be explained by a simple anisotropic multiple-scattering model without invoking any depth dependence of attenuation properties. As anisotropic scattering is a prominent feature of high-frequency wave propagation in the Earth, its effect should be properly modeled to extract the depth-dependent attenuation structure from Qc measurements at the local scale (epicentral distance less than 100~km). An additional outcome of this study is the demonstration that the lapse-time dependence of Qc contains information on the heterogeneity power spectrum of the crust. It may therefore be combined with other methods such as peak delay time analysis to develop precise models of heterogeneity.

(2) The good coincidence between the intrinsic quality factor and the coda quality factor at large lapse time found in this work provides a simple technique to measure the absorption properties of the crust. In this respect the choice of coda window is crucial. Within a limited and fixed range of epicentral distance, we recommend plotting Qc as a function of coda window length Lw for different choices of coda onset tw to ensure visually that the estimate of Qc is not hampered by transient phenomena occurring at short lapse time. Only the plateau value of Qc can be considered as an approximation of Qi. This procedure is particularly important when performing a regionalization of Qc over a broad region.

(3) The model of scattering and absorption of the Pyrenees obtained in this study is preliminary and subject to revision in several respects. In terms of numerical modeling, it would be necessary to include the coupling among P and S waves to properly model the coda envelopes at short lapse time. Although it probably plays a minor effect on the lapse time dependence of Qc the reflection/refraction effects at the Moho should also be incorporated in a more realistic calculation. Concerning the interpretation of data, a more systematic exploration of the parameter space (in particular the correlation length and the smoothness exponent) should be conducted in future works in order to better delineate the robust features of our scattering model. As the average attenuation properties of the Pyrenees do not differ much from what is observed in the tectonically quiet central France, it appears that the interesting information on the pyrenean structure is contained in the lateral variations of Qc observed in our data.

(4) Qc maps show that the amplitude and the frequency dependence of attenuation strongly vary along the Pyrenean range. The Paleozoic Axial Zone mainly exhibits lower seismic attenuation than the surrounding regions, except at the longitude of the Maladeta Massif, east of the Adour fault. Seismic waves in the Western Pyrenees, more particularly at the

location of the Basques Massifs and the Nappe des Marbres, are strongly attenuated. Similarly the Neogene structures of the North-East Catalunya show strong seismic attenuation at high frequency.

(5) In addition to coda Q analysis, envelope broadening of high-frequency seismic waves gives complementary information on the origin of seismic attenuation in the Pyrenees, more particularly on the nature of the crustal inhomogeneities. The peak delay time maps highligth a strong East-West dichotomy in the scattering properties of the Pyrenean crust with stronger inhomogeneities in the Western Pyrenees, as previously proposed by Sens-Schonfelder et al. (2009) The Eastern Pyrenees exhibit a stronger frequency dependence of the peak delay time than the Western Pyrenees.

(6) The comparison of Qc and peak delay time maps allows a qualitative discussion about the relative contributions of absorption and scattering to the seismic attenuation in the Pyrenean crust. Anelastic absorption appears to be dominant in the Eastern Pyrenees at high frequency, whereas both absorption and scattering are strong in the Western Pyrenees. We propose a thermal origin for the strong seismic attenuation at the location of the Neogene structures in the Eastern Pyrenees. Indeed, the Eastern Pyrenees have been affected by a late extensional event with volcanism, and the region presents a rather strong geothermal activity in comparison to the Ebro Basin or the Western Pyrenees. In the Western Pyrenees, we argue that the attenuation properties of the crust (strong absorption and scattering) are mainly due to sub-crustal or mantle intrusions related to the complex tectonic history of the region.

VI – Références

- Aki, K. and B. Chouet (1975). Origin of coda waves: Source attenuation and scattering effects, J. Geophys. Res., 80, 3322–3342.
- Carcolé, E. and H. Sato (2010). Spatial distribution of scattering loss and intrinsic absorption of short-period S waves in the lithosphere of Japan on the basis of the Multiple Lapse Time Window Analysis of Hi-net data, Geophys. J. Int., 180, 268–290.
- Chazalon, A., M. Campillo, R. Gibson and E. Carreno (1993). Crustal wave propagation anomaly across the Pyrenean range. Comparison between observations and numerical simulations, Geophys. J. Int., 115, 829–838.
- Choukroune, P., F. Roure, B. Pinet and E. Team (1990). Main results of the ECORS Pyrenees profile, Tectonophysics, 173, 411–423.
- Correig, A., Mitchell, B., & Ortiz, R., 1990. Seismicity and coda Q values in the eastern Pyrenees: First results from the La Cerdanya seismic network, Pure Applied Geophys., 132(1), 311–329.
- Del Pezzo, E., R. Allota, and D. Patané (1990). Dependence of Qc (coda Q) on coda duration time interval: model or depth effect?, Bull. Seis. Soc. Am., 80, 1028–1033.
- Gagnepain-Beyneix, J. (1987). Evidence of spatial variations of attenuation in the western Pyrenean range, Geophys. J. R. Ast. Soc., 89, 681–704.
- Gusev, A. (1995). Vertical profile of turbidity and coda Q, Geophys. J. Int., 123, 665–672.

- Gusev, A. and I. Abubakirov (1987). Monte-carlo simulation of record envelope of a near earthquake, Phys. Earth Planet. Int., 49, 30–36.
- Fehler, M., Hoshiba, M., Sato, H., & Obara, K., (1992). Separation of scattering and intrinsic attenuation for the Kanto-Tokai region, Japan, using measurements of s-wave energy versus hypocentral distance, Geophys. J. Int., 108(3), 787–800.
- Hennino, R., N. Trégourès, N. Shapiro, L. Margerin, M. Campillo, B. Van Tiggelen, and R. Weaver (2001). Observation of equipartition of seismic waves, Phys. Rev. Lett., 86, 3447–3450.
- Hoshiba, M. (1991). Simulation of multiple-scattered coda wave excitation based on the energy conservation law, Phys. Earth Planet. Int., 67, 123–136.
- Ibanez, J., E. Del Pezzo, F. De Miguel, M. Herraiz, G. Alguacil, and J. Morales (1990). Depth-dependent seismic attenuation in the Granada zone (southern spain), Bull. Seism. Soc. Am., 80, 1232–1244.
- Klimes, L. (2002). Correlation functions of random media, Pure Appl. Geophys., 159, 1811–1831.
- Larose, E., L. Margerin, B. Van Tiggelen, and M. Campillo (2004). Weak localization of seismic waves, Phys. Rev. Lett., 93, 48501.
- Margerin, L., M. Campillo, and B. Van Tiggelen (2000). Monte Carlo simulation of multiple scattering of elastic waves, J. Geophys. Res., 105, 7873–7892.
- Margerin, L., M. Campillo, B. Van Tiggelen, and R. Hennino (2009). Energy partition of seismic coda waves in layered media: theory and application to Pinyon Flats Observa- tory, Geophys. J. Int., 177, 571–585.
- Mitchell, B., L. Cong, and G. Ekstro ̈m (2008). A continent-wide map of 1-Hz Lg coda Q variation across Eurasia and its relation to lithospheric evolution, J. Geophys. Res, 113, B04303.
- Mukhopadhyay, S., J. Sharma, R. Massey, and J. Kayal (2008). Lapse-time dependence of coda Q in the source region of the 1999 Chamoli earthquake, Bull. Seism. Soc. Am., 98, 2080–2086.
- Obara, K. & Sato, H., 1995. Regional differences of random inhomogeneities around the volcanic front in the Kanto-Tokai area, Japan, revealed from the broadening of S wave seismogram envelopes, J. Geophys. Res., 100, 2103–2103.
- Petukhin, A. G. & Gusev, A. A., 2003. The duration-distance relationship and average envelope shapes of small Kamtchatka earthquakes, Pure Appl.Geophys., 160, 171–1743.
- Rautian, T. G. and V. I. Khalturin (1978). The use of the coda for determination of the earthquake source spectrum, Bull. Seism. Soc. Am., 68, 923–948.
- Ryzhik, L., G. Papanicolaou, and J. B. Keller (1996) Transport equations for elastic and other waves in random media, Wave motion, 24, 327–370.
- Saito, T., H. Sato, and M. Ohtake (2002). Envelope broadening of spherically outgoing waves in three-dimensional random media having power law spectra, J. Geophys. Res., 107, 2089–2103.
- Saito, T., Sato, H., Ohtake, M., & Obara, K., 2005. Unified explanation of envelope broadening and maximum-amplitude decay of high-frequency seismograms based on the envelope simulation using the Markov

approximation: Forearc side of the volcanic front in northeastern Honshu, Japan, J. Geophys. Res, 110, B01304.

- Sato, H. (1989). Broadening of seismogram envelopes in the randomly inhomogeneous lithosphere based on the parabolic approximation: Southeastern Honshu, Japan, J. Geophys. Res, 94, 17735.
- Sato, H., M. C. Fehler, and T. Maeda (2012). Seismic wave propagation and scattering in the heterogeneous Earth, Springer, Berlin, 2nd edn.
- Sens-Schönfelder, C., L. Margerin, and M. Campillo (2009). Laterally heterogeneous scattering explains Lg blockage in the Pyrenees, J. Geophys. Res., 114, B07309.
- Shapiro, N.M., M. Campillo, L. Margerin, S. K. Singh, V. Kostoglodov, and J. Pacheco (2000). The energy partitioning and the diffusive character of the seismic coda, Bull. Seism. Soc. Am., 90, 655–665.
- Souriau, A. and M. Granet (1995). A tomographic study of the lithosphere beneath the pyrenees from local and teleseismic data, J. Geophys. Res., 100, 18117.
- Souriau, A., E. Chaljub, C. Cornou, L. Margerin, M. Calvet, J. Maury, M. Wathelet, F. Grimaud, C. Ponsolles, C. Pequegnat, and P. Guegen (2011). Multimethod char- acterization of the French-pyrenean valley of Bagn`eres-de-Bigorre for seismic-hazard evaluation: Observations and models, Bull. Seism. Soc. Am., 101, 1912–1937.
- Takahashi, T., Sato, H., Nishimura, T., & Obara, K., 2007. Strong inhomogeneity beneath Quaternary volcanoes revealed from the peak delay analysis of S-wave seismograms of microearthquakes in northeastern Japan, Geophys. J. Int., 168(1), 90–99.
- Takahashi, T., H. Sato, T. Nishimura, and K. Obara (2009). Tomographic inversion of the peak delay times to reveal random velocity fluctuations in the lithosphere: method and application to northeastern Japan, Geophys. J. Int., 178, 1437–1455.
- Tselentis, G. A. (1993). Depth-dependent seismic attenuation in Western Greece, Tectonophysics, 225, 523–528.
- Woodgold, C. (1994). Coda Q in the Charlevoix, Quebec, region: lapse-time dependence and spatial and temporal comparisons, Bull. Seism. Soc. Am., 84, 1123–1131.

VII - Annexes

Conferences:

- M. Calvet and L. Margerin (2013) Lapse time dependence of coda Q: Anisotropic multiple-scattering models and application to the Pyrenees, Poster, AGU San Francisco.
- L. Margerin and M. Calvet (2013) Lapse time dependence of coda Q: Anisotropic multiple-scattering models and application to the Pyrenees, Poster, EGU Vienne.

Publications:

- Calvet, M. and Margerin, L., 2013. Lapse time dependence of coda q: anisotropic multiple- scattering models and application to Pyrenees, Bull. Seism. Soc. Am., 103, in press.
- Calvet, M., Sylvander, M., Margerin, L., and Villasenor, A. Spatial variations of seismic attenuation in the Pyrenees : coda Q and peak delay time analysis, submitted to Tectonophysics

Bulletin of the Seismological Society of America, Vol. 103, No. 3, pp. –, June 2013, doi: 10.1785/0120120239

Lapse-Time Dependence of Coda Q: Anisotropic Multiple-Scattering Models and Application to the Pyrenees

by Marie Calvet and Ludovic Margerin

Abstract The coda quality factor of short-period S waves (Q_c) excited by local earthquakes in the Pyrenees has been measured as a function of the length of the coda window (L_W) for different choices of the onset time of the coda (t_W). In the 2–16 Hz frequency band, we observe a transient regime characterized by an increase of Q_c with L_W, followed by a stabilization around a plateau the value of which depends on the central frequency of the signal. Using Monte Carlo simulations of wave transport in a variety of random media ($\approx$1200 models), we demonstrate that the lapse-time dependence of Q_c in the Pyrenees may be modeled by multiple anisotropic scattering of seismic waves, without invoking any depth dependence of the attenuation properties in the crust. In our model, anisotropic scattering is quantified by the ratio between the transport mean free path and the mean path (l^*/l). At 6 Hz, the data require an anisotropy factor $l^*/l \geq 5$, a transport mean free path $l^* \approx 400$ km, and an intrinsic quality factor $Q_i \approx 800$. From the frequency-dependent plateau of Q_c at large lapse time, we infer an intrinsic quality factor of the form $Q_i \approx 400 f^{0.4}$ in the Pyrenees. We also show how the rapid increase of the lapse-time dependence of Q_c with frequency may be exploited to put constraints on the power spectrum of heterogeneities in the crust.

Introduction

Since its inception by Aki and Chouet (1975), the interpretation of the quality factor of coda waves (Q_c) has been the subject of numerous debates in the seismological literature. Aki and Chouet (1975) observed that the shape of the coda envelope of local earthquakes was remarkably independent of the source location and orientation. In addition, they found that a simple algebro-exponential equation could be used to parameterize the coda decay as

$$E(t, f) = S(f) t^{-\alpha} e^{-2\pi f t / Q_c}, \qquad (1)$$

where E is the power spectrum, $S(f)$ is a frequency-dependent source (and/or site) term, t is the lapse time, f is the frequency, α is a positive exponent, and Q_c is the frequency-dependent quality factor of coda waves. It was pointed out by Aki and Chouet (1975) that the exponent α cannot be determined from the data only. In other words, the coda decay may be fitted equally well by different values of α with an impact typically $<20\%$ on the estimated Q_c value. Thus, in data analyses the value of α is fixed *a priori*. In the early years of coda studies, most investigators favored a single-scattering interpretation in a homogeneous half space. This model is compatible with equation (1) with an exponent α equal to 2 and a quality factor Q_c, which depends simultaneously on scattering and absorption through the formula (Shapiro *et al.*, 2000):

$$Q_c^{-1} = Q_{sc}^{-1} + Q_i^{-1}, \qquad (2)$$

where Q_{sc} and Q_i denote the scattering and absorption quality factor, respectively. As array analyses demonstrated that coda waves were likely dominated by shear waves, Q_c was thought to represent the quality factor of shear waves including scattering and absorption processes. In the late eighties and early nineties, the single-scattering model was challenged by the introduction of the radiative transfer equation and numerical Monte Carlo simulations, which put forward the important role of multiple scattering in the generation of coda waves (Gusev and Abubakirov, 1987; Hoshiba, 1991). Direct confirmations of the importance of multiple scattering were provided by the observation of seismic-wave equipartition (Hennino *et al.*, 2001) and weak localization (Larose *et al.*, 2004). Multiple scattering leads to a radically different interpretation of Q_c. In particular, at long lapse time, coda waves enter in the diffusive regime, which implies

$$Q_c^{-1} = Q_i^{-1} \qquad (3)$$

in a simple uniform half-space (Shapiro *et al.*, 2000). Comparison of equations (2) and (3) highlights the role of the physical model underlying the interpretation of Q_c.

The dependence of Q_c on the lapse time in the coda and its relation to the depth dependence of attenuation properties in the lithosphere is another topic of interest that has been discussed recurrently in the literature. Rautian and Khalturin (1978) were among the first authors to propose that, although remarkably stable, the envelope of coda waves could not be fitted with a single Q_c parameter, independent of the time in the coda. Combining coda observations in different epicentral distance ranges and lapse times, they found the general trend that coda waves are generally less attenuated (show higher Q_c) at long lapse times (large epicentral distances) than at short lapse times (short epicentral distances). Similar observations were made by Roecker *et al.* (1982) in the Hindu-Kush region. The lapse time dependence of coda Q was interpreted by Rautian and Khalturin (1978) as a consequence of the overall decrease of attenuation of seismic waves with depth. Elaborating further on this idea and using a single-scattering interpretation, Gusev (1995) developed a stratified model of scattering properties in the lithosphere exhibiting a strong decrease of the strength of the scattering with depth. A number of studies throughout the world reported an increase of Q_c with lapse time (e.g., Ibanez *et al.*, 1990; Tselentis, 1993; Woodgold, 1994; Mukhopadhyay *et al.*, 2008, to cite a few only) and, with few exceptions, generally ascribed this observation to depth-dependent attenuation properties in the Earth. Del Pezzo *et al.* (1990) nevertheless pointed out that the increase of Q_c with time may stem simply from the inability of equation (1) to capture the full complexity of the scattering process in the Earth. For instance, the transition from the single scattering to the diffusive regime may result in an apparent dependence of Q_c with lapse time, even in a half-space with uniform attenuation properties. As pointed out, however, by Hoshiba (1991) based on a multiple isotropic scattering model, such an effect is too small to explain the full dependence of Q_c on lapse time.

Isotropic scattering, that is, the independence of the scattering pattern on the incoming and outgoing propagation directions, does a generally poor job at fitting the shape of S coda envelopes at short lapse time (e.g., Gusev and Abubakirov, 1987; Hoshiba, 1995). Gusev and Abubakirov (1996) showed that envelope records of body waves are generally much better fitted by anisotropic scattering models and proposed a generic model of heterogeneity compatible with seismological observations. The broadening of energy envelopes with epicentral distance is a clear manifestation of multiple forward scattering in Earth's lithosphere (Sato, 1989; Saito *et al.*, 2002). Thus, the purpose of the present paper is to clarify the role of multiple anisotropic scattering in the lapse-time dependence of coda Q using numerical simulations and observations from the Pyrenees. We first review briefly the method of data analysis and present our observations of lapse-time dependence of Q_c in different frequency bands. We show that Q_c stabilizes after a given lapse time. Next, we present the multiple-scattering model and discuss its limitations. The core of the paper illustrates with the aid of numerical simulations of wave transport through a variety of random media that the lapse-time dependence of Q_c is well explained by multiple anisotropic scattering. This allows us to give estimates of the scattering properties of the pyrenean crust based on the observed lapse-time dependence of Q_c. Finally, our results are discussed and compared to other studies.

Observations

Data Selection and Processing

We collected all available waveform data from various institutions that operate seismological networks on both the French and Spanish sides of the Pyrenees. This database is a coordinated effort through the European project INTERREG SISPYR. We selected ~5000 waveforms from 159 earthquakes that occured between 2001 and 2010, with a local magnitude >3.0. This data set includes short-period seismometer data from RSSP (Réseau de Surveillance Sismique des Pyrénées), accelerometer data from RAP (Réseau Accélérométrique Permanent) and IGC (Institut Geolologic de Catalunya), and broadband seismometer data from IGC and IGN (Instituto Geografico Nacional). Short-period velocimeter and accelerometer records are triggered data. The selected events are located within 20–250 km epicentral distance, with a majority of events occurring between 2 and 12 km depth. Locations of epicenters and stations are reported on Figure 1.

We estimate the power spectral density $E(t, f)$ at lapse time t in the coda using the procedure outlined by Aki and Chouet (1975). The waveforms are deconvolved from the station response, and acceleration records are integrated to get the three components of velocity. Passband Butterworth filters of order 4 are applied to the data in three frequency bands: 2–4, 4–8, and 8–16 Hz. The squared vertical traces are smoothed with a moving average window, the typical duration of which is of the order of 16 cycles. The coda envelopes are subsequently corrected for the algebraic term $t^{-\alpha}$ of equation (1) with $\alpha = 3/2$. After selecting a time window of duration L_W starting at a lapse time t_W after the earthquake occurrence, a least-squares linear fit of $\ln[E(t, f)t^{3/2}]$ as a function of t yields an estimate of Q_c in each frequency band. The values of Q_c are accepted when the signal-to-noise ratio is >4 and the correlation coefficient of the linear regression is >0.98.

At this point, it seems worthwhile to justify the value $\alpha = 3/2$ adopted in this work, which differs from previous investigations. Rautian and Khalturin (1978) examined this point in detail and concluded that the data cannot guide us in the choice of α. In particular, they write: "For most frequencies, the estimates of Q for $n = 0.5, 0.75$, or 1.0 differ by less than 20 per cent and the data are inadequate to choose among these values." (Note that $n = \alpha/2$.) The value of α must, therefore, be fixed *a priori* in accordance with the interpretation model. Because our approach relies on wave multiple scattering, which is known to converge towards a diffusion process after a few mean free times (Sato *et al.*, 2012), we

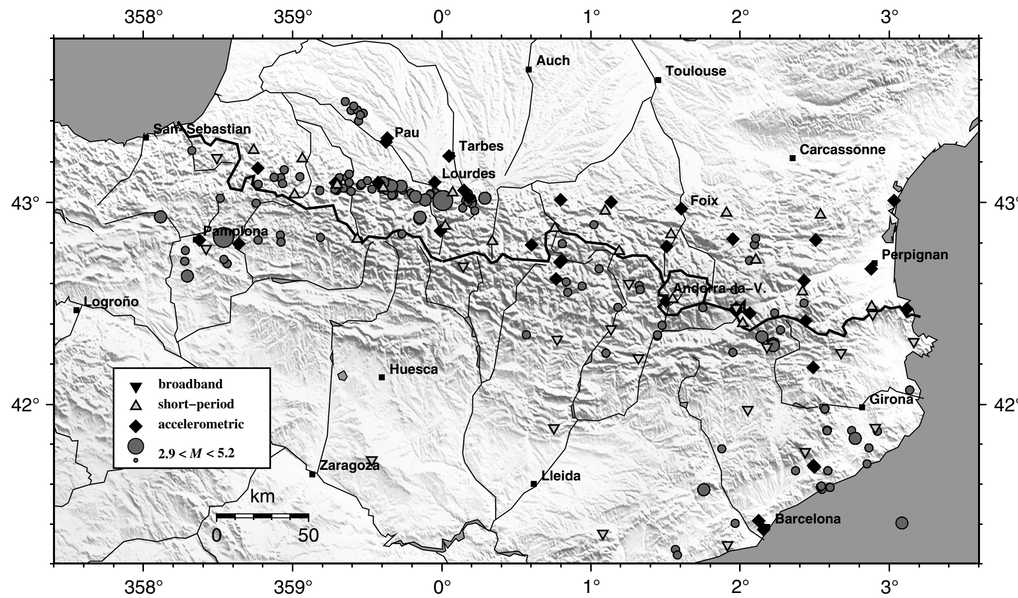

Figure 1. Location map of earthquakes and seismological stations. See inset for symbol explanation.

adopt the value $\alpha = 3/2$ expected from 3D diffusion theory in full-space. Although this is not shown in the paper, we did perform the data analysis with other choices of α. This affects only marginally the measurement of coda Q. As an example, in the case $\alpha = 2$, we found slightly higher values of Q_c (typically +10%), but the lapse-time dependence is intact.

Lapse-Time Dependence of Q_c at 6 Hz

In this paragraph, we consider data band-passed around a central frequency of 6 Hz. To characterize the lapse-time dependence of Q_c, we vary the position of the coda window with respect to the origin time of the earthquakes ($t_W \in [30–120]$ s) and/or the length of the coda window ($L_W \in [20–135]$ s). As the shape of the seismogram envelope is strongly affected by the source-station distance, we select local records with epicentral distances between 50 and 80 km. Figure 2 shows the values of Q_c at 6 Hz as a function of the window length (L_W) for two onset times of the coda ($t_W = 30$ s and $t_W = 50$ s). Note that twice the ballistic time of shear waves lies in the range 28–45 s, so that our choice of coda onset time is close to the classical $2t_S$ introduced by Aki and Chouet (1975). Figure 2 compiles all measurements along the pyrenean range and clearly displays an overall increase of Q_c with L_W, as previously reported in the literature. Some nuance must nevertheless be brought to this statement because the dependence of Q_c on L_W is strongly affected by the value of t_W. As shown in Figure 2, Q_c typically ranges from 450 to 800 for $L_W \in [30–130]$ s at $t_W = 30$ s, but Q_c is

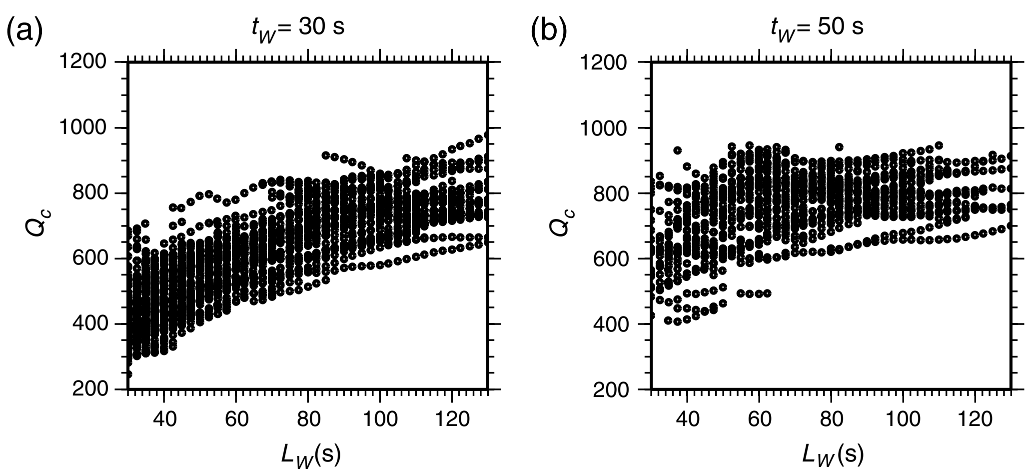

Figure 2. Q_c as a function of the length of the coda window L_W, measured at 6 Hz in the Pyrenees. Two examples of coda onset are shown: (a) $t_W = 30$ s and (b) $t_W = 50$ s after the origin time of the earthquake. Epicentral distances range between 50 and 80 km.

largely time independent at $t_W = 50$ s. Similarly, for sufficiently large L_W we observe that Q_c tends to a constant (800 ± 200), independent of t_W. We emphasize that the range of fluctuations of Q_c (± 200) is likely due to strong lateral variations of the attenuation in the Pyrenees and does not reflect the uncertainty of individual measurements, which is typically one order of magnitude lower.

To confirm these observations, estimates of Q_c as a function of epicentral distance are shown in Figure 3. The window length is fixed ($L_W = 30$ s), and three choices of coda onset t_W are explored: $t_W = 2t_S$, with t_S the ballistic time of shear waves in the crust, $t_W = 50$ s, and $t_W = 80$ s. For $t_W = 2t_S$, Q_c increases with epicentral distance ($r \in [10–180]$ km) and reaches the plateau value 800 ± 200 reported earlier, for r typically > 100 km (Fig. 3a). The opposite behavior is observed in Figure 3b for $t_W = 50$ s. In this case, the average value of Q_c is roughly constant at short epicentral distances and decreases rapidly for $r > 100$ km. It is also worth noting that there is a large scatter in the data points at short epicentral distance. This observation is consistent with the lapse-time dependence of Q_c shown in Figure 2. In particular, at epicentral distance $r > 150$ km, the ballistic time of the shear waves is $t_S > 43$ s. Because the coda onset is at $t_W = 50$ s, Q_c is estimated in the very early coda where the energy decay is faster, which explains the lower values of Q_c. When mapping lateral variations of Q_c, it is, therefore, crucial that the same range of epicentral distance and onset time t_W be adopted throughout the region of interest. Only a careful examination of the data can guide the choice of time windows and epicentral distances that allow for a robust estimate of Q_c. For sufficiently large t_W (80 s in Fig. 3c), Q_c is approximately constant (800 ± 200) throughout the range of epicentral distances we have explored. From the analysis of Figures 2 and 3, we conclude that Q_c does not increase indefinitely with lapse time in the Pyrenees but rather tends to a plateau the value of which depends on the local attenuation properties. The modeling of the transient regime and the convergence toward the plateau will be the main target of this work.

Frequency Dependence of Q_c

In this paragraph, we compare the lapse-time dependence of Q_c in three frequency bands: 2–4, 4–8, and 8–16 Hz, at fixed coda onset ($t_W = 30$ s). Figure 4 clearly illustrates the increase of Q_c with the length of the coda window up to $L_W \approx 80$ s in all frequency bands. After this transient regime, Q_c reaches a plateau that globally increases with frequency. The overall increase of the lapse-time dependence of Q_c from low to high frequencies is a key observation to constrain the form of heterogeneity in the Pyrenees, as will be demonstrated later in this paper. To facilitate the comparison

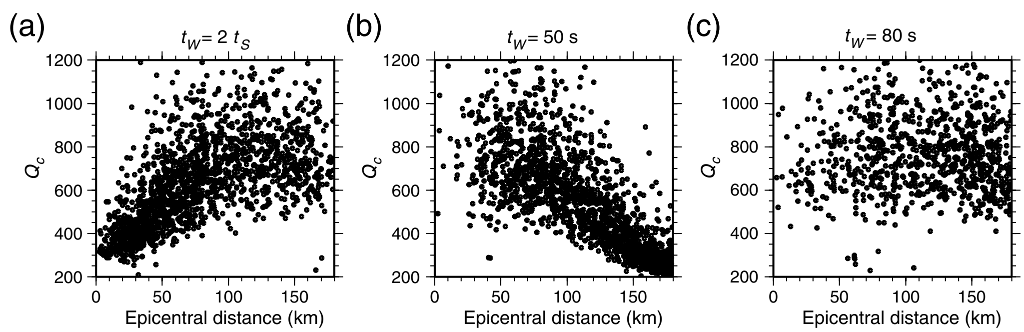

Figure 3. Q_c as a function of epicentral distance at 6 Hz in the Pyrenees for three choices of coda onset: (a) $t_W = 2t_s$, (b) $t_W = 50$ s, and (c) $t_W = 80$ s. The length of the coda window is fixed: $L_W = 30$ s.

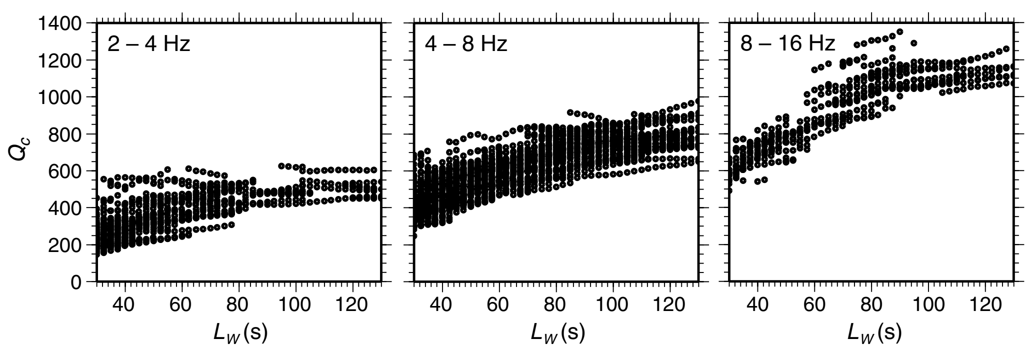

Figure 4. Lapse-time dependence of Q_c in three frequency bands as indicated in each panel. The coda starts at $t_W = 30$ s, and the epicentral distance ranges between 50 and 80 km.

with other studies, the measurements are summarized by a simple power law of the form $Q_c = Q_0 f^n$. At large L_W (typically $L_W \approx 120$ s), Q_c varies as $295(\pm 25) f^{0.55(\pm 0.015)}$, whereas at shorter L_W ($L_W \approx 35$ s), Q_c varies as $106(\pm 21) f^{0.75\pm 0.08}$. Although earlier studies reported on the frequency dependence of Q_c in the Pyrenees, a straightforward comparison is problematic because the choice of coda window varies from one author to the other (Gagnepain-Beyneix, 1987; Pujades *et al.*, 1990; Mitchell *et al.*, 2008). On the one hand, Gagnepain-Beyneix (1987) finds Q_0 and n in the range 30–140 and 0.7–1.1, respectively. These measurements are compatible with our results for short lapse time. On the other hand Mitchell *et al.* (2008) find Q_0 and n in the range 200–300 and 0.6–0.7, respectively. These measurements are consistent with our findings at large lapse time. The differences among the various studies published so far on the Pyrenees may presumably be ascribed to the choice of coda window. Indeed, Gagnepain-Beyneix (1987) analyzed data from nearby earthquakes ($r < 30$ km) using $t_W = 2t_S$ and a window length $L_W \in [20–50]$ s, which mostly samples the early coda. This is in sharp contrast with the work of Mitchell *et al.* (2008) who used earthquakes recorded at regional distances and analyzed the coda starting at a group velocity $u = 3.15$ km/s, with a time window of several hundreds of seconds. The systematic exploration of the relation between Q_c and L_W applied to our data set therefore reconciles the observations of Gagnepain-Beyneix (1987) and Mitchell *et al.* (2008). In Heterogeneity and Multiple-Scattering Models section, we present the physical model of wave scattering adopted in this study.

Heterogeneity and Multiple-Scattering Models

As outlined in the introduction, there are two key ingredients to model high-frequency seismic waves: (1) multiple scattering, which is responsible for the generation of coda waves and (2) anisotropic scattering, which is required to explain envelope broadening. Thus, the basic question addressed in this work is as follows: to what extent does multiple anisotropic scattering in a statistically homogeneous medium explain the lapse-time dependence of Q_c observed in the Pyrenees? This physical model is in sharp contrast with a single-scattering interpretation in depth-dependent attenuation structures. If anisotropic scattering has an impact on the lapse-time dependence of Q_c, however, its effect must be quantified to have access to the stratification of heterogeneity in the lithosphere. Our study represents a first effort in this direction. In what follows, we describe in detail the basic ingredients of our model.

In Earth's lithosphere, the fluctuations of velocity are conveniently encapsulated in the formula

$$V(\mathbf{x}) = c[1 + \xi(\mathbf{x})], \tag{4}$$

where c is the background velocity and $\xi(\mathbf{x})$ is a random function of position (Sato *et al.*, 2012). In this study, the mean velocity is fixed at $c = 3.5$ km/s which is a good approximation of the S-wave velocity in the pyrenean crust (Souriau and Granet, 1995). In multiple-scattering applications, random media are usually characterized by the autocorrelation function of the fluctuations defined as

$$R(\mathbf{x}, \mathbf{y}) = \langle \xi(\mathbf{x}) \xi(\mathbf{x} + \mathbf{y}) \rangle, \tag{5}$$

where the brackets denote an average over an ensemble of realization (Sato *et al.*, 2012). In this work we assume that the random medium is homogeneous and isotropic, which implies that the autocorrelation function depends on $r = |\mathbf{x} - \mathbf{y}|$ only. The magnitude of the fluctuations is quantified by the mean-squared velocity fluctuation $\epsilon^2 = R(0)$. A completely equivalent description of the random medium is provided by the heterogeneity power spectrum P, which is the Fourier transform of R. A large variety of power spectra relevant to geophysical applications has been proposed by Klimeš (2002). In this work, the usual Gaussian and Von-Karman power spectra will be adopted to represent the crustal heterogeneity. The Gaussian power spectrum is used to describe smooth random media where fluctuations all have a similar size a, also known as the correlation length. Von-Karman spectra are characterized by three parameters (a, ϵ^2, ν) and describe a large variety of random media where small-scale fluctuations are superposed on a smooth background. The roughness of the medium, that is, its content in short wavelength features, is controlled by the exponent $\nu > 0$, such that the power spectrum $P(k)$ decays like $k^{-2\nu-3}$ for $ka \gg 1$, with k the wavenumber. The most frequently encountered version of the Von-Karman spectrum is the exponential medium that corresponds to $\nu = 0.5$ (see Appendix). Media with $0 < \nu < 1$ are said to be rich in short wavelength. Note that ν may also be taken > 1.

The gross scattering properties of random media are encapsulated in two parameters: the mean free path l and the transport mean free path l^*. l is the characteristic length between two scattering events, and l^* is the propagation distance required for a wave to lose memory of its initial direction. The ratio l^*/l, called anisotropy factor hereafter, quantifies the amount of anisotropic scattering. A complete description of elastic-wave scattering should incorporate the polarization of the waves and mode conversions (Margerin *et al.*, 2000; Przybilla *et al.*, 2006; Sens-Schönfelder *et al.*, 2009). Mode conversions are particularly important to describe the coda of P waves and the convergence toward equipartition. A number of studies around the world have reported the rapid stabilization of energy ratios in the high-frequency coda, which is usually interpreted as a marker of equipartition (e.g., Hennino *et al.*, 2001; Margerin *et al.*, 2009; Yamamoto and Sato, 2010). A stabilization of the vertical-to-horizontal kinetic energy ratio was observed in the Pyrenees by Souriau *et al.* (2011) only a few seconds after the S-wave onset. This strongly supports the idea that coda waves in the Pyrenees are close to equipartition, thereby implying that the transport of seismic energy is dominated largely by shear waves. In addition, numerical Monte Carlo simulations generally suggest that the depolarization of shear waves is extremely rapid (Margerin *et al.*, 2000). As a consequence, it seems reasonable to model the coda of *S* waves within the acoustic approximation, which neglects polarization and mode conversions. This approximation greatly alleviates the numerical effort and allows the exploration of a large variety of random media.

The analytical expressions of l and l^* for scalar waves in Gaussian, exponential, and general Von-Karman media are given in the Appendix. In Figure 5, we have plotted l, l^*, and the anisotropy factor l^*/l as a function of the correlation length for two Von-Karman power spectra with $\nu = 0.5$ (Fig. 5a) and $\nu = 3.0$ (Fig. 5b). For the two power spectra shown in Figure 5, l decreases continuously with a (and ϵ^2). Interestingly, l^* goes through a minimum at a correlation length $a_{\min}$, which decreases as ν increases. From Figure 5 (and the results included in the Appendix), we find that l and l^* scale like $k^{-4}a^{-3}$ at low adimensional frequency ($ka \ll 1$). At large adimensional frequency ($ka \gg 1$), l, and l^* scale like $k^{-2}a^{-1}$ and a, respectively. The anisotropy factor l^*/l tends to 1 for $a \ll a_{\min}$ and increases like k^2a^2 at

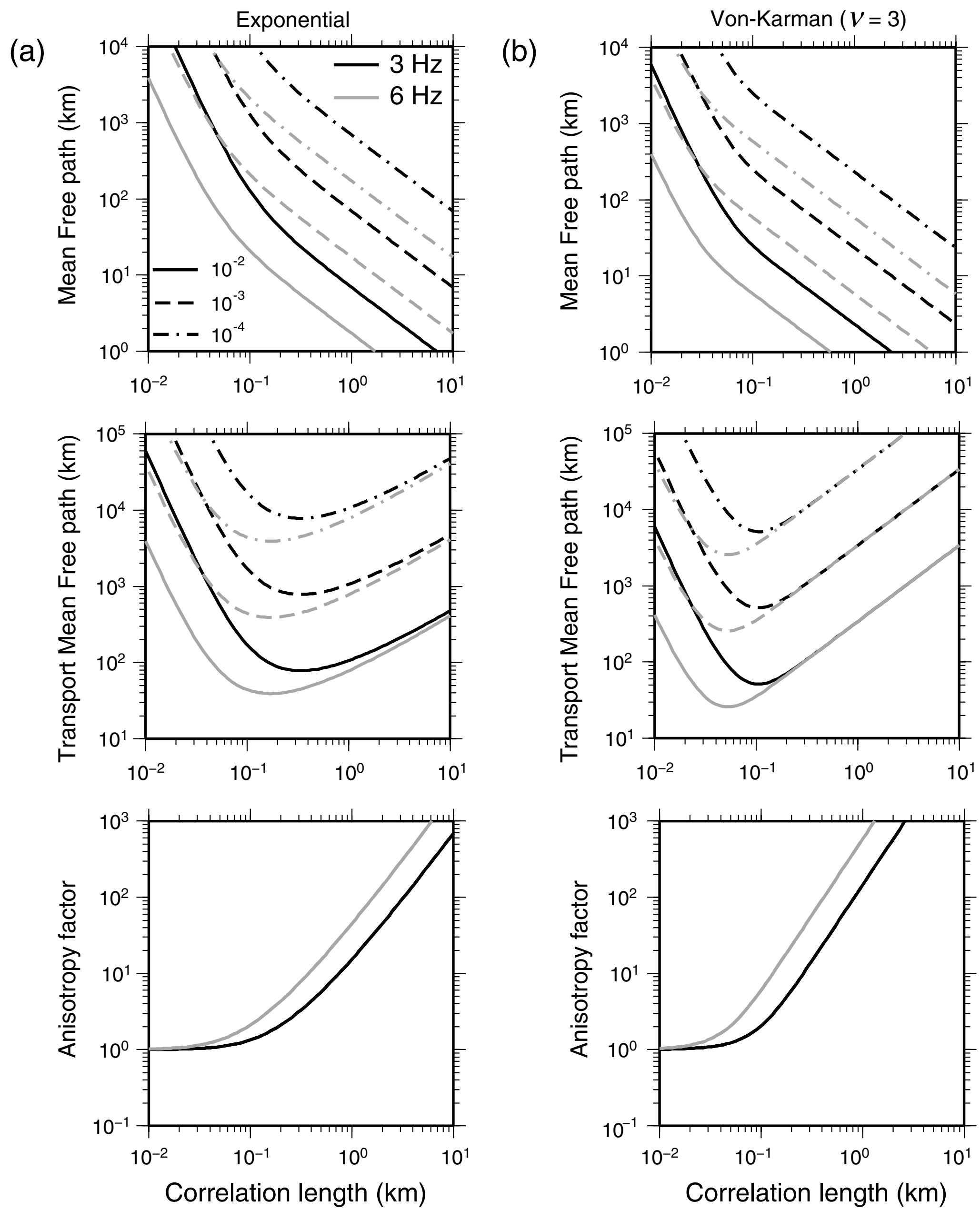

Figure 5. Mean free path (l), Transport mean free path (l^*), and anisotropy factor (l^*/l) as a function of the correlation length a at 3 Hz (black lines) and 6 Hz (gray lines) for (a) an exponential random medium and (b) a Von-Karman random medium with $\nu = 3$. Three values of ϵ^2 are represented: $\epsilon^2 = 10^{-2}$ (solid lines), $\epsilon^2 = 10^{-3}$ (dashed lines), and $\epsilon^2 = 10^{-4}$ (dot-dashed lines).

large correlation length. At fixed correlation length, l^*/l increases like $2\nu - 1$ ($ka \gg 1$). In the limit of weak perturbations, the power spectrum of the velocity fluctuations completely determines the scattering anisotropy, usually encapsulated in the differential scattering cross section:

$$\sigma(\theta) \sim P\left(2k \sin\frac{\theta}{2}\right), \qquad (6)$$

where θ is the angular deviation from the forward direction and P the power spectral density function of random inhomogeneity (Sato *et al.*, 2012). Equation (6) provides an important relation between the degree of smoothness (or roughness) of the medium and the excitation of scattered waves at large angles, particularly in the regime $ka > 1$. As an example, smooth Von-Karman media (large ν, poor in short-wavelength features) tend to favor scattering at small angles compared to rough Von-Karman media (small ν, rich in short-wavelength features). In what follows, ν will be termed the smoothness exponent of the Von-Karman medium.

Multiple anisotropic scattering is accurately modeled with the radiative transfer equation (Ryzhik *et al.*, 1996), which can be solved numerically with the aid of Monte Carlo simulations. In this paper, we employ a simplified version of the Monte Carlo code developed by Margerin *et al.* (2000). The main steps are summarized hereafter. A number of particles (typically 10^7) are launched isotropically from a point source. The distance between two collisions follows an exponential distribution with parameter l, and absorption is simply taken into account by decreasing the weight of each particle by a factor $e^{-2\pi f t/Q_i}$. At each scattering event, the direction of the particle is modified by selecting randomly two angles that statistically reproduce the angular anisotropy of the single-scattering process. This free propagation+scattering process is repeated until the travel time of the particle exceeds the time window of interest. The position of the particle is tracked during its random walk through the scattering medium to obtain the energy distribution as a function of time.

Numerical Results

In this section, we discuss the effects of scattering parameters (anisotropy factor and transport mean free path), heterogeneity power spectrum, and intrinsic absorption on the lapse-time dependence of Q_c at 6 Hz. A large number of coda envelopes (~1200) spanning a large set of random media was computed using the Monte Carlo method. Using the processing approach outlined in Observations, synthetic curves of Q_c versus lapse time were obtained and compared to the pyrenean data shown in Figures 2–4. Our goal is to find a scattering model that can explain the increase of Q_c as a function of lapse time as observed in the Pyrenees at 6 Hz: a monotonic increase of Q_c from $Q_c \approx 450$ at $L_W = 30$ s to $Q_c \approx 800$ at $L_W = 130$ s.

Isotropic Multiple-Scattering Models

Before delving into more complex models, it is interesting to demonstrate explicitly that isotropic multiple scattering is incompatible with the lapse-time dependence of Q_c observed in the Pyrenees. We recall that scattering is isotropic or more generally nonpreferential (equal amount of forward and backward scattered waves) when the wavelength is much larger than the correlation length. In that case, the transport mean free path l^* is equal to the mean free path l (see Fig. 5). In Figure 6, we show the variation of Q_c as a function of the window length L_W estimated both from data and synthetic envelopes for a coda onset at $t_W = 30$ s. To facilitate the comparison between data and models, we represent the average value of synthetic Q_c weighted by the observed distribution of epicentral distances in the range 50–80 km. In the simulations, the mean free path ranges from 100 to 1000 km, as suggested by previous scattering models

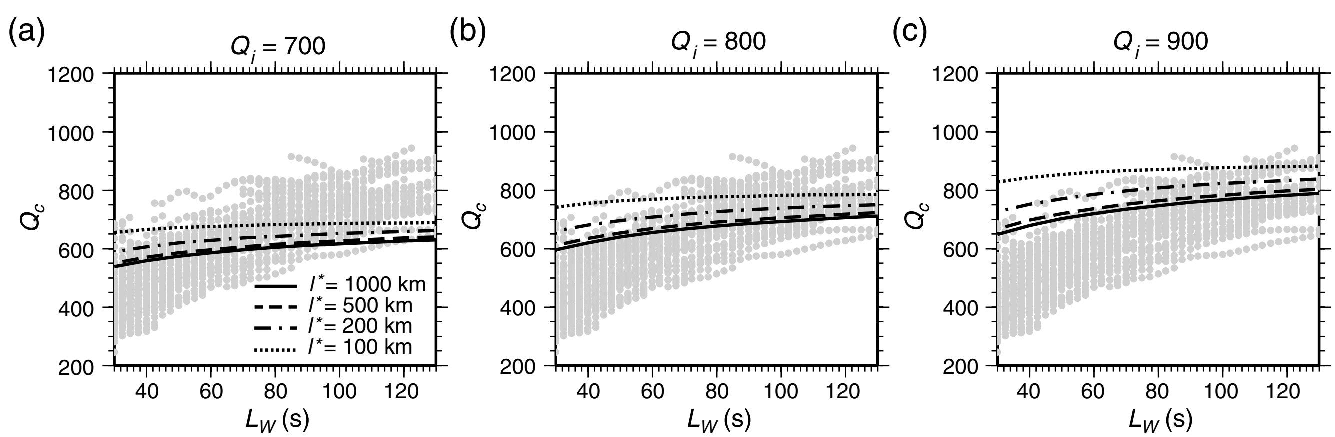

Figure 6. Lapse-time dependence of synthetic codas computed at 6 Hz in a series of isotropic multiple-scattering models with $l^* = 1000$ km (solid line), $l^* = 500$ km (dashed line), $l^* = 200$ km (dot-dashed line), and $l^* = 100$ km (dotted line). Three values of intrinsic quality factor are investigated: (a) $Q_i = 700$, (b) $Q_i = 800$, and (c) $Q_i = 900$. The numerical results (black lines) are superposed on the data (gray dots). The onset of the coda window is the same for synthetics and observations ($t_W = 30$ s).

of the Pyrenees (Sens-Schönfelder *et al.*, 2009). The values of intrinsic attenuation $Q_i = \{700, 800, 900\}$ are dictated by the plateau of Q_c at large L_W. Although the mean free path varies over one order of magnitude, it has little impact on the overall shape and amplitude of the lapse-time dependence of Q_c. Multiple isotropic scattering may explain at most 25% of the observed variation of Q_c, which motivates the introduction of anisotropic scattering models considered in the next paragraphs.

Anisotropic Multiple-Scattering Models

To illustrate the impact of anisotropic scattering, we consider the popular exponential random medium ($\nu = 0.5$) for three anisotropy factors $l^*/l = \{2, 5, 10\}$ and four values of the transport mean free path $l^* = \{100, 200, 500, 1000\}$ km. To match the value of Q_c observed in our data set at large window length L_W, we fix the intrinsic quality factor $Q_i = 800$. By using the same averaging procedure as described in the previous section, we compare in Figure 7 the coda quality factor Q_c in synthetics and observations (top panels). Figures 7a–c show that in an exponential medium, scattering anisotropy increases the lapse-time dependence of Q_c by a factor of roughly two compared to the isotropic case (Fig. 6b). The effect is more pronounced at short window length L_W but is rather insensitive to the value of the anisotropy factor l^*/l and of the transport mean free path l^*. Rather, the transport mean free path (together with the intrinsic attenuation Q_i) controls the overall amplitude of Q_c.

To illustrate the role of the heterogeneity power spectrum, we also consider a Von-Karman medium poor in short-wavelength features ($\nu = 5$) for the same set of anisotropy factors and transport mean free paths as above (Fig. 7, lower panels). As previously noted, the introduction of scattering anisotropy increases the lapse-time dependence of Q_c. In particular for $\nu = 5$, Q_c rises all the more rapidly at short window length as the anisotropy factor is large, and the effect is all the more pronounced as the transport mean free path is short. The two Von-Karman power spectra can hardly be distinguished for small anisotropy factors (Fig. 7a and d), but there are striking differences between the two at sufficiently large anisotropy factors. Comparison of panels c and f in Figure 7 shows that the transport mean free path has little effect on the lapse-time dependence of Q_c in an exponential medium, whereas the rise of Q_c at short time windows is all the more rapid as the transport mean free path l^* is short, in

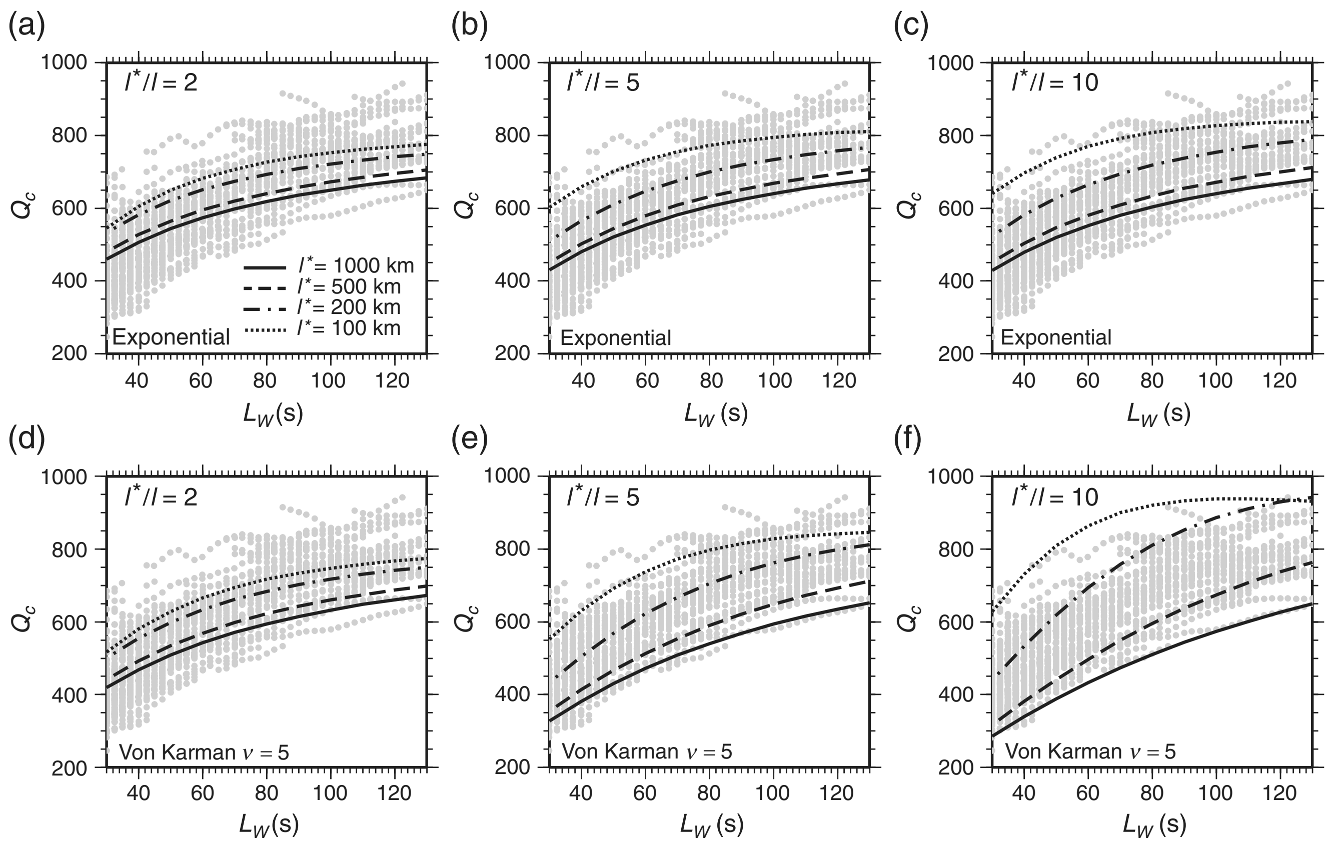

Figure 7. Lapse-time dependence of synthetic codas computed at 6 Hz in a series of anisotropic scattering models with $l^* = 1000$ km (solid line), $l^* = 500$ km (dashed line), $l^* = 200$ km (dot-dashed line), and $l^* = 100$ km (dotted line) for two heterogeneity power spectra: exponential (top) and Von-Karman with $\nu = 5$ (bottom). Three values of the anisotropy factor are investigated: (a, d) $l^*/l = 2$, (b, e) $l^*/l = 5$, and (c, f) $l^*/l = 10$. The intrinsic quality factor is fixed: $Q_i = 800$. The numerical results (black lines) are superposed on the data (gray dots). The onset of the coda window is the same for synthetics and observations ($t_W = 30$ s).

a Von-Karman medium poor in short wavelength ($\nu = 5$). Thus, Figure 7 reveals that in addition to the scattering parameters l and l^*, the medium roughness plays a crucial role in the lapse-time dependence of Q_c. The increase of Q_c observed in our data set—Q_c varies from 450 at $L_W =$ 30 s to 800 at $L_W = 130$ s—requires an anisotropy factor typically >5 and a smoothness exponent typically >1. Better estimates of the scattering properties of the pyrenean crust will be provided in the next section.

The impact of the medium smoothness on Q_c at large anisotropy factor ($l^*/l = 10$) is further examined in Figure 8 where four examples of power spectra (Gaussian and Von-Karman with $\nu = \{1, 3, 5\}$) are compared for the same set of transport mean free paths ($l^* = \{200, 500, 1000\}$ km) and an intrinsic quality factor $Q_i = 800$. The coda quality factor rises all the more rapidly at short window length as the smoothness exponent of the medium increases (compare panels from top to bottom in Fig. 8) and the effect is all the more visible as l^* decreases. Figure 8 also suggests that the transport mean free path and the roughness of the medium deduced from coda-wave observations will be to some extent correlated. Indeed, the lapse-time dependence of Q_c may equally well be fitted by smooth media ($\nu \in [3–5]$) with large transport mean free path ($l^* > 800$ km), or moderately rough media ($\nu \in [1–3]$) and smaller transport mean free path ($l^* < 500$ km).

We remark that in the case of smooth media (Fig. 8c,d), the quality factor seems to increase indefinitely with lapse time. When the calculations are performed at sufficiently large window length L_W, as in Figure 9, however, we find that the synthetic Q_c curve can present an overshoot before converging to a plateau determined by the intrinsic quality factor. The overshoot is all the more pronounced as the anisotropy factor l^*/l and the smoothness exponent ν are larger and is associated with a very rapid increase of Q_c at short lapse time ($L_W \in [30–80]$). We may exploit this theoretical prediction to put some loose constraints on the anisotropy factor and on the medium roughness. In particular, smooth media (e.g., Gaussian media) with large anisotropy factor are less likely to represent the heterogeneity of the pyrenean crust because they predict an increase of Q_c with lapse time usually faster than observed (Figs. 8 and 9).

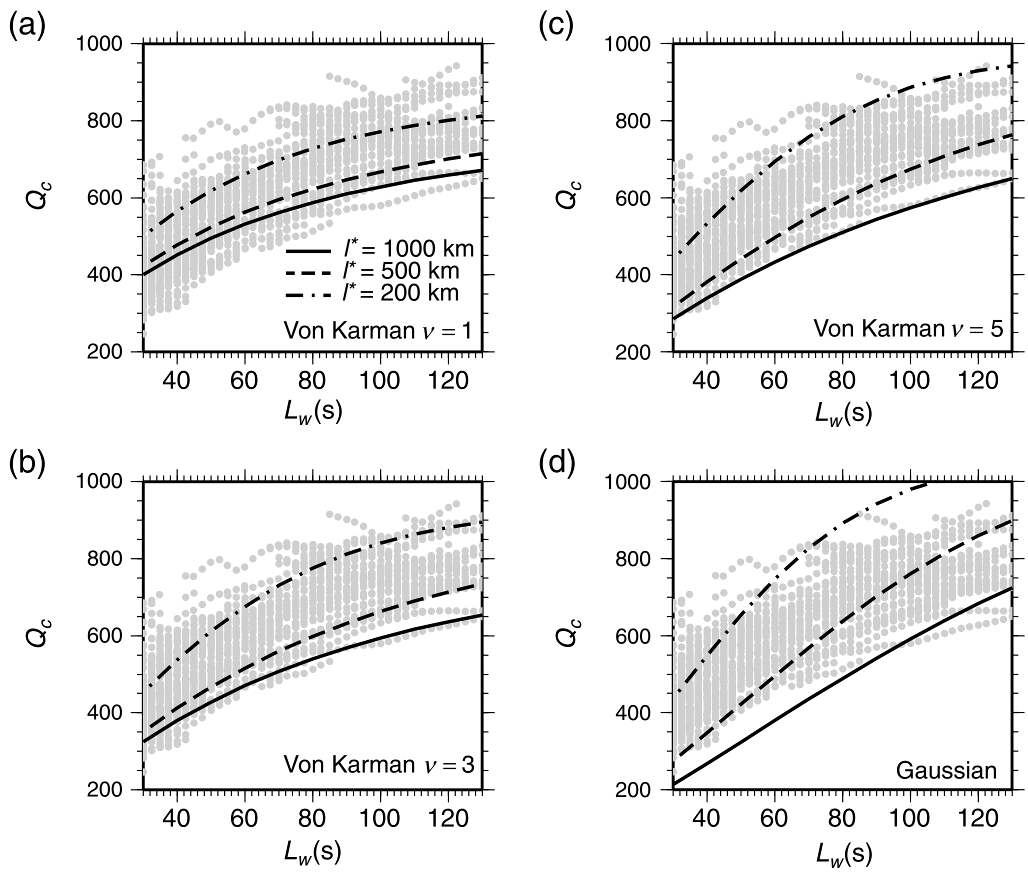

Figure 8. Effect of the roughness of the random medium on the lapse-time dependence of Q_c at 6 Hz. Four heterogeneity power spectra are investigated: Von-Karman with (a) $\nu = 1.0$, (b) $\nu = 3.0$, (c) $\nu = 5.0$, and (d) Gaussian power spectrum, for three values of the transport mean free path $l^* = 1000$ km (solid line), $l^* = 500$ km (dashed line), and $l^* = 200$ km (dot-dashed line). The anisotropy factor and the intrinsic quality factor are fixed: $l^*/l = 10$ and $Q_i = 800$. The numerical results (black lines) are superposed on the data (gray dots). The onset of the coda window is the same for synthetics and observations ($t_W = 30$ s).

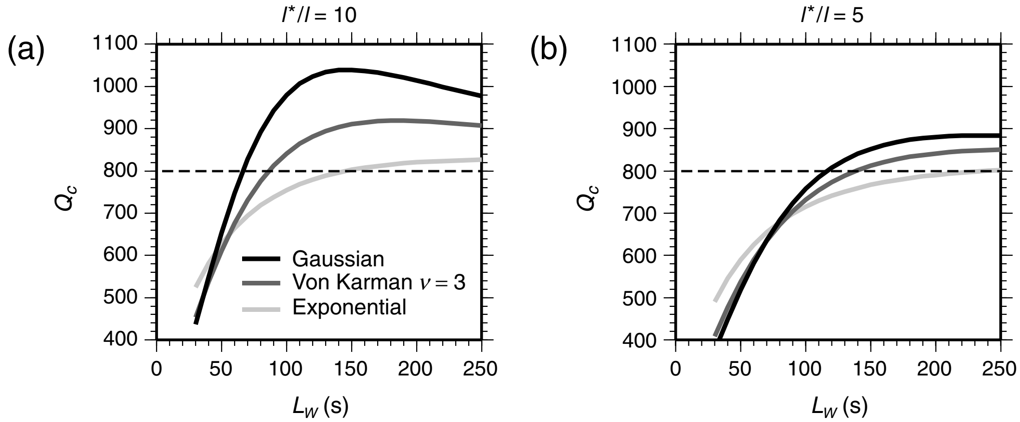

Figure 9. Illustration of the convergence of the coda quality factor Q_c toward the intrinsic quality factor $Q_i = 800$ at large lapse time for three anisotropic scattering models with anisotropy factors (a) $l^*/l = 10$ and (b) $l^*/l = 5$ and transport mean free path $l^* = 200$ km: gaussian medium (black line), Von-Karman medium with $\nu = 3$ (dark gray line), and exponential medium (light gray line). The coda starts at $t_W = 30$ s, and the length of the coda window L_W is indicated on the horizontal axis.

Figure 9 also shows that some care must be taken to infer Q_i from coda Q measurements with real data for which the observation window is necessarily finite due to either noise or recording conditions (e.g., triggered data). The effect of windowing is further studied in Figure 10 where we explore the lapse-time dependence of Q_c for three values of intrinsic attenuation: $Q_i = \{700, 800, 1000\}$. Figure 10 shows the results of the numerical experiments for four values of the transport mean free path $l^* = \{100, 200, 500, 1000\}$ km, an anisotropy factor $l^*/l = 5$, and two

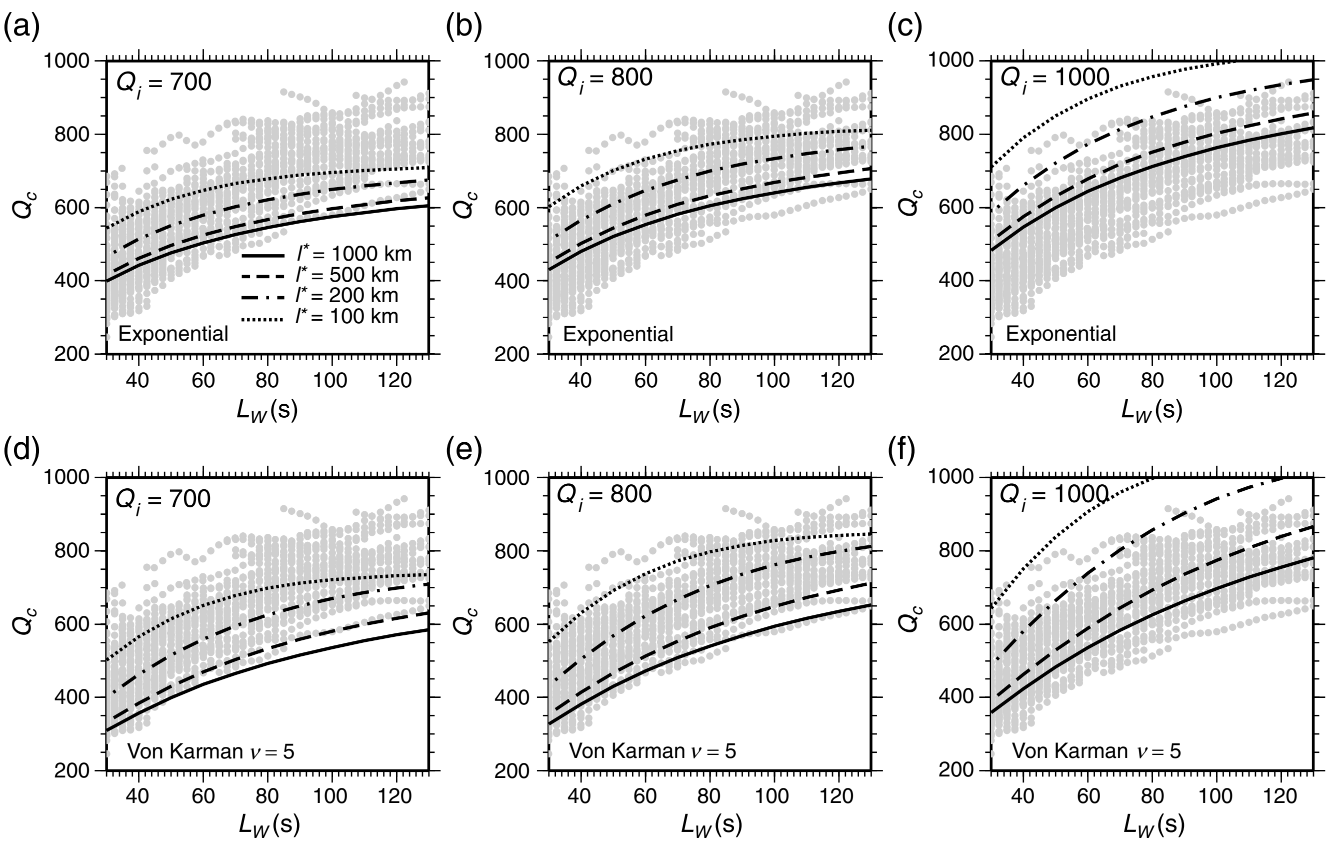

Figure 10. Effect of the intrinsic quality factor Q_i on the lapse-time dependence of Q_c at 6 Hz. Four values of the transport mean free path $l^* = 1000$ km (solid line), $l^* = 500$ km (dashed line), $l^* = 200$ km (dot-dashed line), and $l^* = 100$ km (dotted line) are represented in each panel for two heterogeneity power spectra with an anisotropy rate $l^*/l = 5$: exponential (top) and Von-Karman with $\nu = 5$ (bottom). The intrinsic quality factor increases from left to right: (a, d) $Q_i = 700$, (b, e) $Q_i = 800$, and (c, f) $Q_i = 1000$. The numerical results (black lines) are superposed on the data (gray dots). The onset of the coda window is the same for synthetics and observations ($t_W = 30$ s).

power spectra: exponential (top panels) and Von-Karman with $\nu = 5$ (bottom panels). As expected, the impact of the transport mean free path on the lapse-time dependence of Q_c is all the more visible as the intrinsic quality factor is large. As a consequence, the lapse-time dependence of Q_c increases with the intrinsic quality factor Q_i. This implies some correlation between the values of l^* and Q_i deduced from coda Q measurements at short time windows. In the Pyrenees, the data may equally be fitted by $\{Q_i = 1000, l^* > 500 \text{ km}\}$ or $\{Q_i = 700, l^* < 500 \text{ km}\}$, in the Von-Karman case with $\nu = 5$.

Although the main theme of this paper is the lapse-time dependence of Q_c, it is nevertheless interesting to make a short digression on the distance dependence of Q_c in connection with the estimation of the intrinsic quality factor Q_i. In Figure 11, we represent the variation of Q_c as a function of epicentral distance for three choices of time windows ($t_W = 2t_S$, $t_W = 50$ s, and $t_W = 80$ s). In numerical calculations, two transport mean free paths ($l^* = \{500, 1000\}$ km), two anisotropy factors ($l^*/l = \{2, 5\}$) and four intrinsic quality factors ($Q_i = \{700, 800, 900, 1000\}$) have been considered for two Von-Karman random media ($\nu = 0.5$ [top panels] and $\nu = 5$ [bottom panels]). The theoretical predictions are superposed upon the observations, shown in light gray. It is reassuring to see that the values of the transport mean free path and attenuation deduced from a rapid analysis of the lapse-time dependence of Q_c predict rather well the distance dependence of Q_c for the three choices of coda window. The role of the scattering anisotropy is more apparent in media poor in short wavelengths but is on the whole much less pronounced than in the lapse-time analysis. The curves representing Q_c as a function of epicentral distance all show a plateau for late coda samples. This corresponds to either large epicentral distance for the traditional coda window starting at $t_W = 2t_S$, or short epicentral distances for coda windows starting at fixed lapse time ($t_W = 50$,80 s). The numerical results confirm that the value of the plateau is close to the intrinsic quality factor Q_i. From the analysis of Figure 11, we conclude that the distance dependence of Q_c provides useful information on the plausible range of absorption in the crust but does not strongly constrain the power spectrum of the fluctuations.

On the Attenuation Properties of the Pyrenees

In Numerical Results section, we made a case that a large part if not all the lapse-time dependence of Q_c in the Pyrenees may be ascribed to anisotropic scattering without invoking any depth dependence of the attenuation properties. Following this idea, we combine Q_c measurements in different frequency bands to put some constraints on the nature of heterogeneities in the pyrenean crust. The main purpose is to develop a preliminary scattering model that captures the gross features of the lapse-time dependence of Q_c in the Pyrenees. Let us first recapitulate the principal conclusions that can be drawn from the confrontation of observations and numerical models at 6 Hz. The lapse-time dependence of Q_c requires (1) anisotropy factors of the order of five or larger, (2) smoothness exponent $\nu > 1$, (3) intrinsic quality factor of the order of 900 ± 300, and (4) transport mean free path >100 km. Considering the nonlinearity of the model and the number of parameters, we do not make any attempt to solve an inverse problem. Our modest goal is to show that the frequency dependence of Q_c may give some constraint on the roughness of the crust, that is to say, its content in short-wavelength features.

We adopt the following two-step approach. (1) We infer the frequency dependence of absorption properties by using the close correspondence between Q_i and the coda quality factor Q_c estimated from late coda windows, as put forward in the previous section. The frequency-dependent plateau of Q_c apparent in Figure 4 is parametrized in the form $Q_c = Q_0 f^n$. For the Pyrenees, the values of Q_0 and n deduced from a least-squares fit of the average value of Q_c are 300 and 0.6, respectively. Because Q_c tends to Q_i at large lapse time as illustrated in Figure 9, it appears reasonable to propose a frequency-dependent intrinsic quality factor of the form $Q_i = 300 f^{0.6}$. Because the standard deviation of the data is rather large (± 100), other parameterizations that fall within the uncertainty range are possible. As an example the frequency-dependent relation $Q_i = 400 f^{0.4}$ is equally acceptable and will also be implemented. (2) Assuming an anisotropy factor $l^*/l = 5$, we select a set of Von-Karman random media with $\nu = \{1, 3, 5\}$, which best fit the lapse-time dependence of Q_c at 6 Hz. Considering the different parameterizations of Q_i, three transport mean free paths $l^* = \{250, 500, 1000\}$ km may adequately explain the data. For each power spectrum ($\nu = 1$, 3, 5), we calculate the pair (a, ϵ), which corresponds to a given pair (l^*/l, l^*) at 6 Hz. This yields three different heterogeneity models for each value of ν as summarized in Table 1. From the knowledge of (a, ϵ, ν), we deduce the transport parameters (l, l^*) and the scattering pattern in the 2–4 and 8–16 Hz frequency bands. By numerically solving the radiative transfer equation for each heterogeneity model (a, ϵ, ν) given in Table 1, we theoretically predict the lapse-time dependence of Q_c in all frequency bands. Numerical results are confronted with observations in Figure 12.

In the 2–4 Hz frequency band, the three Von-Karman random media yield very similar predictions. This does not come as a surprise because, as shown in the previous section, Q_c is controlled essentially by the intrinsic quality factor and the transport mean free path for anisotropy factors typically <2 (see Table 1). The agreement with observations in the 2–4 Hz frequency band is worth noting and is consistent with the dominance of nonpreferential scattering around 3 Hz in the Pyrenees (Fig. 12a,d,g). Because the lapse-time dependence is weak, low-frequency Q_c measurements do not provide strong constraints on the medium roughness and on the transport mean free path. The comparison of Figure 12a, d,g and Figure 12c,f,i reveals that only high-frequency data may help discriminate the models presented in Table 1.

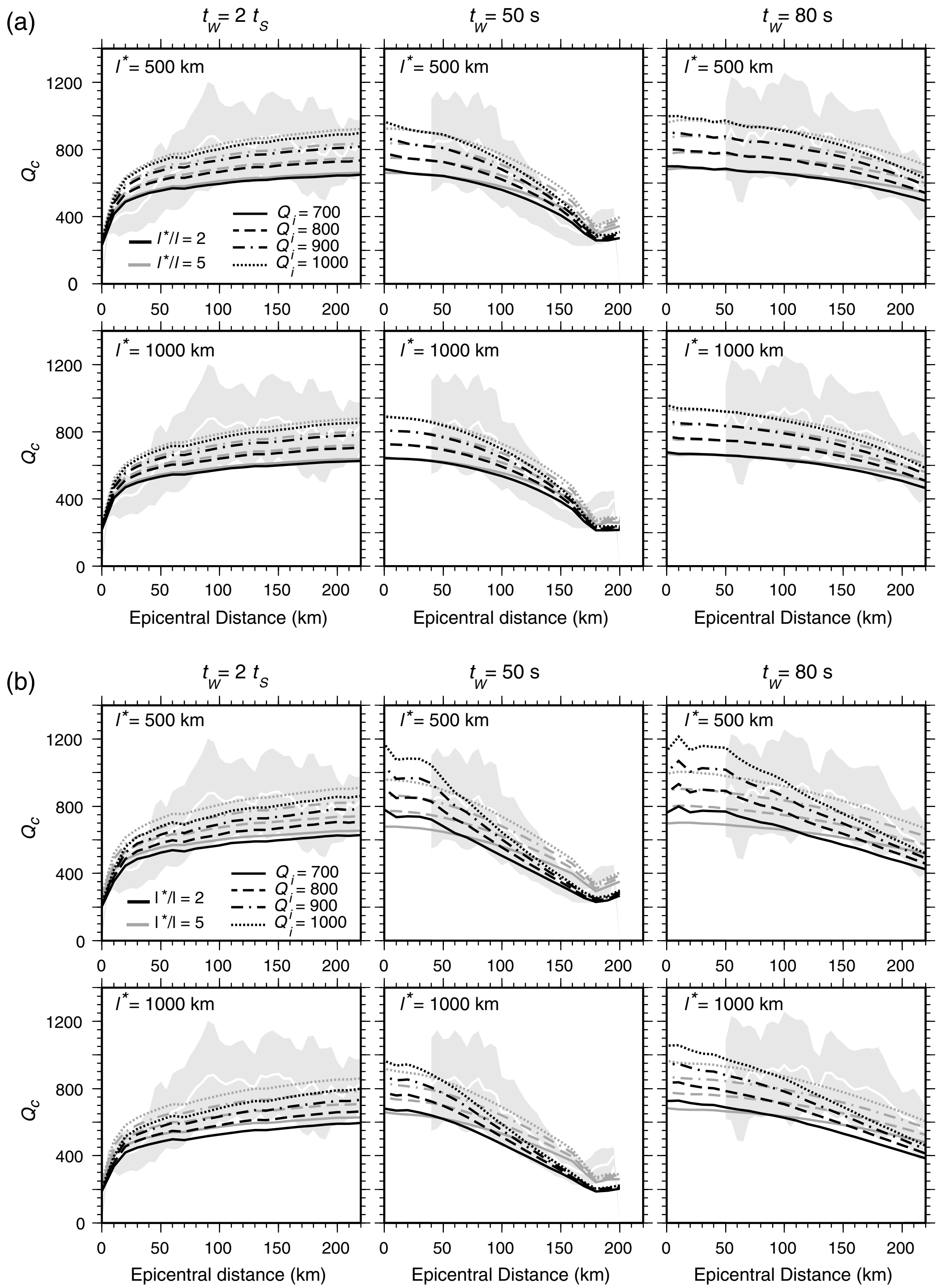

Figure 11. Q_c as a function of epicentral distance at 6 Hz for three choices of coda onset, $t_W = 2t_s$ (left), $t_W = 50$ s (middle), and $t_W = 80$ s (right). Two values of the transport mean free path $l^* = \{500, 1000\}$ km are represented for two heterogeneity power spectra: exponential (a) and Von-Karman with $\nu = 5$ (b). In each panel, two anisotropy factors, $l^*/l = 2$ (gray lines) and $l^*/l = 5$ (black lines), and four values of the intrinsic quality factor, $Q_i = 700$ (solid line), $Q_i = 800$ (dashed line), $Q_i = 900$ (dot-dashed line), and $Q_i = 1000$ (dotted line), are considered. The numerical results are superposed on the data (gray area). The coda window length is the same for synthetics and observations ($L_W = 30$ s).

Table 1
Statistical and Scattering Properties of the Random Media Investigated in the Section, "On the Attenuation Properties of the Pyrenees"

				l (km)			l^* (km)		
Power Spectrum	Model	a (m)	ϵ (%)	3 Hz	6 Hz	12 Hz	3 Hz	6 Hz	12 Hz
Von-Karman $\nu = 1.0$	Model 1	160	3.7	230	50	13	485	250	190
	Model 2	160	2.6	460	100	25	970	500	380
	Model 3	160	1.8	920	200	50	1930	1000	760
Von-Karman $\nu = 3.0$	**Model 1**	**90**	**3.5**	**230**	**50**	**13**	**420**	**250**	**235**
	Model 2	**90**	**2.5**	**450**	**100**	**25**	**830**	**500**	**470**
	Model 3	90	1.8	900	200	50	1650	1000	940
Von-Karman $\nu = 5.0$	Model 1	70	3.6	220	50	13	390	250	250
	Model 2	70	2.5	430	100	25	780	500	490
	Model 3	70	1.8	870	200	50	1560	1000	980

Independent of the medium roughness, the anisotropy factor increases while the transport mean free path decreases at high frequency, which in turn implies a stronger lapse-time dependence of Q_c, as observed in pyrenean data in the 8–16 Hz band. Comparison of panels c, f, and i in Figure 12 leads us to select preferred average models of heterogeneity for the pyrenean range, also indicated in boldface in Table 1. A Von-Karman medium with a smoothness exponent $\nu = 3$, a correlation length $a = 90$ m, root mean-squared velocity fluctuations $\epsilon \in [2.5\%–3.5\%]$, and intrinsic quality factor of the form $Q_i = 400 f^{0.4}$ agrees well with observations at all frequencies. Von Karman models with $\nu = 1$ (resp. $\nu = 5$) predict too weak (resp. strong) lapse-time dependence of Q_c in the [8,16] Hz frequency band. Our preferred models yield a transport mean path $l^* \in [420–830]$ km and an intrinsic quality factor $Q_i = 620$ at 3 Hz, in excellent agreement with previous estimates by Sens-Schönfelder *et al.* (2009) who obtained $Q_i = 623$ and $l^* = 761$ km from the analysis of Lg coda at 3 Hz. Sens-Schönfelder *et al.* (2009) assumed a model of heterogeneity of exponential type ($\nu = 0.5$), which differs from our estimate ($\nu = 3$). This is not a severe discrepancy as we have demonstrated that low-frequency data do not give constraints on the roughness of the crust.

Discussion

Single-Scattering Versus Multiple-Scattering Interpretations

Using data from the Pyrenees, we may provide one more demonstration of the necessity to introduce depth-dependent scattering properties to explain the observed lapse-time dependence of Q_c within the single-scattering approximation. Figure 13a displays the variation of Q_c with window length L_W (coda onset is fixed at $t_W = 30$ s), as predicted by the anisotropic single-scattering model of Sato (1982) using an exponential correlation function with a fixed anisotropy factor $l^*/l = 5$, the transport mean free path $l^* = \{100, 200, 500, 1000\}$ km, and an intrinsic quality factor $Q_i = 1000$. From the comparison between model and data at 6 Hz in Figure 13a, we infer that the transport mean free path should increase roughly from ~200 km at shallow depth to > 1000 km at large depth in a stratified model of heterogeneity. Such an increase has been reported many times in the literature (see e.g., Mukhopadhyay *et al.*, 2008; Rahimi *et al.*, 2010; Padhy *et al.*, 2011; Vieira Barros *et al.*, 2011, among recent publications) based on the single-scattering interpretation. The reader should keep in mind that single scattering is nothing but the first term of the multiple-scattering series that we calculate numerically in our Monte Carlo simulations. In Figure 13b, we compare in more details the single- and multiple-scattering results for two values of the transport mean free path $l^* = \{100, 1000\}$ km. It is apparent that even for $l^* = 1000$ km, the full numerical solution disagrees with the single-scattering approximation. This disagreement is all the more visible for shorter l^*. This means that the single-scattering approximation is limited to $l^* > 1000$ km. The comparison of Figure 13a and Figure 10c also reveals that the variation of the amplitude of Q_c with the transport mean free path is completely opposite in single- and multiple-scattering models. The difference between the lapse-time dependence of Q_c predicted by the two models is striking. In particular, without invoking any depth dependence of attenuation properties, multiple anisotropic scattering explains most of the observed variation of Q_c with the window length.

Our study highlights the fact that a signature of depth-dependent scattering and/or absorption properties may only be detected once the effect of scattering anisotropy and multiple scattering have been properly quantified. This conclusion should hold for the space and time scales involved in this study: lapse time typically of the order of 200 s and epicentral distances typically < 100 km, that is, for waves that propagate mostly within the crust. At larger temporal and spatial scales, lapse time and epicentral distance in the range 200–2000 s and 100–600 km, respectively, Rautian and Khalturin (1978) showed that the coda decay may be fitted piecewise by equation (1) with coda Q generally smaller at short lapse time than at large lapse time (see Roecker *et al.*,

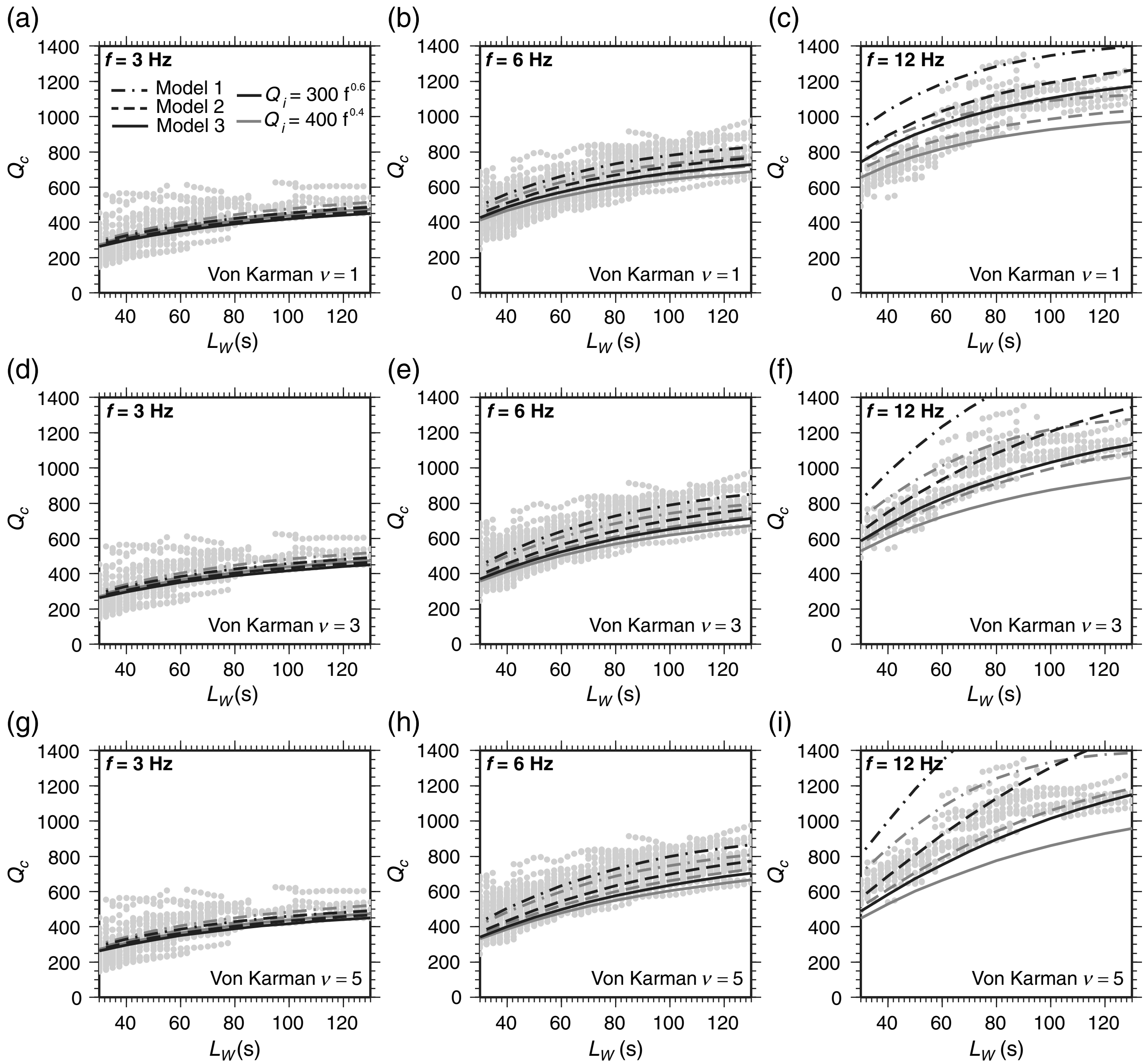

Figure 12. Lapse-time dependence of Q_c for synthetic codas computed at 3, 6, and 12 Hz. Three Von-Karman power spectra with $\nu = 1.0$ (a–c), $\nu = 3.0$ (d–f), and $\nu = 5.0$ (g–i) are considered. In each panel, three couples of statistical parameters (a, ϵ^2) given in Table 1 are investigated: Model 1 (dot-dashed lines), Model 2 (dashed lines), and Model 3 (solid lines). Two frequency-dependent intrinsic quality factors are explored: $Q_i = 300f^{0.6}$ (black lines) and $Q_i = 400f^{0.4}$ (gray lines). The numerical results (black and gray lines) are superposed on the data (gray dots). The onset of the coda window is the same for synthetics and observations ($t_W = 30$ s) in the three frequency bands.

1982; Gusev, 1995, for similar conclusions). Explaining such observations, which span a broad range of temporal and spatial scales, goes beyond the scope of our model and presumably points toward a drastic change of scattering properties at the transition between crust and mantle.

On the Scattering and Absorption Properties of the Pyrenees

As recently put forward by Carcolé and Sato (2010) based on a thorough study of coda attenuation in Japan, there exists a strong connection between intrinsic attenuation (Q_i) and the coda quality factor Q_c. In particular, in the multiple-scattering regime the simple relation, equation (3), applies at large lapse time in a statistically homogeneous half-space. A uniform depth distribution of seismic and scattering properties in the lithosphere may nevertheless be too restrictive an assumption. It has been argued by Korn (1990) and Margerin *et al.* (1998) that the lithosphere may be better represented by a heterogeneous crust overlying a transparent mantle in some regions. In this configuration, the leakage of diffuse waves

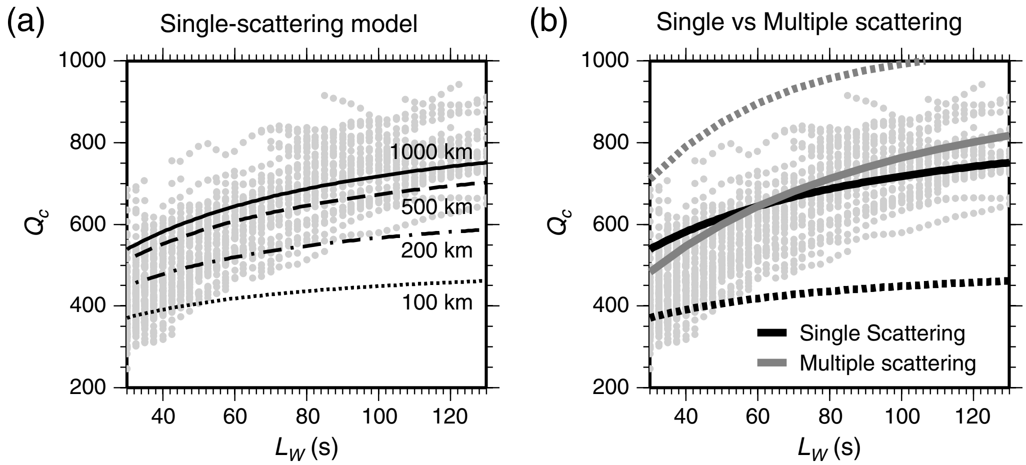

Figure 13. (a) Lapse-time dependence of synthetic codas computed at 6 Hz in four anisotropic single-scattering models. Four values of the transport mean free path, $l^* = \{100, 200, 500, 1000\}$ km, are considered for an exponential random medium with fixed anisotropy and intrinsic quality factor ($l^*/l = 5$, $Q_i = 1000$). (b) Comparison of the lapse-time dependence of Q_c in single-scattering and multiple-scattering models depicted by black and gray lines, respectively. Two values of the transport mean free path are considered, $l^* = 1000$ km (solid lines) and $l^* = 100$ km (dotted lines). The intrinsic absorption and the anisotropic factor are fixed: $Q_i = 1000$ and $l^*/l = 5$. In each panel, the numerical results (lines) are superposed on the data (gray dots). The onset of the coda window is the same for synthetics and observations ($t_W = 30$ s).

from crust to mantle entails an apparent attenuation quantified by a quality factor Q_{leak}. The ratio between the crustal thickness H and the transport mean free path controls the efficacy of leakage. Typically the effect is maximum for $l^*/H \sim 1$ and becomes negligible for $l^* \gg H$. Based on the numerical study of Margerin *et al.* (1999), we may approximate the leakage quality factor as $Q_{\text{leak}} \approx 1000f$, assuming a crustal thickness of the order of 40 km (Choukroune *et al.*, 1990) and a transport mean free path of the order of 600 km (Sens-Schönfelder *et al.*, 2009; this study). We may therefore conclude that the leakage effect is on the whole negligible in the Pyrenees. Note that in some anomalous regions, the transport mean free path may be much smaller, which may locally enhance the role of leakage (Sens-Schönfelder *et al.*, 2009).

From the observation of coda-wave attenuation, we propose a relation of the form $Q_i = Q_0 f^n$ with Q_0 of the order of 400 and n of the order of 0.4 to parametrize the intrinsic attenuation in the Pyrenees in the 2–16 Hz band. The frequency dependence of Q_i is relatively weak but still measurable. The exponent n deduced from our data set is in line with other studies based on the multiple lapse window analysis (Ugalde *et al.*, 1998; Vargas *et al.*, 2004; Carcolé and Sato, 2010, for example). At 3 Hz, the absorption length (of the order of 110 km) and the transport mean free path (~600 km) found in this study agree perfectly with the finding of Sens-Schönfelder *et al.* (2009) based on the analysis of Lg waves propagating through the range. The mean free path is of the order of 330 km, which suggests that absorption is slightly dominant over scattering in the Pyrenees. Lacombe *et al.* (2003) obtained similar estimates in central France from an analysis of Lg coda waves.

The crustal heterogeneity in the Pyrenees has been parameterized with a Von-Karman power spectrum, which models satisfactorily our observations with a correlation length $a = 100$ m and a smoothness exponent $\nu = 3$. These estimates should definitely not be taken at face value as they do not result from a genuine inversion process. It is worth noting that our model of crustal heterogeneity is in sharp contrast with the one proposed for northern Japan by Takahashi *et al.* (2009). From the analysis of envelope broadening with distance, these authors inferred a correlation length of 5 km and a smoothness exponent typically < 1. The difference may find its origin in (1) the different geological conditions, (2) the different type of data analyzed, (3) the physical model underlying data interpretation, and (4) the limited range of parameters explored in our study. Evaluating the role of each factor goes way beyond the scope of the present study. In the near future, we intend to analyze the broadening of seismogram envelopes with distance and frequency to put to the test our heterogeneity model and to revise it if necessary.

Conclusions

The principal message conveyed by this article is that most if not all the lapse-time dependence of Q_c observed in the Pyrenees may be explained by a simple anisotropic multiple-scattering model without invoking any depth dependence of attenuation properties. As anisotropic scattering is a prominent feature of high-frequency wave propagation in the Earth, its effect should be properly modeled to extract the depth-dependent attenuation structure from Q_c measurements at the local scale (epicentral distance < 100 km). An additional outcome of this study is the demonstration that the lapse-time dependence of Q_c contains information on the heterogeneity power spectrum of the crust. It may, therefore, be combined with other methods such as peak delay time analysis to develop precise models of heterogeneity.

The good coincidence between the intrinsic quality factor and the coda quality factor at large lapse time found in this work provides a simple technique to measure the absorption properties of the crust. In this respect the choice of coda window is crucial. Within a limited and fixed range of epicentral distance, we recommend plotting Q_c as a function of coda window length L_W for different choices of coda onset t_W to ensure visually that the estimate of Q_c is not hampered by transient phenomena occurring at short lapse time. Only the plateau value of Q_c can be considered as an approximation of Q_i. This procedure is particularly important when performing a regionalization of Q_c over a broad region. If different epicentral distance ranges and/or different coda windows are mixed, it may well happen that the lateral variations of Q_c deduced from observations are measurement artifacts.

The model of scattering and absorption of the Pyrenees obtained in this study is preliminary and subject to revision in several respects. In terms of numerical modeling, it would be necessary to include the coupling among P and S waves to properly model the coda envelopes at short lapse time. Although it probably plays a minor effect on the lapse-time dependence of Q_c, the reflection/refraction effects at the Moho should also be incorporated in a more realistic calculation. Concerning the interpretation of data, a more systematic exploration of the parameter space (in particular the correlation length and the smoothness exponent) should be conducted in future works to better delineate the robust features of our scattering model. As the average attenuation properties of the Pyrenees do not differ much from what is observed in the tectonically quiet central France, it appears that the interesting information on the pyrenean structure is contained in the lateral variations of Q_c observed in our data. Future works should focus on the mapping of attenuation properties along the range and their relation with the propagation anomalies detected by Chazalon *et al.* (1993) and Sens-Schönfelder *et al.* (2009).

Data and Resources

Accelerometer data are available at the Réseau Accélérométrique Permanent in Grenoble (France) on request, or at http://www-rap.obs.ujf-grenoble.fr (last accessed October 2012). Short-period data are available at the Réseau National de Surveillance Sismique in Strasbourg (France) at http://renass.u-strasbg.fr/ (last accessed October 2012). Figures have been drawn with the Generic Mapping Tool (Wessel and Smith, 1991).

Acknowledgments

The authors would like to thank the different organisms that operate seismological networks in the Pyrenees for making their data available in the framework of the Système d'Information Sismique des Pyrénées project: the Instituto Geografico Nacional (IGN), the Institut Geológic de Catalunya (IGC), the RAP program and the Réseau de Surveillance Sismique des Pyrénées (RSSP). This work was funded by the European Regional Development Fund (ERDF/FEDER), Programme Opérationnel de Coopération Territoriale France-Espagne-Andorre program.

References

Aki, K., and B. Chouet (1975). Origin of coda waves: Source attenuation and scattering effects, *J. Geophys. Res.* **80,** 3322–3342.

Carcolé, E., and H. Sato (2010). Spatial distribution of scattering loss and intrinsic absorption of short-period S waves in the lithosphere of Japan on the basis of the multiple lapse time window analysis of Hi-net data, *Geophys. J. Int.* **180,** 268–290.

Chazalon, A., M. Campillo, R. Gibson, and E. Carreno (1993). Crustal wave propagation anomaly across the Pyrenean range. Comparison between observations and numerical simulations, *Geophys. J. Int.* **115,** 829–838.

Choukroune, P., F. Roure, B. Pinet, and E. Team (1990). Main results of the ECORS Pyrenees profile, *Tectonophysics* **173,** 411–423.

Del Pezzo, E., R. Allota, and D. Patané (1990). Dependence of Q_c (coda Q) on coda duration time interval: Model or depth effect? *Bull. Seismol. Soc. Am.* **80,** 1028–1033.

Gagnepain-Beyneix, J. (1987). Evidence of spatial variations of attenuation in the western Pyrenean range, *Geophys. J. Roy. Astron. Soc.* **89,** 681–704.

Gusev, A. (1995). Vertical profile of turbidity and coda Q, *Geophys. J. Int.* **123,** 665–672.

Gusev, A., and I. Abubakirov (1987). Monte-Carlo simulation of record envelope of a near earthquake, *Phys. Earth Planet. In.* **49,** 30–36.

Gusev, A., and I. Abubakirov (1996). Simulated envelopes of non-isotropically scattered body waves as compared to observed ones: Another manifestation of fractal heterogeneity, *Geophys. J. Int.* **127,** 49–60.

Hennino, R., N. Trégourès, N. Shapiro, L. Margerin, M. Campillo, B. Van Tiggelen, and R. Weaver (2001). Observation of equipartition of seismic waves, *Phys. Rev. Lett.* **86,** 3447–3450.

Hoshiba, M. (1991). Simulation of multiple-scattered coda wave excitation based on the energy conservation law, *Phys. Earth Planet. Int.* **67,** 123–136.

Hoshiba, M. (1995). Estimation of nonisotropic scattering in western Japan using coda wave envelopes: Application of a multiple nonisotropic scattering model, *J. Geophys. Res.* **100,** 645–657.

Ibanez, J., E. Del Pezzo, F. De Miguel, M. Herraiz, G. Alguacil, and J. Morales (1990). Depth-dependent seismic attenuation in the Granada zone (southern spain), *Bull. Seismol. Soc. Am.* **80,** 1232–1244.

Klimeš, L. (2002). Correlation functions of random media, *Pure Appl. Geophys.* **159,** 1811–1831.

Korn, M. (1990). A modified energy flux model for lithospheric scattering of teleseismic body waves, *Geophys. J. Int.* **102,** 165–175.

Lacombe, C., M. Campillo, A. Paul, and L. Margerin (2003). Separation of intrinsic absorption and scattering attenuation from L_g coda decay in central France using acoustic radiative transfer theory, *Geophys. J. Int.* **154,** 417–425.

Larose, E., L. Margerin, B. Van Tiggelen, and M. Campillo (2004). Weak localization of seismic waves, *Phys. Rev. Lett.* **93,** 48501.

Margerin, L., M. Campillo, and B. Van Tiggelen (1998). Radiative transfer and diffusion of waves in a layered medium: New insight into coda Q, *Geophys. J. Int.* **134,** 596–612.

Margerin, L., M. Campillo, N. M. Shapiro, and B. V. Tiggelen (1999). Residence time of diffuse waves in the crust as a physical interpretation for coda Q. Application to seismograms recorded in Mexico, *Geophys. J. Int.* **138,** 343–352.

Margerin, L., M. Campillo, and B. Van Tiggelen (2000). Monte Carlo simulation of multiple scattering of elastic waves, *J. Geophys. Res.* **105,** 7873–7892.

Margerin, L., M. Campillo, B. Van Tiggelen, and R. Hennino (2009). Energy partition of seismic coda waves in layered media: Theory and application to Pinyon Flats Observatory, *Geophys. J. Int.* **177,** 571–585.

Mitchell, B. J., L. Cong, and G. Ekström (2008). A continent-wide map of 1-Hz *Lg* coda Q variation across Eurasia and its relation to lithospheric evolution, *J. Geophys. Res.* **113,** B04303, doi: 10.1029/2007JB005065.

Mukhopadhyay, S., J. Sharma, R. Massey, and J. Kayal (2008). Lapse-time dependence of coda Q in the source region of the 1999 Chamoli earthquake, *Bull. Seismol. Soc. Am.* **98,** 2080–2086.

Padhy, S., N. Subhadra, and J. Kayal (2011). Frequency-dependent attenuation of body and coda waves in the Andaman Sea basin, *Bull. Seismol. Soc. Am.* **101,** 109–125.

Przybilla, J., M. Korn, and U. Wegler (2006). Radiative transfer of elastic waves versus finite difference simulations in two-dimensional random media, *J. Geophys. Res.* **111,** B04305, doi: 10.1029/2005JB003952.

Pujades, L., J. Canas, J. Egozcue, M. Puigvi, J. Gallart, X. Lana, J. Pous, and A. Casas (1990). Coda-Q distribution in the Iberian Peninsula, *Geophys. J. Int.* **100,** 285–301.

Rahimi, H., K. Motaghi, S. Mukhopadhyay, and H. Hamzehloo (2010). Variation of coda wave attenuation in the Alborz region and central Iran, *Geophys. J. Int.* **181,** 1643–1654.

Rautian, T. G., and V. I. Khalturin (1978). The use of the coda for determination of the earthquake source spectrum, *Bull. Seismol. Soc. Am.* **68,** 923–948.

Roecker, S. W., B. Tucker, J. King, and D. Hatzfeld (1982). Estimates of *Q* in central Asia as a function of frequency and depth using the coda of locally recorded earthquakes, *Bull. Seismol. Soc. Am.* **72,** 129–149.

Ryzhik, L., G. Papanicolaou, and J. B. Keller (1996). Transport equations for elastic and other waves in random media, *Wave Motion* **24,** 327–370.

Saito, T., H. Sato, and M. Ohtake (2002). Envelope broadening of spherically outgoing waves in three-dimensional random media having power law spectra, *J. Geophys. Res.* **107,** 2089–2103.

Sato, H. (1982). Coda wave excitation due to nonisotropic scattering and nonspherical source radiation, *J. Geophys. Res.* **87,** 8665–8674.

Sato, H. (1989). Broadening of seismogram envelopes in the randomly inhomogeneous lithosphere based on the parabolic approximation: Southeastern Honshu, Japan, *J. Geophys. Res.* **94,** 17735.

Sato, H., M. C. Fehler, and T. Maeda (2012). *Seismic wave propagation and scattering in the heterogeneous Earth*, Second Ed., Springer, Berlin.

Sens-Schönfelder, C., L. Margerin, and M. Campillo (2009). Laterally heterogeneous scattering explains *Lg* blockage in the Pyrenees, *J. Geophys. Res.* **114,** B07309, doi: 10.1029/2008JB006107.

Shapiro, N. M., M. Campillo, L. Margerin, S. K. Singh, V. Kostoglodov, and J. Pacheco (2000). The energy partitioning and the diffusive character of the seismic coda, *Bull. Seismol. Soc. Am.* **90,** 655–665.

Souriau, A., and M. Granet (1995). A tomographic study of the lithosphere beneath the Pyrenees from local and teleseismic data, *J. Geophys. Res.* **100,** no. B9, 18117–18134, doi: 10.1029/95JB01053.

Souriau, A., E. Chaljub, C. Cornou, L. Margerin, M. Calvet, J. Maury, M. Wathelet, F. Grimaud, C. Ponsolles, C. Pequegnat, and P. Guegen (2011). Multimethod characterization of the French-pyrenean valley of Bagnères-de-Bigorre for seismic-hazard evaluation: Observations and models, *Bull. Seismol. Soc. Am.* **101,** 1912–1937.

Takahashi, T., H. Sato, T. Nishimura, and K. Obara (2009). Tomographic inversion of the peak delay times to reveal random velocity fluctuations in the lithosphere: Method and application to northeastern Japan, *Geophys. J. Int.* **178,** 1437–1455.

Tselentis, G. A. (1993). Depth-dependent seismic attenuation in western Greece, *Tectonophysics* **225,** 523–528.

Ugalde, A., L. Pujades, J. Canas, and A. Villasenor (1998). Estimation of the intrinsic absorption and scattering attenuation in northeastern Venezuela (southeastern Caribbean) using coda waves, *Pure Appl. Geophys.* **153,** 685–702.

Vargas, C., A. Ugalde, L. Pujades, and J. Canas (2004). Spatial variation of coda wave attenuation in northwestern Colombia, *Geophys. J. Int.* **158,** 609–624.

Vieira Barros, L., M. Assumpção, R. Quintero, and V. Ferreira (2011). Coda wave attenuation in the Parecis basin, Amazon craton, Brazil: Sensitivity to basement depth, *J. Seismol.* **15,** no. 2, 391–409.

Wessel, P., and W. H. F. Smith (1991). Free software helps map and display data, *Eos Trans. AGU* **72,** 441.

Woodgold, C. (1994). Coda *Q* in the Charlevoix, Quebec, region: Lapse-time dependence and spatial and temporal comparisons, *Bull. Seismol. Soc. Am.* **84,** 1123–1131.

Yamamoto, M., and H. Sato (2010). Multiple scattering and mode conversion revealed by an active seismic experiment at Asama volcano, Japan, *J. Geophys. Res.* **115,** B07304, doi: 10.1029/2009JB007109.

Appendix

Scattering and Transport Mean Free Path for Gaussian, Exponential, and Von-Karman Random Media

In this appendix, we summarize basic facts about the most popular models of heterogeneity in seismological applications. The power spectral density function of Gaussian, exponential, and Von-Karman random media are defined as

$$P_G(k) = (2\pi)^{3/2} a^3 \epsilon^2 \exp(-k^2 a^2/2), \tag{A1}$$

$$P_E(k) = \frac{8\pi a^3 \epsilon^2}{(1 + k^2 a^2)^2}, \tag{A2}$$

and

$$P_{VK}(k) = \frac{8\pi^{3/2} \epsilon^2 a^3 \Gamma(\nu + 3/2)}{\Gamma(\nu)(1 + k^2 a^2)^{\nu+3/2}}, \tag{A3}$$

where k is the wave number, ϵ^2 is the total variance of the squared slowness fluctuations, a is the correlation length, and Γ denotes the gamma function (Sato *et al.*, 2012). The corresponding scattering and transport mean free paths are readily evaluated using the definitions given by Sato *et al.* (2012):

$$l_G = \frac{4}{k^2 a \epsilon^2 \sqrt{2\pi}[1 - \exp(-2k^2 a^2)]}, \tag{A4}$$

$$l_G^* = \frac{2^{3/2} a}{\epsilon^2 \sqrt{\pi}[1 - (1 + 2k^2 a^2)\exp(-2k^2 a^2)]}, \tag{A5}$$

$$l_E = \frac{1 + 4k^2 a^2}{2k^4 a^3 \epsilon^2}, \tag{A6}$$

$$l_E^* = \frac{4a}{\epsilon^2[\ln(1+4k^2a^2) + 1/(1+4k^2a^2) - 1]}, \qquad (A7)$$

$$l_{VK} = \frac{(1+2\nu)\Gamma(\nu)}{\epsilon^2\sqrt{\pi}k^2a\Gamma(\nu+3/2)[1-(1+4k^2a^2)^{-\nu-1/2}]}, \qquad (A8)$$

and

$$l_{VK}^* = \frac{(4\nu^2-1)\Gamma(\nu)a}{\epsilon^2\sqrt{\pi}\Gamma(\nu+3/2)[1-(2\nu-1)k^2a^2(1+4k^2a^2)^{-\nu-\frac{1}{2}}-(1+4k^2a^2)^{-\nu+\frac{1}{2}}]}, \qquad (A9)$$

where $k = \omega/c$, with ω the circular frequency and c the S-wave velocity.

IRAP, Institut de Recherche en Astrophysique et Planétologie
CNRS, Université de Toulouse
Observatoire Midi-Pyrénées
14 avenue Edouard Belin
31400 Toulouse, France
Marie.Calvet@irap.omp.eu

Manuscript received 23 July 2012

Spatial variations of seismic attenuation in the Pyrenees: coda Q and peak delay time analysis

Marie Calvet[(a)*] , Matthieu Sylvander [(a)], Ludovic Margerin [(a)], Antonio Villaseñor [(b)]

[(a)] IRAP, CNRS , Université de Toulouse

Observatoire Midi-Pyrénées, 14 avenue Edouard Belin, F-31400 Toulouse, France

[(b)] Institute of Earth Sciences Jaume Almera,

ICTJA-CSIC, Lluis Sole i Sabaris s/n, 08028 Barcelona, Spain

* Corresponding author : Marie.Calvet@irap.omp.eu (Phone: +33 561333014)

Abstract

Lateral variations of seismic attenuation in the Pyrenees are explored from the analysis of local earthquakes records. Scattering loss and intrinsic absorption both control the propagation of short period S waves through the crust. The role of intrinsic and scattering attenuation is analyzed in two steps. Firstly, the coda quality factor Q, which quantifies the energy decay of coda waves, is estimated at large lapse time in five frequency bands and interpreted as intrinsic absorption. Next, we systematically measure the peak delay time defined as the time lag from the direct S-wave onset to the maximum amplitude arrival. This parameter quantifies the strength of multiple forward scattering due to random inhomogeneities along the seismic ray path. Comparison of coda-Q and peak delay time measurements allows a qualitative interpretation of the origin of seismic attenuation (scattering/absorption) in the Pyrenean crust.

At low frequency, coda-Q variations mainly depend on the tectonic units of the Pyrenees, with stronger absorption in sedimentary basins, and smaller absorption in Paleozoic basements. At high frequency, coda-Q is low at the location of Neogene structures in the Eastern Pyrenees. A more enigmatic low-Q anomaly is also observed at the location of the Maladeta Massif in the Central Pyrenees. In all frequency bands, peak delay time measurements systematically show stronger scattering in the Western Pyrenees.

In the Labourd-Mauléon area, absorption and scattering are both important at low frequency. The Western Pyrenees also correspond to a high-velocity/density anomaly revealed from tomography and gravity data analysis. This suggests that the high level of inhomogeneities and absorption may be related to intrusion of mantle and/or sub-crustal

materials. In the Eastern Pyrenees, absorption appears dominant over scattering at high frequency. We hypothesize that thermal effects induced by crustal thinning may explain the strong absorption observed in this area.

Keywords: Seismic Attenuation, Coda waves, Wave Scattering, Crustal Structure, Pyrenees

1 Introduction

In complement to seismic velocity measurements, attenuation provides valuable informations about the structure of the Earth. It is also an important parameter for the quantitative evaluation of earthquake ground motion. Three mechanisms can be invoked to explain seismic wave attenuation: (1) anelastic absorption which mainly depends on temperature, melt or fluid content, and chemical composition, (2) scattering of seismic waves generated by small-scale velocity fluctuations and (3) focusing due to propagation in 3-D structures. The separation of these different effects is still a significant challenge but various methods have been proposed to estimate the relative contribution of anelasticity and scattering to the seismic attenuation in the Earth lithosphere (see Sato et al., 2012, for a review).

Substantial regional variations in the attenuation of high-frequency seismic waves have been documented in several studies (see Romanowicz & Mitchell, 2007, for a review). Few studies have explored the seismic attenuation in the French lithosphere (e.g. Campillo et al., 1985; Campillo & Plantet, 1991; Chevrot & Cansi, 1996; Lacombe et al., 2003), but some of them have detected differences between distinct tectonic units. For example, attenuation at 1 Hz may be stronger in the Alps than in the Pyrenees (Drouet et al., 2008, 2010). In Spain, Pujades et al. (1990) and Payo et al. (1990) have shown that seismic attenuation at 1 Hz may be higher in the Pyrenees than in Galicia or in the Ebro Basin. But only a few studies specifically concern the Pyrenees. These studies either focus on a specific area (Gagnepain-Beyneix, 1987; Correig et al., 1990) or propose an estimation of the seismic attenuation for the entire Pyrenean range (Drouet et al., 2005;

Calvet & Margerin, 2013). However, there is some evidence of strong lateral variations of both seismic absorption and scattering properties in the Pyrenees, as illustrated by the L_g blockage phenomenon observed in the western part of the range (Chazalon et al., 1993; Sens-Schönfelder et al., 2009).

Because of easy applicability, many determinations of seismic attenuation have involved so far the use of coda waves of local earthquakes. Coda Q measurements (noted Q_c hereafter) was extensively used in seismology for lithospheric or crustal attenuation studies (Aki & Chouet, 1975; Mitchell, 1995; Sato et al., 2012). However Q_c depends simultaneously on the scattering and anelastic properties of the crust. By using the MLTWA method developed by Fehler et al. (1992), Carcolé & Sato (2010) have recently obtained high resolution maps of scattering and intrinsic attenuation for Japan. They also demonstrated that the spatial variations of intrinsic absorption and Q_c are highly correlated. In complement to coda Q measurements, analyses of high-frequency seismic envelopes have been used to discuss the relative contribution of intrinsic absorption and scattering loss to the total seismic attenuation (Sato, 1989; Obara & Sato, 1995; Saito et al., 2002; Petukhin & Gusev, 2003; Saito et al., 2005; Takahashi et al., 2007). Multiple scattering due to random velocity inhomogeneities in the crust increases the apparent duration of the S-wave pulse. On the contrary, intrinsic absorption truncates it. The seismic wave envelop results from a competition between scattering and absorption (Saito et al., 2005).

In this study, we propose to explore more systematically the regional variations of Q_c and pulse broadening in order to discuss the origin (scattering and/or absorption) of the lateral variations of seismic attenuation in the Pyrenees. To characterize the spatial variations of attenuation in the Pyrenees, we take advantage from a dense seismic network. Several Institutes in France and Spain operate about 70 permanent seismic stations in the Pyrenees, and two temporary experiments have been conducted since 2010 on both sides of the mountain range. The paper is organized as follows. First, we summarize the main tectonic and seismological structures of the Pyrenees (section 2). Then, we present our data set in section 3. Coda-Q and pulse broadening measurements are discussed in section 4 and 5, respectively. The origin of the observed spatial variations of both observables is discussed in section 6. Conclusions are given in section 7.

2 Structure of the Pyrenees

2.1 Seismotectonic settings

The Pyrenees are an asymmetrical, double-wedge continental belt about 400 km long and 150 km wide which exhibits a North-South structure described by three main tectonic units: the Paleozoic Axial Zone (PAZ), the North Pyrenean Zone (NPZ) and the South Pyrenean Zone (SPZ) (Choukroune, 1992). These principal units are shown in Figure 1. The North Pyrenean Fault (NPF) is the major tectonic feature in the Pyrenees. It is observed at the surface in the central and eastern parts of the range. The NPF is also characterized by metamorphic rocks and lherzolite outcrops (Lagabrielle & Bodinier, 2008). Other important fault systems are the Adour fault with a NW-SE orientation in the Central Pyrenees, and the Têt and Tech faults in Eastern Pyrenees. Intricate fault systems related to the Western Mediterranean opening are observed at the southeast end of the Pyrenees and in the Catalan Coastal Ranges. The PAZ is largely inherited from

Hercynian structures and includes several granitic massifs such as the Maladeta Massif. It also includes the highest summits. The NPF marks the boundary between the PAZ and the NPZ. The NPZ corresponds to the former Eurasian margin thinned during the Cretaceous extension phase. It is mainly composed of highly deformed Mezosoic flysh deposits. It also includes large Paleozoic outcrops such as the North Pyrenean Massifs in the central part of the range (noted NPM in Figure 1) and the Basque Massifs to the west. To the north, the NPZ sediments override the Aquitaine Basin along the North Pyrenean Frontal Thrust. To the south, the South Pyrenean zone (SPZ) is composed of Mesozoic and Cenozoic sediments which overthrust the molasse of the Ebro Basin.

The Pyrenees have been affected by several successive orogens. From 120 to 80 Ma, the Pyrenean domain and the Hercynian structures experienced an extension episode related to the opening of the Bay of Biscay with the rotation of the Iberian plate. During this episode, the crust was thinned and affected by dense lower crust and upper mantle intrusions in the western and central part of the Pyrenees. Two competing plate-kinematic models have been proposed to describe the rotation of Iberia with respect to Europe: a scissor-type opening model (Srivastava et al., 2000; Rosenbaum et al., 2002) or a left-lateral strike-slip opening model (Le Pichon & Sibuet, 1971; Jammes et al., 2009). Recently, Vissers & Meijer (2012) have proposed a third geodynamical scenario consistent with both seafloor magnetic anomaly data and geological observations: during the progressive opening of the Bay of Biscay, the mantle lithosphere subducted and became gravitationnally unstable leading to asthenospheric upwelling with magmatism and metamorphism. The second stage for the formation of the Pyrenees is the North-South collision of the Eurasian and Iberian plates about 65 Ma ago, with less shortening in the Western Pyrenees than in the Central Pyrenees (Vergés et al., 2002). The Eastern Pyrenees also experienced Neogene extension during the rotation of the Corsica-Sardinia block. Neogene to Quaternary volcanism has affected the Catalan Coastal Ranges and the south-eastern Pyrenees in the Olot region (Martí et al., 1992).

The seismic activity of the Pyrenees is known from historical catalogues as well as from instrumental seismological studies. The present-day seismicity in the Pyrenees is moderate with an average of one event per year with a magnitude greater than 4 (Souriau & Pauchet, 1998; Rigo et al., 2005; Ruiz et al., 2006). The geographical distribution of Pyrenean earthquakes is very inhomogeneous. To the west, a diffuse activity is observed in the southern part of the range around Pamplona. In the Central Pyrenees, the seismicity is mostly in the North Pyrenean Zone but without any clear evidence of relashionship with the surface location of the NPF (Souriau et al., 2001; Rigo et al., 2005). The seismicity becomes much more diffuse in the eastern part of the Pyrenees with a clear southward shift of the seismicity. The current tectonic regime in the Pyrenees still remains uncertain (Souriau et al., 2001; Nocquet & Calais, 2004; Rigo et al., 2005) even if most of the recent significant earthquakes exhibit East-West extensional fault plane solutions more particularly in the Central Pyrenees (Chevrot et al., 2011).

2.2 Seismic structure of the Pyrenean crust

Crustal structures in the Pyrenees have been widely explored using seismic and gravity data. Geophysical studies based on refraction and ECORS deep penetration seismic profiles (Choukroune et al., 1990) show a large Moho jump along the NPF. The crust is much thicker on the Iberian side (50-55 km) than on the French side (28-30 km). From refraction profiles, there is some evidence that the crust south of the NPF has a 50 km maximal thickness beneath the centre of the range, and is progressively thinned to 23 km to the East (Gallart et al., 1981; Mauffret et al., 2001) and to 40 km to the West (Gallart et al., 1980, 2001). The lower crust in the western part of the NPZ displays much higher P wave velocity than in the PAZ likely due to mantle intrusions into the lower crust (Daignieres et al., 1981).

The crustal seismic tomography by Souriau & Granet (1995) has revealed two high-velocity bodies (both for P waves and S waves) in the Central and Western parts of the North Pyrenean Zone (Figure 2a). These two fast seismic anomalies also correspond to high density bodies (Casas et al., 1997; Vacher & Souriau, 2001; Jammes et al., 2010) as suggested by positive Bouguer anomalies (Figure 2c). Such gravity anomalies could be related to lower crust or mantle material uplifted through the upper crust during the extension episode preceding the collision (Vacher & Souriau, 2001; Jammes et al., 2009, 2010). In Figure 2b, we also show the mean crustal V_P/V_S ratio computed at several seismic monitoring stations from Wadati diagrams. We observe that Paleozoic materials are characterized by rather low V_P/V_S ratios whereas the Mauléon Basin, Pamplona Basin and the SPZ (in Central Pyrenees) exibit larger V_P/V_S values. In contrast, the seismic attenuation structure of the Pyrenean crust is relatively poorly known. Recently, Sens-Schönfelder et al. (2009) and Calvet & Margerin (2013) have shown that absorption may be slightly dominant over scattering at low frequency with probably some lateral variations. In particular, scattering and absorption may be significantly stronger in the Western Pyrenees than in the surrounding regions (Sens-Schönfelder et al., 2009).

3 Data Selection

In this study, we analyse velocity waveform data recorded by permanent and temporary seismic networks in the Pyrenees. We collect around 10000 waveform data recorded at 117 stations from 741 earthquakes which occured between 2001 and 2011, with a local magnitude (M_L) larger than 2.0. Focal depths vary between 1 km and 20 km. Location of epicenters, local magnitude and origin time of earthquakes have been determined by the Réseau de Surveillance Sismique des Pyrénées (RSSP). Our dataset mainly contains short period velocimetric waveforms from RSSP (20 stations). We also include accelerometric data from RAP (Réseau Accélérométrique Permanent - 23 stations) and IGC (Institut Geològic de Catalunya - 13 stations), and broadband velocimetric data from IGC (14 stations) and IGN (Instituto Geogràfico Nacional - 8 stations). These data have been collected in the framework of the european project SISPYR (http://www.sispyr.eu). We also selected a few broadband records from the PYROPE (http://w3.dtp.obs-mip.fr/RSSP/PYROPE/) and IBERARRAY (http://iberarray.ictja.csic.es) experiments which have been deployed in the Pyrenees at the end of 2010. Most of the short period velocimetric and accelerometric data are recorded by triggered systems whereas broadband stations record continuously. Locations of epicenters and stations are reported on Figure 3. Epicentral distances range from 1 km to 400 km.

4 Coda Q observations

4.1 Definition of coda Q

Aki & Chouet (1975) have observed that the energy envelop of seismic coda waves decays as:

$$E(t,f) = S(f)t^{-\alpha}e^{-2\pi ft/Q_c(f)} \tag{1}$$

where E is the power spectral density, $S(f)$ is a frequency-dependent source and/or site term, t is the lapse time, f is the frequency, α is a positive exponent, and Q_c is the frequency-dependent quality factor of coda waves. It is well documented that independent estimates of Q_c and α cannot be achieved from data only. Therefore, the value of α must be fixed a priori, but the impact on the estimated Q_c value is typically less than 20% (Aki & Chouet, 1975). The value of α and the interpretation of the coda quality factor Q_c depend on the physical model used to describe coda waves. A single-scattering interpretation of the seismic coda in a homogeneous half-space is compatible with Eq.(1) for an exponent α equal to 2. In that case, the coda quality factor Q_c depends simultanueously on the scattering and absorption as follows (Sato et al., 2012):

$$Q_c^{-1} = Q_{sc}^{-1} + Q_i^{-1} \tag{2}$$

where Q_{sc} and Q_i are the scattering and intrinsic absorption quality factor, respectively. However, the observation of seismic wave equipartition puts forward the role of multiple scattering in the generation of coda waves (Hennino et al., 2001). For example, in the Central Pyrenees, Souriau et al. (2011) have demonstrated that the equipartition regime may be reached only a few seconds after the S-wave onset. Within the multiple scattering interpretation of coda waves, the physical meaning of Q_c is radically different. After a few mean free times, multiple-scattered waves reach a diffusion regime which implies that

$$Q_c = Q_i \tag{3}$$

in a uniform half-space (Sato et al., 2012). In the present study, we adopt a multiple scattering interpretation of Q_c with $\alpha = 3/2$ in Eq. (1) (Paasschens, 1997).

4.2 Q_c measurements methodology

Prior to estimating the power spectral density $E(t, f)$ at lapse time t in the coda, we deconvolve the waveform from the station response and accelerometer records are integrated to get the vertical component of velocity. For Q_c measurements, only events with a local magnitude greater than 2.5 are processed. Using a bandpass Butterworth filter of order 4, data are filtered in five frequency bands: 1 - 2 Hz, 2 - 4 Hz, 4 - 8 Hz, 8 - 16 Hz, 16 - 32 Hz. In each frequency band, we smooth the squared vertical traces with a moving window whose typical duration is of the order of 16 cycles. The smoothed envelopes are thus corrected for the algebraic terms $t^{-3/2}$. In each frequency band, an estimate of Q_c is obtained from a least-square linear fit of $E(t, f)t^{3/2}$ as a function of t in a coda window of duration L_W starting at a lapse time t_W. The values of Q_c are accepted when the signal-to-noise ratio is greater than 4 and the correlation coefficient of the linear regression is greater than 0.7.

4.3 Lapse-time and frequency dependence of Q_c

In Figure 4, we represent all estimates of Q_c in the frequency band 4 - 8 Hz as a function of epicentral distance. The coda window length is fixed at $L_W = 30$ s and three possible choices of coda onset t_W are explored: (a) $t_W = 2t_s$ -commonly adopted in the seismological literature- where t_s is the ballistic time of S wave in the crust, (b) $t_W = 50$ s after the origin time of the earthquakes, and (c) $t_W = 80$ s. The purpose of this plot is to identify the range of epicentral distances and lapse time which allow stable measurement of Q_c. For $t_W = 2t_s$, Q_c increases with epicentral distance ($R \leq 100$ km) and reaches a plateau value $\sim 800 \pm 250$ at large epicentral distances ($R > 100$ km). For $t_W = 50$ s, Q_c is almost independent of distance for $R \leq 100$ km, with an amplitude close to 800, and decreases rapidly at larger epicentral distances. At sufficiently large t_W (80 s, Figure 4c), Q_c is stable (800 ± 250) throughout the epicentral distance range we have explored.

The choice of coda window is thus crucial to map the lateral variations of seismic attenuation. If different coda windows are mixed (early and late coda window), it may happen that the lateral variations of Q_c are measurement artifacts. For a selected range of epicentral distances, we must fix the coda onset t_W and the coda window length L_W, to facilitate the physical interpretation of Q_c. In particular, we must be sure that its estimate is not hampered by the transient regime occurring at short lapse time (Calvet & Margerin, 2013). However the number of signals which allow measurements at sufficiently large lapse time is limited by the length of the triggered seismic records and by the noise level. The best compromise is to measure Q_c for epicentral distances smaller than 90 km and for a 30 s coda window starting 50 s after the origin time of the earthquakes. This range of parameters corresponds to the plateau apparent in Figure 4. Our choice of coda window allows good spatial coverage of the Pyrenees and ensures that Q_c provides a reliable estimate of the absorption quality factor Q_i (see Figure 4b). As discussed by Calvet & Margerin (2013), absorption is to be understood as the combined effect of anelasticity and leakage (Margerin et al., 1999), the latter being negligible except in locally strongly scattering area. The range of fluctuations of Q_c (± 250) around the plateau value (~ 800 in the frequency band 4-8Hz) is typically one order of magnitude larger than the uncertainty of individual measurements. We can thus confidently propose that the fluctuations are due to strong variations of absorption properties along the Pyrenean range.

Adopting the selection criteria discussed above, the total numbers of Q_c measurements in the five frequency bands are: 2190 (1 - 2 Hz), 2260 (2 - 4 Hz), 2296 (4 - 8 Hz), 2293 (8 - 16 Hz), 2035 (16 - 32 Hz). These measurements can be summarized by a simple power law of the form $Q_0 f^n$ where Q_0 is the value of Q_c at 1 Hz and n is an exponent which accounts for the frequency dependence. A simple fit yields $Q_0 = 220(\pm 84)$ and $n = 0.64 \pm 0.15$ for the Pyrenees. Previous studies have also reported a frequency dependence of Q_c in the Pyrenees. In the Western Pyrenees, on the western end of the Axial Zone, Gagnepain-Beyneix (1987) finds Q_0 and n in the range $[30 - 140]$ and $[0.7 - 1.1]$, respectively. In the Eastern Pyrenees, close to Andorra, Correig et al. (1990) obtain $Q_0 \sim 14$ and $n \sim 1.13$, indicating stronger attenuation at 1 Hz in the Western Pyrenees. These two studies focused on the analysis of nearby earthquakes (epicentral distances smaller than 40-30 km) using a coda window starting at $t_W = 2\,t_s$ which mostly samples the early coda. This choice of coda window may largely underestimate Q_c-values (see Figure 4a) and cannot be easily interpreted in terms of absorption. On the contrary, our results are close to those of Mitchell et al. (2008) ($Q_0 \in [200 - 300]$ and $n \in [0.6 - 0.7]$) obtained at large lapse time.

4.4 Spatial distribution of Q_c in the Pyrenees

4.4.1 Mapping Methodology

Usually, the classical quality factor regionalization approach adopted with coda waves considers that the sensitivity is distributed within ellipsoidal shells whose size increases with the lapse time in the coda (e.g. Mitchell, 1995; Vargas et al., 2004; Mitchell et al., 2008). Recent progresses in the modeling of seismic coda waves challenges this view. In particular, in the multiple scattering regime, the coda wave sensitivity strongly depends on the type of perturbation (elastic or anelastic), and is not distributed within an ellipsoid. In diffusive propagation model, it has been verified that the coda waveform sensitivity to slowness or scattering perturbation is larger at the locations of the source and the station (Pacheco & Snieder, 2005; Rossetto et al., 2011). The sensitivity kernels of coda wave intensity to local variations of absorption still have to be derived, but we expect similar spatial sensitivity. Consequently, we adopt a very simple Q_c regionalization approach which consists of assigning Q_c values to ray paths between stations and hypocentres. As the sensitivity of coda waves may be stronger near the station and the source, we should select Q_c measurements for rather small epicentral distances. We tested various epicentral distance ranges, but to preserve good spatial coverage in Q_c maps, we decided to select all the data for epicentral distance smaller than 90 km.

For simplicity, we only consider 2D lateral variations of Q_c . Seismic ray paths are calculated considering that the S-wave velocity is homogeneous (about 3.5 km.s^{-1}). The depth distribution of hypocentres, indicates that most of the ray paths are located in the first 20 kms of the crust. We divide the Pyrenean crust into rectangular $0.1° \times 0.1°$ blocks. As many ray paths propagate through one block and each ray path indicates a different value of Q_c, we propose to allocate the mean values of Q_c to each block. Only blocks crossed by more than 2 ray paths are retrieved. Finally, for each block, we take an average of the mean value over the nearest nine blocks to smooth the spatial variations.

4.4.2 Main characteristics of the Q_c maps

Figure 5 shows the spatial distribution of Q_c and the ray path density in the five frequency bands. The spatial coverage of the Pyrenees is rather good, more particularly in areas characterized by a strong density of seismic stations and earthquakes. Strong absorption (small Q_c values) is indicated in red colors whereas low absorption (large Q_c values) is indicated in blue colors.

At low-frequency, we observe a rather good correlation between attenuation structures and the main tectonic units of the Pyrenees described by Choukroune (1992). In the 1-2 Hz map, Precambrian and Paleozoic basements in the Eastern (from NPF to the Catalan Coastal Range) and the Central Pyrenees (between the North Pyrenean Thrust and the southern limit of the PAZ) are characterized by smaller attenuation (larger Q_c values) than the South Pyrenean Zone, the Mauléon, Pau and Pamplona Basins. However, the Paleozoic Basque Massifs exhibit stronger attenuation than other Paleozoic structures of the Pyrenees. Q_c maps also reveal a North-South low-Q_c anomaly at the longitude of the Hercynian Maladeta Massifs (longitude 1.5°) which crosses the Pyrenees from the

Aquitaine Basin to the Ebro Basin. On average, similar Q_c structures are observed in the 2-4 Hz map, except for the Mauléon Basin where attenuation becomes smaller than in the sediments of Pamplona and Pau Basins. In conclusion, our low-frequency Q_c maps are characterized by rather strong absorption in the Western Pyrenees and small absorption in the Eastern Pyrenees with in average stronger absorption in sedimentary structures than in Paleozoic materials.

At high frequency (> 4 Hz), the Q_c pattern in the Pyrenees change drastically and cannot be easily related to the principal tectonic units. The most striking feature is the low-Q_c anomaly clearly delimited by the Neogene structures (Olot and La Selva volcanic areas) in the Eastern Pyrenees. We also observe that the North-South low-Q_c anomaly already detected at low frequency spreads from the Maladeta Massif to the Adour Fault. Surprisingly, the sediments in Aquitain and Ebro Basins as well as the Hercynian massifs of the Paleozoic Axial Zone in the Eastern Pyrenees exhibit similar seismic absorption. In the Westernmost Pyrenees, the strong attenuation anomaly is now limited to the Basque Massifs. We will discuss all these features in section 6.

5 Peak delay time observations

5.1 Definition of the peak delay time

In randomly heterogeneous media, an impulsive seismic wave radiated from the source broadens as its travel distance increases. The broadening of energy envelopes with epicentral distance is a clear manifestation of multiple forward scattering in Earth's lithosphere (Sato, 1989; Saito et al., 2002). The strength of multiple scattering due to random heterogeneities along the seismic ray path can be quantified by the peak delay time (noted T_{pd} hereafter) defined as the time lag from the S-wave onset to the maximum of the amplitude. Peak delay time measurements have been mainly used to characterize the scattering properties of the Japanese lithosphere (Obara & Sato, 1995; Saito et al., 2005; Takahashi et al., 2007, 2009) or in the Kamchatka region (Petukhin & Gusev, 2003). In comparison, the scattering properties of the French crust are really poorly known (Lacombe et al., 2003; Sens-Schönfelder et al., 2009; Calvet & Margerin, 2013). In this study, we propose a first attempt at measuring and mapping the peak delay time T_{pd} in the Pyrenees.

5.2 T_{pd} measurements

We select data from permanent stations for earthquakes with a local magnitude greater than 2.0. We consider records with hypocentral distances smaller than 80 km in order to focus on crustal phases only. The waveforms are first deconvolved from the recording system response. Seismograms are filtered in four frequency bands (2 - 4 Hz, 4 - 8 Hz, 8 - 16 Hz, 16 - 32 Hz) in forward and backward directions to avoid any phase delay caused by using the fourth-order bandpass Butherworth filter. Next, we compute the root mean square of the sum of the two horizontal velocity components. The envelopes are smoothed with a moving time window whose typical duration is twice the central period of each frequency band. We only used waveform data which show a clear S-wave onset (quantified by the picking weight). S-wave onsets have been collected from local seismicity catalogues and are the same for each frequency band. T_{pd} is measured in seconds in a 40 s time window starting from the S-wave onset. We obtained 5157 T_{pd} measurements in each frequency band.

5.3 Hypocentral distance and frequency dependence of T_{pd}

Figure 6 shows T_{pd} as a function of the hypocentral distance R in the four frequency bands. Typically, at 80 km epicentral distance, the peak delay time can reach 4 s. Large values of T_{pd}, while absorption is also important (see previous section), reveal that scattering is rather strong in the Pyrenean crust. Although data are widely scattered, we observed that $\log_{10}(T_{pd})$ increases almost linearly with the logarithm of the hypocentral distance. The general features of T_{pd} variations with hypocentral distance have been previously investigated by using a Markov approximation of the parabolic wave equation (Sato, 1989; Saito et al., 2002). At fixed frequency, it can be shown that $\log_{10}(T_{pd})$ varies linearly with the logarithm of the hypocentral distance depending on the heterogeneity power spectrum of the random medium and on intrinsic absorption (Saito et al., 2002). Black solid lines in Figure 6 show the linear regression of $\log_{10}(T_{pd})$ against hypocentral distance $\log_{10}(R\ )$:

$$\log_{10} T_{pd}(f) = A_r(f) + B_r(f) \log_{10} R \tag{4}$$

The regression coefficients A_r and B_r are given in Table 1. The comparison of the linear regression coefficients in the frequency band 4-32 Hz reveals that T_{pd} slightly increases with frequency (at fixed hypocentral distance). Saito et al. (2002) have verified that envelope broadening strongly increases with frequency as the content of the random media in short-wavelength increases. Our measurements thus suggest that the Pyrenean crust may be poor in short-wavelength components. This interpretation is in good agreement with Calvet & Margerin (2013) who have proposed that the Pyrenean crust inhomogeneity may be described by a Von-Karman random medium with a hurst exponent larger than 1. However, to confirm our interpretation, we also need to consider the effect of absorption on the frequency dependence of T_{pd}. Coda Q measurements at large lapse time indicate that the average absorption quality factor in the Pyrenees varies as $\approx 220f^{0.64}$. Consequently, the absorption time decreases with frequency as $f^{-0.36}$. We hypothesize that the decrease of the absorption time with frequency hampers the broadening effect of small-scale heterogeneities and results in a slow increase of T_{pd} with frequency (Saito et al., 2002). A more quantitative interpretation in terms of heterogeneity power spectrum would be possible (Saito et al., 2005; Takahashi et al., 2009) but goes beyond the scope of the present article.

A part of the dispersion of T_{pd} measurements at a given hypocentral distance could be due to regional variations of scattering along the range. Thus, we propose to explore the spatial variations of envelope broadening after removing the hypocentral dependence described by the regression lines given in Table 1.

5.4 Spatial distribution of T_{pd} in the Pyrenees

5.5 Mapping methodology

For the mapping of peak delay times, we follow the method proposed by Takahashi et al. (2007). First, for each frequency band, we remove the hypocentral dependence by computing the peak delay time deviation defined as follows:

$$\Delta \log_{10} T_{pd} = \log_{10} T_{pd}(f) - (A_r(f) + B_r(f) \log_{10} R) \tag{5}$$

As envelope broadening is considered to be the result of multiple forward scattering by inhomogeneities, $\Delta \log_{10} T_{pd}$ may represent the relative strength of accumulated scattering contribution along each ray path. A small $\Delta \log_{10} T_{pd}$ thus implies the absence of strong medium heterogeneities along the ray path from the hypocentre to the station, whereas strong $\Delta \log_{10} T_{pd}$ indicates that a strongly inhomogeneous region is located somewhere along the ray path. For the mapping, we adopt the same approach as the one used for Q_c maps. We only consider 2D spatial variations and we divide the Pyrenean crust into rectangular $0.1° \times 0.1°$ blocks. Next, we allocate the mean values of $\Delta \log_{10} T_{pd}$ to each block. Only blocks that are crossed by more than 5 ray paths are considered. Finally, in each block, we take an average of the mean values over the nearest nine blocks to smooth the spatial variations.

5.5.1 Main characteristics of ΔT_{pd} maps

Figure 7 shows the distribution of peak delay time deviation in four frequency bands. Blocks with small values of $\Delta \log_{10} T_{pd}$ are indicated by blue colors while blocks of large $\Delta \log_{10} T_{pd}$ values are in red. The top panel shows the ray path density.

First we observe that there is no clear correlation between the $\Delta \log_{10} T_{pd}$ maps and the three main tectonic units. The main feature is an East-West dichotomy in the $\Delta \log_{10} T_{pd}$ spatial distribution. The Western Pyrenees (west to the Adour Fault) exhibit larger $\Delta \log_{10} T_{pd}$ values than the Central and Eastern Pyrenees. It may indicate the presence of strong inhomogeneities in the western part of the range. Indeed, as absorption and scattering have a competitive effect on the peak delay time, large $\Delta \log_{10} T_{pd}$ values suggest that scattering may be dominant, at least equal, in comparison to absorption at low frequency. The small variations of $\Delta \log_{10} T_{pd}$ with frequency also suggest that the power spectrum of inhomogeneities is poor in small-scale components (Sato, 1989; Saito et al., 2002).

In the Central and Eastern Pyrenees, the Paleozoic Axial Zone and the North Pyrenean Zone show rather small $\Delta \log_{10} T_{pd}$ values in all frequency bands. This feature could be due either to weak scattering or to strong absorption. But Q_c maps show that absorption is low in the PAZ except around the Maladetta Massif (Figures 7). Thus, scattering is probably weak on average in the PAZ and NPZ.

Eastern Pyrenees, more particularly to the east of intermountain basins of Empordà and La Selva, exhibit rather strong $\Delta \log_{10} T_{pd}$ values in the $2-4$ Hz frequency band. But the amplitude of the peak delay time deviation decreases as frequency increases. This frequency feature suggests that the crust in the Eastern Pyrenees is richer in small-scale structures than in the Western Pyrenees. However the effect of absorption should be also taken into account to propose a robust conclusion. In the Eastern Pyrenees, we also observe two high $\Delta \log_{10} T_{pd}$ regions located in the southern thrusts of the Axial zone, close to the compressive faults of Tech and Ribes-Camprodon . These high $\Delta \log_{10} T_{pd}$ anomalies match with regions characterized by strong deformation (Choukroune & Séguret, 1973) and may be related to small scale heterogeneities produced by strong crustal thickening (Vergés et al., 2002).

6 Discussion

In this section we propose to discuss Q_c and ΔT_{pd} maps in relation with other geophysical and geological observations. Globally, there is no clear correlation between geological structures and attenuation maps in the Pyrenees in all frequency bands. Usually, seismic waves are less attenuated in crystalline materials than in sedimentary ones (Sato et al., 2012). In the Pyrenees, this classical feature is maybe observed only at low frequency. In the next paragraphs, we propose a more detailed discussion.

6.1 The Eastern Pyrenees

The Eastern Pyrenees, south of the Têt and Tech faults, are characterized by rather small S-wave velocity (Souriau & Granet, 1995; Villaseñor et al., 2007), small (strong) absorption and rather large (small) $\Delta \log_{10} T_{pd}$ values at low (high) frequency. It may indicate that absorption is predominant at high frequency whereas scattering is strong at low frequency. However we can not quantitatively conclude on the predominance of scattering against absorption (and vice versa). Strong absorption and slightly low velocities suggest a thermal origin of these anomalies and/or the presence of fluids and melt, but rather small V_P/V_S ratio (Figure 2b) in this area does not favor a fluid interpretation of the strong absorption observed at high frequency. However, we clearly observe that low values of Q_c are mainly found in the Neogene fields at the east to Olot. Indeed, the Eastern Pyrenees have been strongly affected by the Neogene and Quaternary extensional events which have induced a crustal and lithospheric thinning towards the Mediterranean Sea as revealed by seismic data (Gallart et al., 1981; Mauffret et al., 2001), gravity data (Zeyen & Fernàndez, 1994; Vergés et al., 2002; Ayala et al., 2003; Gunnell et al., 2008) and heat flow measurements (Lucazeau & Vasseur, 1989; Fernandez & Banda, 1989). The Eastern Pyrenees have been also affected by alkaline volcanism in the late Mediterranean extensional phase. The main volcanic structures are located west to Banyoles-Olot and along the border of the intermountain basin of La Selva. Moreover, numerous thermal springs and associated geothermal anomalies located along faults or at the margins of graben-like structure in the Catalan Coastal Range also confirm a stronger geothermal activity in this part of the Eastern Pyrenees (Fernandez & Banda, 1989; Cabal & Fernàndez, 1995). In contrast, seismic absorption is smaller west of the volcanics units, in the Ebro Basin, where no strong geothermal anomalies have been detected (Fernandez & Banda, 1989). We thus propose that thermal effects induced by the crustal thinning and volcanism may explain strong attenuation in this area.

6.2 The Western Pyrenees

In the Western Pyrenees, ΔT_{pd} and Q_c maps reveal strong crustal inhomogeneities and strong absorption, respectively. The Pau Basin is characterized by rather strong absorption at low frequency (Figure 5), low-velocities and high V_P/V_S ratio (Daignieres et al., 1981). It could be explained by the presence of oil and gas in the sediments. In the South Pyrenean Zone, the Pamplona Basin is also characterized by low shear wave velocity (Souriau & Granet, 1995; Villaseñor et al., 2007) high V_P/V_S ratio (Figure 2b), and strong absorption (Figure 5). However, Q_c varies differently with frequency in the Pau and Pamplona Basins. The difference in the attenuation properties of the two basins may be ascribed to geographical variations either in the chemical composition of sedimentary materials and/or fluids, or in the distribution of melts and fluids, or in the density and connectivity of the fractures (and consequently in fluids circulation) (e.g., Leary, 1995).

Analyses of Lg waveforms have suggested the presence of small-scale heterogeneities in the Western Pyrenees. Indeed, no crustal phases appear in seismic records of Lg waves when ray paths cross the western part of the range (Chazalon et al., 1993; Sens-Schönfelder et al., 2009). Chazalon et al. (1993) have demonstrated that neither a realistic Moho jump nor a large-scale high-velocity body in the crust can cause such extinction. They speculate that the attenuation of crustal phases may be due to high scattering by small-scale heterogeneities in the Western Pyrenees. This hypothesis has been confirmed by Sens-Schönfelder et al. (2009) who demonstrated that a large-scale body with strong intrinsic absorption and strong scattering may explain the Lg blockage phenomenom. Their best model is characterized by an intrinsic quality factor Q_i about 180 and a scattering quality factor about 340 (at 3 Hz). In the Western Pyrenees, absorption and scattering may be respectively about 4 times and 10 times larger than in the surrounding regions. Our $\Delta \log T_{pd}$ and Q_c maps show qualitatively that scattering and absorption are on average strong in the Western Pyrenees at low frequency. Even if we do not perform robust inversions, our results are in good agreement with those of Sens-Schönfelder et al. (2009).

The Basque and Labourd Massifs are characterized by strong attenuation in all frequency bands. The Mauléon Basin seems to have a distinct behaviour with slightly less absorption at high frequency than the surrounding Massifs. Slightly higher V_P/V_S ratio in the Mauléon and Pamplona Basins in comparison to the Basque and Labourd Massifs (see Figure 2b) suggests the presence of more melts or fluids in the basins than in Paleozoic Massifs. Geographical variations in the fluid contents may also explain a part of the frequency-dependence of absorption in the Mauléon Basin. However, the fluid hypothesis is not compatible with the high seismic velocities observed in this region (Figure 2a). Alternatively, seismic properties of the Labourd-Mauléon area may be ascribed to the chemical and/or mechanical properties of the crustal materials. The strong positive Bouguer anomaly observed in the Mauléon-Labourd area (Vacher & Souriau, 2001; Jammes et al., 2010) (see also Figure 2c) have been interpreted as mantle intrusions which could also explain high seismic velocities and strong absorption. Sens-Schönfelder et al. (2009) argue that S-wave absorption in the Western Pyrenees is too strong for crustal materials (Sato et al., 2012). As mantle materials are more ductile, their presence may induce stronger seismic absorption.

Peak delay time measurement reveals that scattering is strong in the Western Pyrenees. What is the possible origin of scattering in this area? Close to the surface, it is observed that Cretaceous sediments are locally associated with remnants of subcrustal and mantle rocks in the Labourd Massifs and the Mauléon Basin. Particularly, the Mauléon Basin contains a number of outcrops, ranging from a few meters to 3 km in diameter, rich in serpentinized mantle peridotites (Lagabrielle & Bodinier, 2008; Jammes et al., 2009). Interestingly, Sens-Schönfelder et al. (2009) obtain a typical size for heterogeneities in the western Pyrenean crust around 800 m. Intrusion of mantle or subcrustal material is thus a possible mechanism to explain both the strong seismic scattering and absorption observed in the Western Pyrenees.

6.3 The Central Pyrenees

In all frequency bands, a low-Q_c anomaly (strong absorption) extends from the North Pyrenean Zone to the South Pyrenean Zone. At the same location, small $\Delta \log T_{pd}$ values show that scattering may be smaller than in the Western Pyrenees. East to this low-Q_c anomaly, we also observe that most of the Paleozoic materials are characterized by small absorption (Figure 5). This East-West dichotomy in the Axial Zone with a transition at the location of the Maladeta Massif can not be easily explained from tectonic and geological arguments except maybe that most of the Hercynian granitic massifs, the large massifs of gneiss (age ∼470 Ma) and the older meta-sediments (Upper Proterozoic to Ordovician) are located in this high-Q_c area (Baudin et al., 2008). We also observe that the Pyrenean seismicity shifts southward at the location of the low-Q_c anomaly. A deep structure in the crust may be at the origin of this attenuation anomaly. Interestingly, an anomalous body has been detected in this area by seismic tomography and analysis of Bouguer anomalies. This high-density and high-velocity crustal body is located south to Saint Gaudens , in the North Pyrenean Zone,(see Figure 2), on the northern border of this Q_c-anomaly. As proposed for the Labourd-Mauléon area, more ductile mantle or sub-crustal materials could be at the origin of the observed strong absorption. However, we observe that the Saint Gaudens and Labourd-Mauléon anomalies have a rather distinct seismic behaviour. The Saint Gaudens anomaly exhibits smaller absorption, smaller scattering and smaller V_P/V_S ratio than the Labourd-Mauléon one. In both cases, the positive correlation between seismic velocity and attenuation cannot be explained by thermal effects but suggests that seismic properties may be related to the chemical composition. Variations in the chemical/mineralogical composition of these deep materials may be at the origin of the distinct seismic behaviour between the two high density/velocity anomalies. However, from the comparison of gravity and seismic data, Vacher & Souriau (2001) propose a similar mineralogical origin for these two bodies, even if more detailed investigations may be necessary. A part of the difference in absorption between the Saint Gaudens and Labourd-Mauléon anomalies may be also due to a difference in the amount of mantle materials in the crust.

7 Conclusions

A first attempt at mapping seismic wave attenuation in the Pyrenees has been proposed, based on coda Q and peak delay time analysis in the $[1-32]$ Hz frequency band. Q_c maps show that the amplitude and the frequency dependence of attenuation strongly vary along the Pyrenean range. The Paleozoic Axial Zone exhibits mainly lower seismic attenuation than the surrounding regions, except at the longitude of the Maladeta Massif, east of the Adour fault. Seismic waves in the Western Pyrenees, more particularly at the location of the Basques Massifs and the Nappe des Marbres, are strongly attenuated. Similarly the Neogene structures of North-East Catalonia show strong seismic attenuation at high frequency. In addition to coda Q analysis, envelope broadening of high-frequency seismic waves gives complementary information on the origin of seismic attenuation in the Pyrenees, more particularly on the nature of the crustal inhomogeneities. The peak delay time maps highligth a strong East-West dichotomy in the scattering properties of the Pyrenean crust with stronger inhomogeneities in the Western Pyrenees, as previously proposed by Sens-Schönfelder et al. (2009). The Eastern Pyrenees exhibit a stronger frequency dependence of the peak delay time than the Western Pyrenees.

The comparison of Q_c and peak delay time maps allows a qualitative discussion about the relative contributions of absorption and scattering to the seismic attenuation in the Pyrenean crust. Anelastic absorption appears to be dominant in the Eastern Pyrenees at high frequency, whereas both absorption and scattering are strong in the Western Pyrenees. We propose a thermal origin for the strong seismic attenuation at the location of the Neogene structures in the Eastern Pyrenees. Indeed, the Eastern Pyrenees have been affected by a late extensional event with volcanism, and the region presents a rather strong geothermal activity in comparison to the Ebro Basin or the Western Pyrenees. In the Western Pyrenees, we argue that the attenuation properties of the crust (strong absorption and scattering) are mainly due to sub-crustal or mantle intrusions related to the complex tectonic history of the region.

Although some correlations have been observed between Q_c, $\Delta \log_{10} T_{pd}$, seismic velocity and V_P/V_S ratio, our findings need to be clarified in several aspect. First, seismic structures in the eastern and western edges of the range are not correctly resolved in the tomography by Souriau & Granet (1995), more particularly the lateral extension of the Labourd-Mauléon high-velocity anomaly. High-resolution crustal tomography may be soon available through to the deployment of the PYROPE and IBERARRAY seismic networks. Second, we only provide coda-Q and peak delay times deviation maps which have been interpreted qualitatively in terms of absorption and scattering. Future works should explore the sensitivity of coda-Q measurements to the lateral and depth variations of absorption. It is clear that our simple mapping approach to Q_c measurements only gives the gross features of the lateral variations of attenuation without any constraint on the depth behavior. Next, we will consider an inversion of the peak delay times, after correction for absorption, in order to better quantify the spatial distribution of the velocity random fluctuations in the Pyrenean crust. Absorption and scattering maps may bring new insights into the structures of the Pyrenees but also offer new elements for interpreting geophysical data (Bouguer anomaly, seismic tomography), seismicity distribution and geological observations. Moreover, such attenuation maps should also significantly improve strong motion prediction in the Pyrenees.

Acknowledgements

The authors would like to thank the different organisms that operate temporary and permanent seismological networks in the Pyrenees for making their data available. The authors are also grateful to Marc Calvet, Alexis Rigo, Annie Souriau and Thomas Theunissen for helpful discussions. This work was funded by the European Regional Development Fund (ERDF/FEDER) – POCTEFA program– (SISPyr project) and the Agence Nationale de la Recherche (ANR - PYROPE). The temporary network IberArray was funded by Consolider-Ingenio 2010 project TOPO-IBERIA (CSD2006-00041).

References

Aki, K. & Chouet, B., 1975. Origin of coda waves: Source attenuation and scattering effects, *J. Geophys. Res.*, **80**, 3322–3342.

Ayala, C., Torne, M., & Pous, J., 2003. The lithosphere–asthenosphere boundary in the western Mediterranean from 3D joint gravity and geoid modeling: tectonic implications, *Earth Planet. Sci. Lett.*, **209**(3), 275–290.

Baudin, T., Barnolas, A., Gil, I., & Martin-Alfageme, S., 2008. *Carte géologique des Pyrénées à 1/400 000*, Bureau de Recherches Géologiques et Minières, BRGM-ITGE.

Cabal, J. & Fernàndez, M., 1995. Heat flow and regional uplift at the north-eastern border of the Ebro basin, NE Spain, *Geophys. J. Int.*, **121**(2), 393–403.

Calvet, M. & Margerin, L., 2013. Lapse time dependence of coda q: anisotropic multiple-scattering models and application to Pyrenees, *Bull. Seism. Soc. Am.*, **103**, in press.

Campillo, M. & Plantet, J., 1991. Frequency dependence and spatial distribution of seismic attenuation in France: experimental results and possible interpretations, *Phys. Earth Planet. Int.*, **67**(1-2), 48–64.

Campillo, M., Plantet, J., & Bouchon, M., 1985. Frequency-dependent attenuation in the crust beneath central France from Lg waves: data analysis and numerical modeling, *Bulletin of the Seismological Society of America*, **75**(5), 1395–1411.

Carcolé, E. & Sato, H., 2010. Spatial distribution of scattering loss and intrinsic absorption of short-period S waves in the lithosphere of Japan on the basis of the Multiple Lapse Time Window Analysis of Hi-net data, *Geophys. J. Int.*, **180**(1), 268–290.

Casas, A., Kearey, P., Rivero, L., & Adam, C., 1997. Gravity anomaly map of the Pyrenean region and a comparison of the deep geological structure of the western and eastern Pyrenees, *Earth Planet. Sci. Lett.*, **150**(1), 65–78.

Chazalon, A., Campillo, M., Gibson, R., & Carreno, E., 1993. Crustal wave propagation anomaly across the Pyrenean range. Comparison between observations and numerical simulations, *Geophys. J. Int.*, **115**(3), 829–838.

Chevrot, S. & Cansi, Y., 1996. Source spectra and site-response estimates using the coda of Lg waves in western Europe, *Geophys. Res. Lett.*, **23**(13), 1605–1608.

Chevrot, S., Sylvander, M., & Delouis, B., 2011. A preliminary catalog of moment tensors for the Pyrenees, *Tectonophysics*, **150**, 239–251.

Choukroune, P., 1992. Tectonic evolution of the Pyrenees, *An. Rev. Earth Planet. Sci.*, **20**, 143–158.

Choukroune, P. & Séguret, 1973. *Carte structurale des Pyrénées*, Université des Sciences et Techniques du Languedoc. Laboratoire de géologie structurale.

Choukroune, P., Roure, F., Pinet, B., & Team, E., 1990. Main results of the ECORS pyrenees profile, *Tectonophysics*, **173**(1-4), 411–423.

Correig, A., Mitchell, B., & Ortiz, R., 1990. Seismicity and coda Q values in the eastern Pyrenees: First results from the La Cerdanya seismic network, *Pure Applied Geophys.*, **132**(1), 311–329.

Daignieres, M., Gallart, J., & Banda, E., 1981. Lateral variation of the crust in the North Pyrenean Zone, *Ann. Geophys*, **37**(3), 435–456.

Drouet, S., Souriau, A., & Cotton, F., 2005. Attenuation, seismic moments, and site effects for weak-motion events: application to the Pyrenees, *Bull. Seism. Soc. Am.*, **95**(5), 1731–1748.

Drouet, S., Chevrot, S., Cotton, F., & Souriau, A., 2008. Simultaneous inversion of source spectra, attenuation parameters, and site responses: application to the data of the French accelerometric network, *Bull. Seism. Soc. Am.*, **98**(1), 198–219.

Drouet, S., Cotton, F., & Guéguen, P., 2010. vs30, κ, regional attenuation and Mw from accelerograms: application to magnitude 3–5 French earthquakes, *Geophys. J. Int.*, **182**(2), 880–898.

Fehler, M., Hoshiba, M., Sato, H., & Obara, K., 1992. Separation of scattering and intrinsic attenuation for the Kanto-Tokai region, Japan, using measurements of s-wave energy versus hypocentral distance, *Geophys. J. Int.*, **108**(3), 787–800.

Fernandez, M. & Banda, E., 1989. An approach to the thermal field in northeastern Spain, *Tectonophysics*, **164**(2-4), 259–266.

Gagnepain-Beyneix, J., 1987. Evidence of spatial variations of attenuation in the western Pyrenean range, *Geophys. J. Roy. Astr. Soc.*, **89**(2), 681–704.

Gallart, J., Daignieres, M., Banda, E., Surinach, E., & Hirn, A., 1980. The eastern Pyrenean domain: lateral variations at crust-mantle level, *Ann. Geophys*, **36**(2), 141–158.

Gallart, J., Banda, E., & Daignières, M., 1981. Crustal structure of the Paleozoic Axial Zone of the Pyrenees and transition to the North Pyrenean Zone, *Ann. Geophys*, **37**(3), 457–480.

Gallart, J., Díaz, J., Nercessian, A., Mauffret, A., & Dos Reis, T., 2001. The eastern end of the Pyrenees: Seismic features at the transition to the NW Mediterranean, *Geophys. Res. Lett.*, **28**(11), 2277–2280.

Gunnell, Y., Zeyen, H., & Calvet, M., 2008. Geophysical evidence of a missing lithospheric root beneath the Eastern Pyrenees: Consequences for post-orogenic uplift and associated geomorphic signatures, *Earth Planet. Sci. Lett.*, **276**(3-4), 302–313.

Hennino, R., Trégourès, N., Shapiro, N., Margerin, L., Campillo, M., Van Tiggelen, B., & Weaver, R., 2001. Observation of equipartition of seismic waves, *Phys. Rev. Lett.*, **86**(15), 3447–3450.

Jammes, S., Manatschal, G., Lavier, L., & Masini, E., 2009. Tectonosedimentary evolution related to extreme crustal thinning ahead of a propagating ocean: Example of the western Pyrenees, *Tectonics*, **28**, TC4012, doi:10.1029/2008TC002406.

Jammes, S., Tiberi, C., & Manatschal, G., 2010. 3d architecture of a complex transcurrent rift system: The example of the Bay of Biscay–Western Pyrenees, *Tectonophysics*, **489**(1), 210–226.

Lacombe, C., Campillo, M., Paul, A., & Margerin, L., 2003. Separation of intrinsic absorption and scattering attenuation from l_g coda decay in central france using acoustic radiative transfer theory, *Geophys. J. Int.*, **154**, 417–425.

Lagabrielle, Y. & Bodinier, J., 2008. Submarine reworking of exhumed subcontinental mantle rocks: field evidence from the Lherz peridotites, French Pyrenees, *Terra Nova*, **20**(1), 11–21.

Le Pichon, X. & Sibuet, J., 1971. Western extension of boundary between European and Iberian plates during the Pyrenean orogeny, *Earth Planet. Sci. Lett.*, **12**(1), 83–88.

Leary, P., 1995. The cause of frequency-dependent seismic absorption in crustal rock, *Geophys. J. Int.*, **122**(1), 143–151.

Lucazeau, F. & Vasseur, G., 1989. Heat flow density data from France and surrounding margins, *Tectonophysics*, **164**(2-4), 251–258.

Margerin, L., Campillo, M., Shapiro, N. M., & Tiggelen, B. V., 1999. Residence time of diffuse waves in the crust as a physical interpretation for coda q. application to seismograms recorded in Mexico., *Geophys. J. Int.*, **138**, 343–352.

Martí, J., Mitjavila, J., Roca, E., & Aparicio, A., 1992. Cenozoic magmatism of the Valencia trough (Western Mediterranean): Relationship between structural evolution and volcanism, *Tectonophysics*, **203**(1), 145–165.

Mauffret, A., Durand de Grossouvre, B., Tadeu Dos Reis, A., Gorini, C., & Nercessian, A., 2001. Structural geometry in the eastern Pyrenees and western Gulf of Lion (Western Mediterranean), *J. Struc. Geol.*, **23**(11), 1701–1726.

Mitchell, B., 1995. Anelastic structure and evolution of the continental crust and upper mantle from seismic surface wave attenuation, *Reviews of Geophysics*, **33**(4), 441–462.

Mitchell, B., Cong, L., & Ekström, G., 2008. A continent-wide map of 1-hz Lg coda Q variation across Eurasia and its relation to lithospheric evolution, *J. Geophys. Res*, **113**, B04303.

Nocquet, J. & Calais, E., 2004. Geodetic measurements of crustal deformation in the Western Mediterranean and Europe, *Pure Applied Geophys.*, **161**(3), 661–681.

Obara, K. & Sato, H., 1995. Regional differences of random inhomogeneities around the volcanic front in the Kanto-Tokai area, Japan, revealed from the broadening of S wave seismogram envelopes, *J. Geophys. Res.*, **100**, 2103–2103.

Paasschens, J., 1997. Solution of the time-dependent Boltzmann equation, *Phys. Rev. E*, **56**(1), 1135–1141.

Pacheco, C. & Snieder, R., 2005. Time-lapse travel time change of multiply scattered acoustic waves, *The Journal of the Acoustical Society of America*, **118**, 1300–1310.

Payo, G., Badal, J., Canas, J., Corchete, V., Pujades, L., & Serón, F., 1990. Seismic attenuation in Iberia using the coda-Q method, *Geophys. J. Int.*, **103**(1), 135–145.

Petukhin, A. G. & Gusev, A. A., 2003. The duration-distance relationship and average envelope shapes of small Kamtchatka earthquakes, *Pure Appl.Geophys.*, **160**, 171–1743.

Pujades, L., Canas, J., Egozcue, J., Puigvi, M., Gallart, J., Lana, X., Pous, J., & Casas, A., 1990. Coda-Q distribution in the Iberian peninsula, *Geophys. J. Int.*, **100**(2), 285–301.

Rigo, A., Souriau, A., Dubos, N., Sylvander, M., & Ponsolles, C., 2005. Analysis of the seismicity in the central part of the Pyrenees (France), and tectonic implications, *J. Seism.*, **9**(2), 211–222.

Romanowicz, B. & Mitchell, B., 2007. Q in the earth from crust to core, *Treatise on geophysics*, **1**, 731–774.

Rosenbaum, G., Lister, G., & Duboz, C., 2002. Relative motions of Africa, Iberia and Europe during Alpine orogeny, *Tectonophysics*, **359**(1-2), 117–129.

Rossetto, V., Margerin, L., Planès, T., & Larose, E., 2011. Locating a weak change using diffuse waves: Theoretical approach and inversion procedure, *Journal of Applied Physics*, **109**(3), 034903–034903–11.

Ruiz, M., Gallart, J., Díaz, J., Olivera, C., Pedreira, D., López, C., González-Cortina, J., & Pulgar, J., 2006. Seismic activity at the western Pyrenean edge, *Tectonophysics*, **412**(3), 217–235.

Saito, T., Sato, H., & Ohtake, M., 2002. Envelope broadening of spherically outgoing waves in three-dimensional random media having power law spectra, *J. Geophys. Res.*, **107**(B5), doi:10.1029/2001JB000264.

Saito, T., Sato, H., Ohtake, M., & Obara, K., 2005. Unified explanation of envelope broadening and maximum-amplitude decay of high-frequency seismograms based on the envelope simulation using the Markov approximation: Forearc side of the volcanic front in northeastern Honshu, Japan, *J. Geophys. Res*, **110**, B01304, doi:10.1029/2004JB003225.

Sato, H., 1989. Broadening of seismogram envelopes in the randomly inhomogeneous lithosphere based on the parabolic approximation: Southeastern Honshu, Japan, *J. geophys. Res*, **94**, 17–735.

Sato, H., Fehler, M. C., & Maeda, T., 2012. *Seismic wave propagation and scattering in the heterogeneous Earth*, Springer, Berlin, 2nd edn.

Sens-Schönfelder, C., Margerin, L., & Campillo, M., 2009. Laterally heterogeneous scattering explains Lg blockage in the Pyrenees, *J. Geophys. Res.*, **114**, B07309, doi:10.1029/2008JB006107.

Souriau, A. & Granet, M., 1995. A tomographic study of the lithosphere beneath the Pyrenees from local and teleseismic data, *J. Geophys. Res.*, **100**(B9), 18117–18.

Souriau, A. & Pauchet, H., 1998. A new synthesis of Pyrenean seismicity and its tectonic implications, *Tectonophysics*, **290**(3-4), 221–244.

Souriau, A., Sylvander, M., Rigo, A., Fels, J., Douchain, J., & Ponsolles, C., 2001. Sismotectonique des Pyrénées; principales contraintes sismologiques, *Bull. Soc. Geol. France*, **172**(1), 25–39.

Souriau, A., Chaljub, E., Cornou, C., Margerin, L., Calvet, M., Maury, J., Wathelet, M., Grimaud, F., Ponsolles, C., Péquegnat, C., et al., 2011. Multimethod characterization of the French-Pyrenean valley of Bagnères-de-Bigorre for seismic-hazard evaluation: Observations and models, *Bull. Seism. Soc. Am.*, **101**(4), 1912–1937.

Srivastava, S., Sibuet, J., Cande, S., Roest, W., & Reid, I., 2000. Magnetic evidence for slow seafloor spreading during the formation of the Newfoundland and Iberian margins, *Earth Planet. Sci. Lett.*, **182**(1), 61–76.

Takahashi, T., Sato, H., Nishimura, T., & Obara, K., 2007. Strong inhomogeneity beneath Quaternary volcanoes revealed from the peak delay analysis of S-wave seismograms of microearthquakes in northeastern Japan, *Geophys. J. Int.*, **168**(1), 90–99.

Takahashi, T., Sato, H., Nishimura, T., & Obara, K., 2009. Tomographic inversion of the peak delay times to reveal random velocity fluctuations in the lithosphere: method and application to northeastern Japan, *Geophys. J. Int.*, **178**(3), 1437–1455.

Vacher, P. & Souriau, A., 2001. A three-dimensional model of the Pyrenean deep structure based on gravity modelling, seismic images and petrological constraints, *Geophys. J. Int.*, **145**(2), 460–470.

Vargas, C., Ugalde, A., Pujades, L., & Canas, J., 2004. Spatial variation of coda wave attenuation in northwestern Colombia, *Geophys. J. Int.*, **158**(2), 609–624.

Vergés, J., Fernàndez, M., & Martínez, A., 2002. The Pyrenean orogen: pre-, syn-, and post-collisional evolution, *J. Virtual Explorer*, **8**, 57–76.

Villaseñor, A., Yang, Y., Ritzwoller, M., & Gallart, J., 2007. Ambient noise surface wave tomography of the Iberian Peninsula: Implications for shallow seismic structure, *Geophysical Research Letters*, **34**(11), L11304, doi:10.1029/2007GL030164.

Vissers, R. & Meijer, P., 2012. Mesozoic rotation of Iberia: Subduction in the Pyrenees?, *Earth-Science Reviews*, **110**, 93–110.

Zeyen, H. & Fernàndez, M., 1994. Integrated lithospheric modeling combining thermal, gravity, and local isostasy analysis: application to the NE Spanish Geotransect, *J. Geophys. Res.*, **99**(B9), 18089–18.

List of Tables

Table 1: Estimated A_r and B_r parameters with their standard deviation from least-square regression $\log_{10} T_{pd}(f) = A_r(f) + B_r(f) \log_{10} R$ in four frequency bands.

Frequency (Hz)	A_r	SD(A_r)	B_r	SD(B_r)
2.0-4.0	-0.827	0.125	0.649	0.074
4.0-8.0	-1.572	0.125	1.045	0.075
8.0-16.0	-1.859	0.124	1.239	0.075
16.0-32.0	-1.902	0.125	1.323	0.075

List of Captions

Figure 1: Main structural units of the Pyrenees after Choukroune (1992). NPFT: North Pyrenean Frontal Thrust; NPM: North Pyrenean Massifs; SPT: South Pyrenean Thrust. Light grey zones corresponds to Paleozoic material, dark grey zones indicates Quaternary volcanic rocks.

Figure 2: (a) Crustal P-wave tomographic model by Souriau & Granet (1995) at depth 11 km. (b) V_P/V_S ratio computed at some French and Spanish velocimeter stations (c) Bouguer anomalies (computed by International Gravimetric Bureau – http://bgi.omp.obs-mip.fr/). Black thick lines are the main Pyrenean faults.

Figure 3: Location map of earthquakes and seismological stations used for coda-Q and peak delay time measurements. See inset for symbol explanation.

Figure 4: Q_c as a function of the epicentral distance in the frequency band $[4-8]$Hz. Solid line is the mean value and dashed lines correspond to one standard deviation. The coda windows start at $2\,t_s$ (a), 50 s (b), 80 s (c) after the origin time of the earthquake. t_s is the S-wave travel time. The length of the coda window is fixed at 30 s.

Figure 5: Regional variations of Q_c (left) and ray path density (right). Q_c is estimated in five frequency bands from $[1-2]$ Hz (top) to $[16-32]$ Hz (bottom). Blocks with less than two measurements are shown in gray in Q_c maps.

Figure 6: Logarithmic plot of peak delay times (in seconds) as a function of the hypocentral distance (in kilometers) for crustal S waves in four frequency bands. Gray dots are the data, and black lines are the regression lines : $\log_{10}(T_{pd}) = A_r(f) + B_r(f)\log_{10} R$. The values of coefficient A_r and B_r are listed in Table 1.

Figure 7: Distribution of the logarithmic deviation of crustal S-wave peak delay time $\Delta\log_{10}(T_{pd})$ in four frequency bands. We do not consider blocks in which the number of ray paths is less than 5 (gray blocks). The top panel gives the ray path density in all frequency bands.

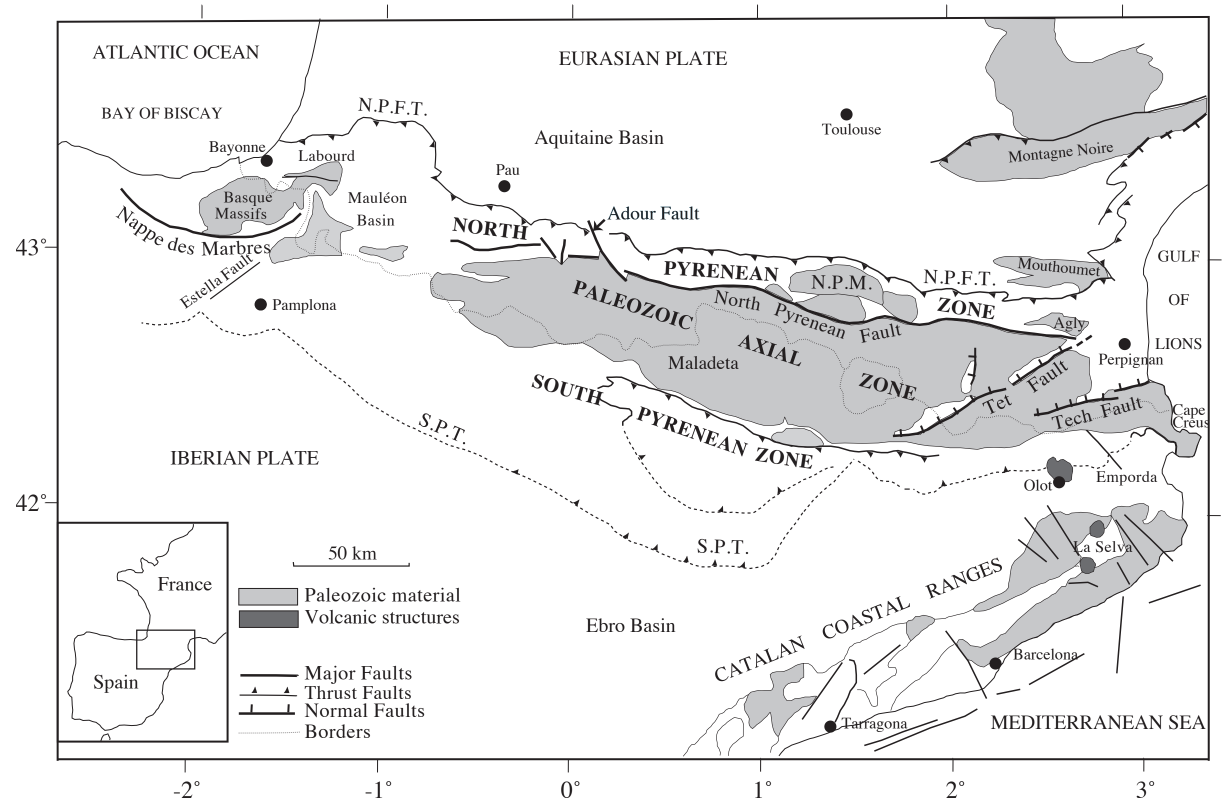
ATLANTIC OCEAN
EURASIAN PLATE
BAY OF BISCAY
N.P.F.T.
Bayonne
Labourd
Aquitaine Basin
Toulouse
Pau
Montagne Noire
Basque Massifs
Mauléon Basin
Adour Fault
Nappe des Marbres
NORTH
PYRENEAN
ZONE
N.P.M.
N.P.F.T.
Mouthoumet
GULF OF LIONS
Estella Fault
Pamplona
PALEOZOIC
AXIAL
ZONE
North Pyrenean Fault
Agly
Perpignan
Maladeta
Tet Fault
Tech Fault
Cape Creus
SOUTH PYRENEAN ZONE
S.P.T.
IBERIAN PLATE
Olot
Emporda
La Selva
France
Spain
50 km
Paleozoic material
Volcanic structures
Major Faults
Thrust Faults
Normal Faults
Borders
Ebro Basin
CATALAN COASTAL RANGES
Barcelona
Tarragona
MEDITERRANEAN SEA
43°
42°
-2°
-1°
0°
1°
2°
3°

Figure 1

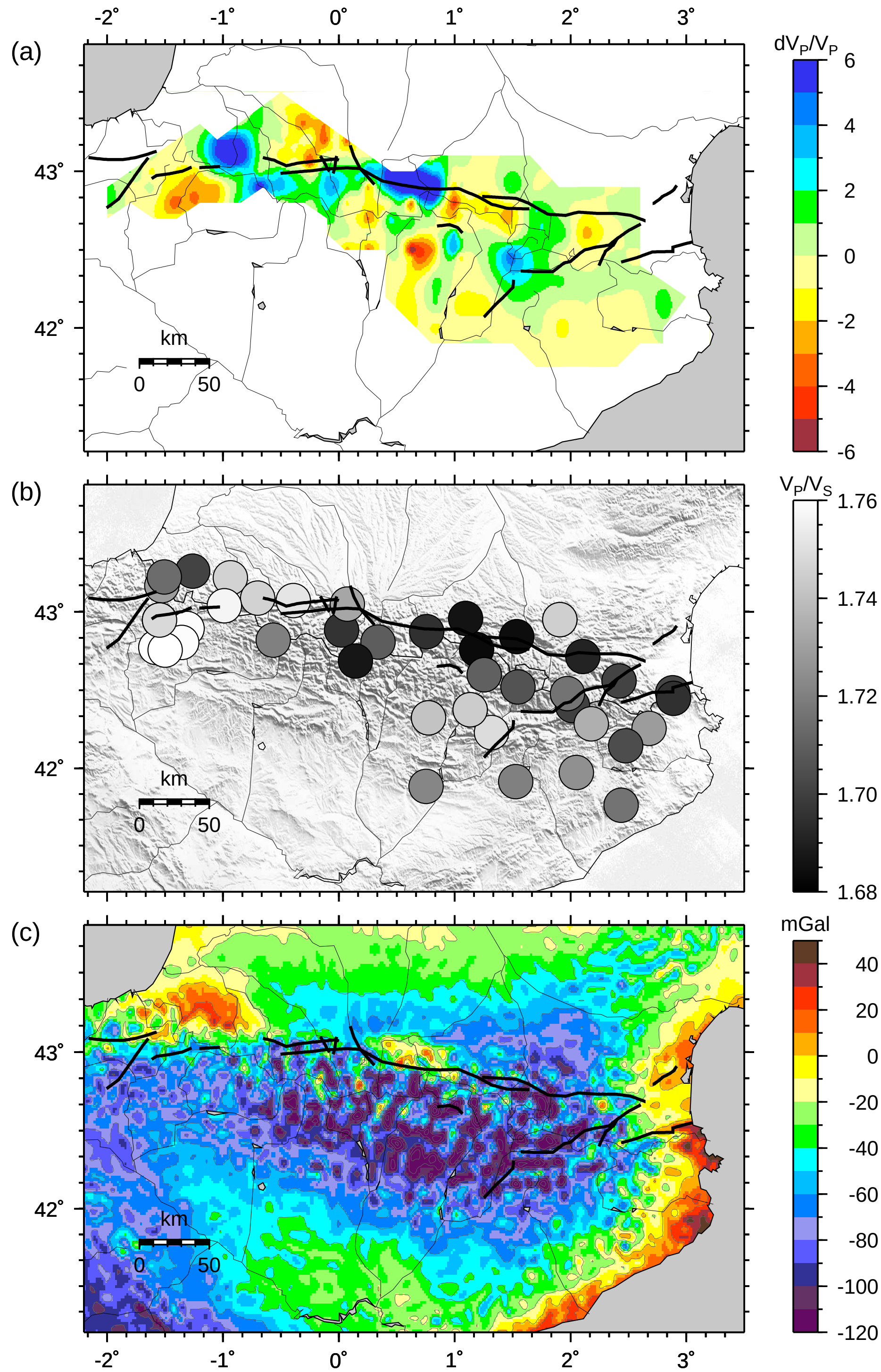

798

799 Figure 2

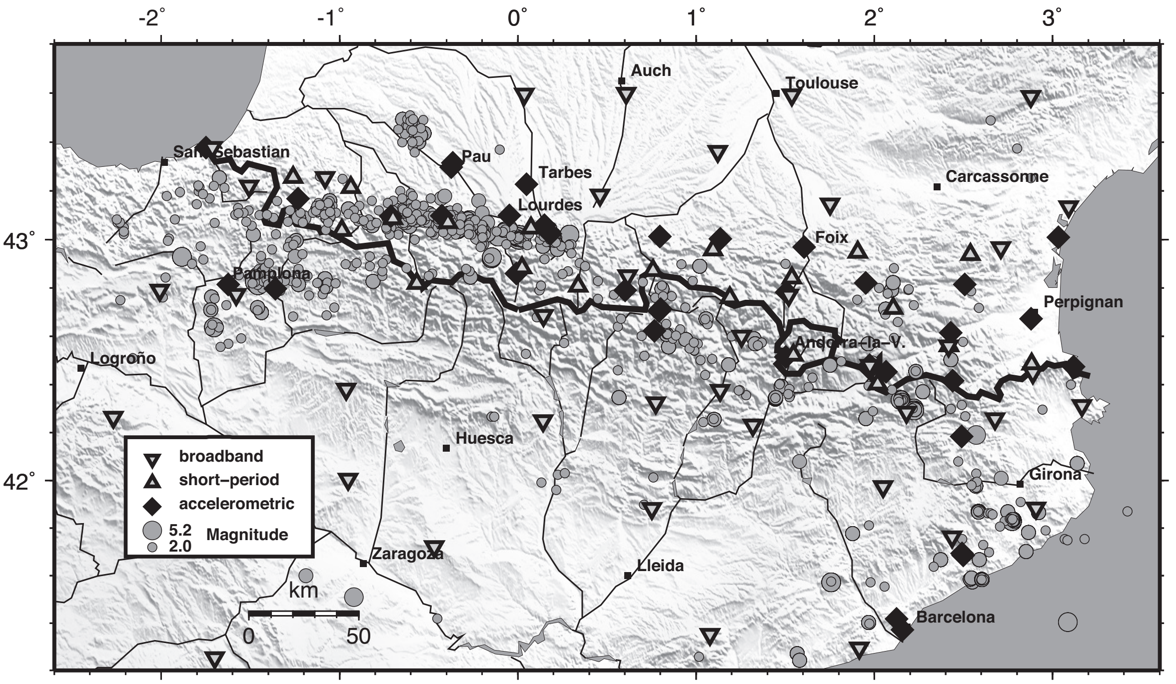
-2°
-1°
0°
1°
2°
3°
43°
42°
Auch
Toulouse
San Sebastian
Pau
Tarbes
Lourdes
Carcassonne
Foix
Pamplona
Perpignan
Andorra-la-V.
Logroño
Huesca
Girona
Zaragoza
Lleida
Barcelona
broadband
short–period
accelerometric
5.2
2.0
Magnitude
km
0
50

Figure 3

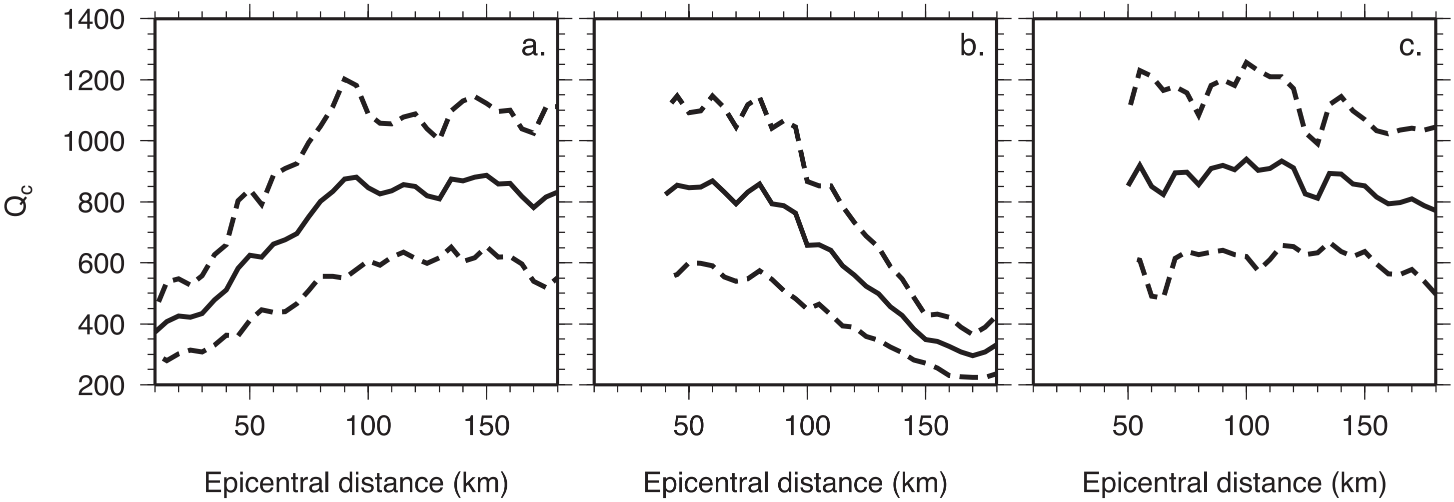

1400
1200
1000
800
600
400
200
Q_c
a.
b.
c.
50
100
150
Epicentral distance (km)
Epicentral distance (km)
Epicentral distance (km)

Figure 4

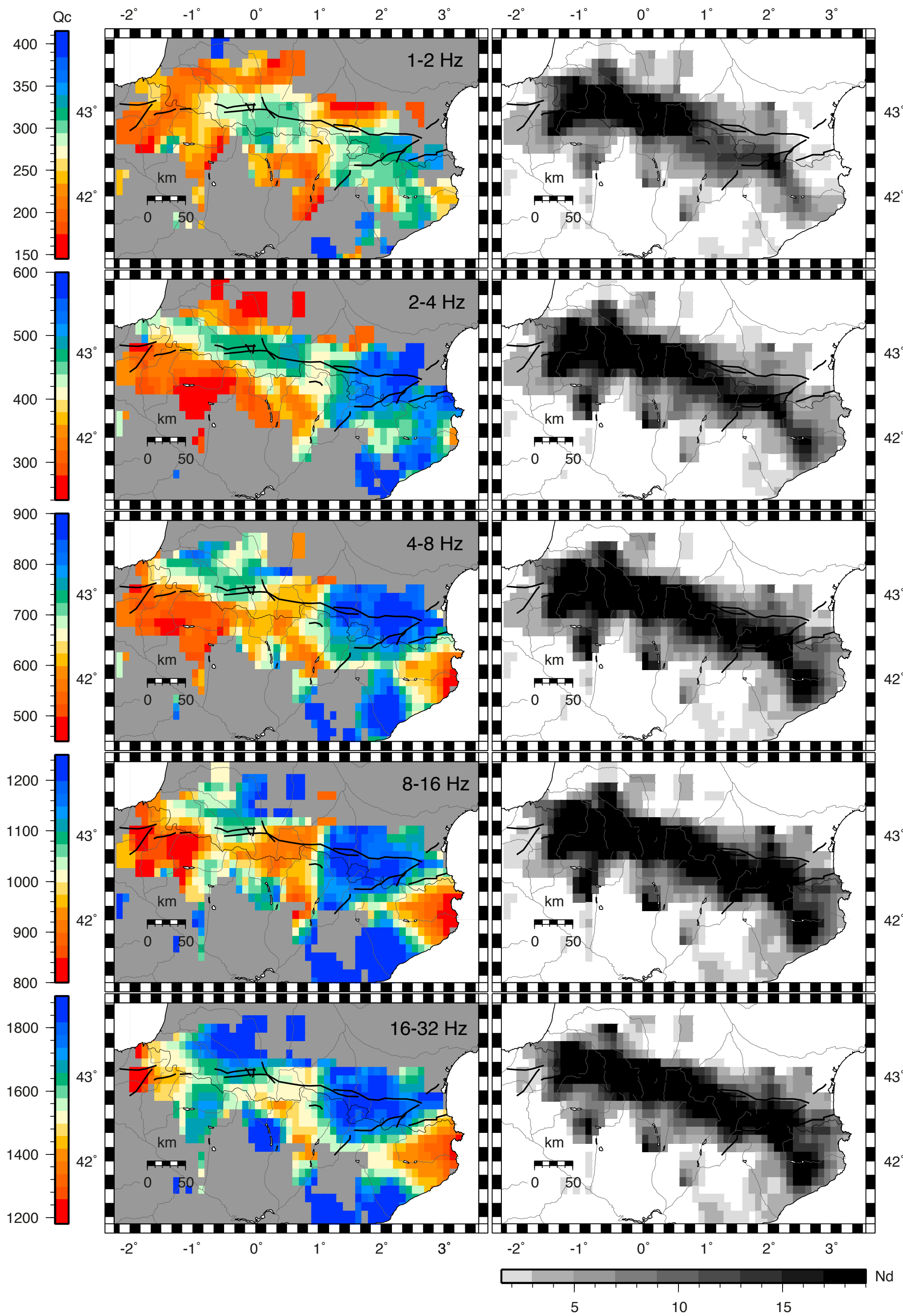
Qc
1-2 Hz
2-4 Hz
4-8 Hz
8-16 Hz
16-32 Hz
km
0 50
-2° -1° 0° 1° 2° 3°
42° 43°
400 350 300 250 200 150
600 500 400 300
900 800 700 600 500
1200 1100 1000 900 800
1800 1600 1400 1200
Nd
5 10 15

Figure 5

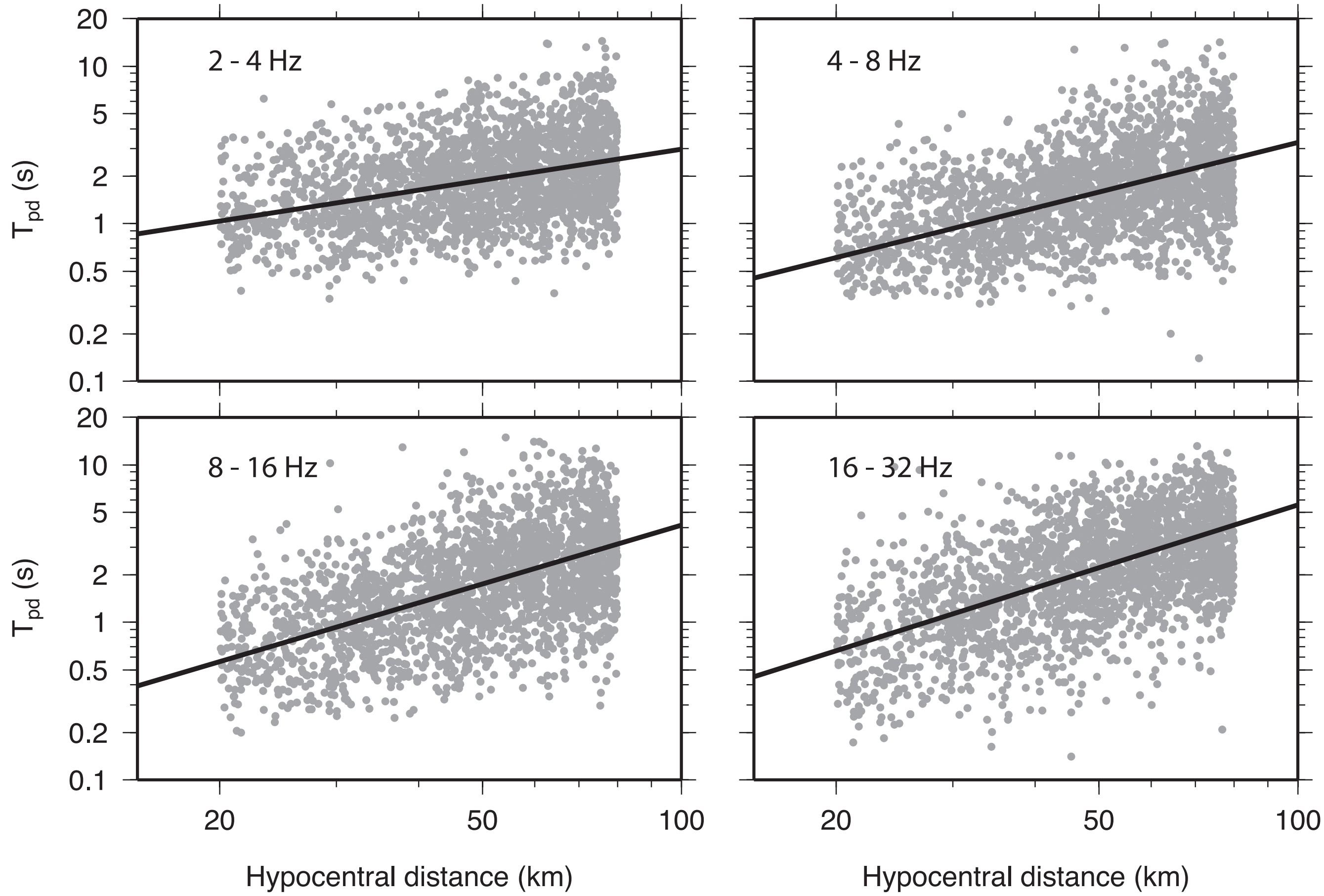
2 - 4 Hz
4 - 8 Hz
8 - 16 Hz
16 - 32 Hz
T_pd (s)
T_pd (s)
20
10
5
2
1
0.5
0.2
0.1
20
50
100
Hypocentral distance (km)
Hypocentral distance (km)

Figure 6

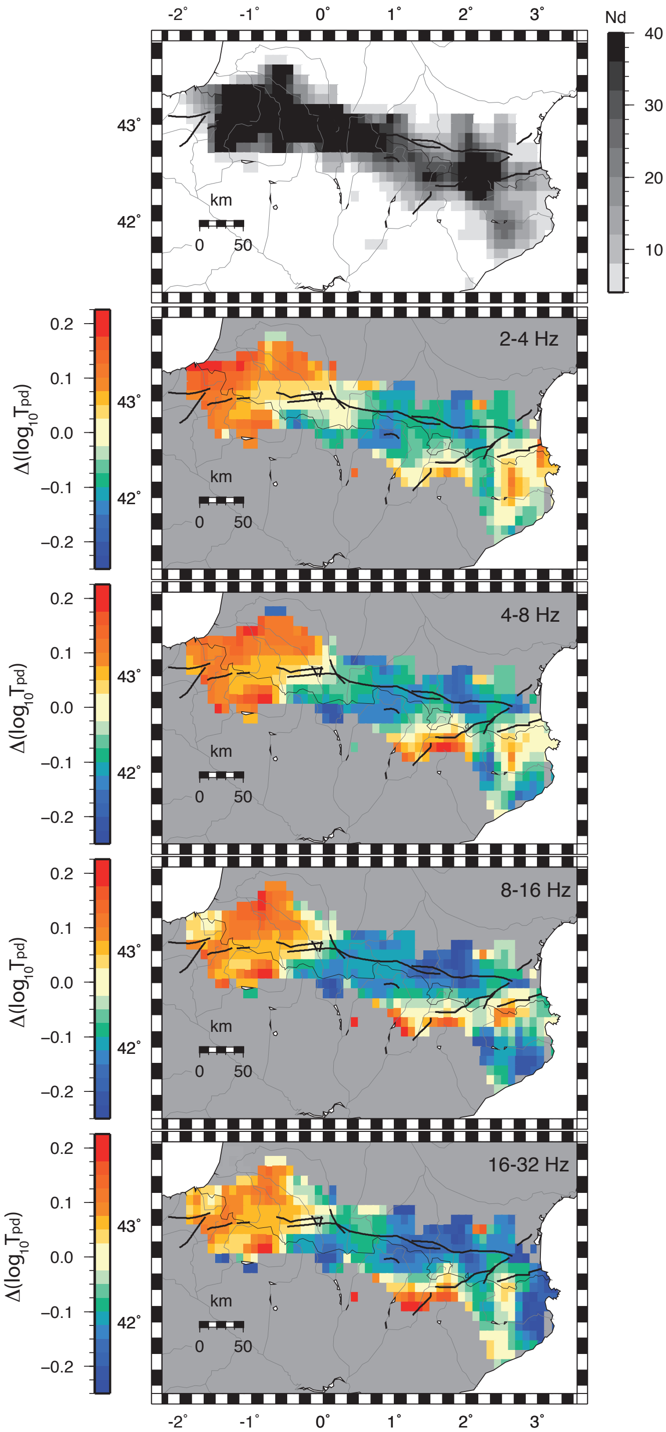

808

809 Figure 7